THERMAL NEUTRON (n,α) STUDIES IN THE RARE EARTH REGION

THERMAL NEUTRON (n,α) STUDIES IN THE RARE EARTH REGION

By

KHALID BEG, M.Sc., F.C.T.L'pool

A Thesis

Submitted to the Faculty of Graduate Studies

in Partial Fulfilment of the Requirements

for the Degree

Doctor of Philosophy

McMASTER UNIVERSITY

October 1967

DOCTOR OF PHILOSOPHY (1967) McMASTER UNIVERSITY
(Chemistry) Hamilton, Ontario

TITLE: Thermal Neutron (n,α) Studies in the Rare Earth Region

AUTHOR: Khalid Beg, M.Sc. (Punjab University, Pakistan)
F.C.T.(Liverpool, United Kingdom)

SUPERVISOR: Professor R. D. Macfarlane

NUMBER OF PAGES: xii,160

SCOPE AND CONTENTS:

Alpha decay from the thermal neutron capture states in Nd^{143}, Sm^{149}, Sm^{147}, Gd^{155} and Eu^{151} has been studied. Precise measurements of the thermal neutron (n,α) effective reaction cross sections ($\hat{\sigma}$) and the Q-values for various alpha transitions have been made. Decay schemes have been proposed and a comparison has been made in each case with those obtained by other workers. Experimental values for cross sections were compared with those calculated using the statistical model approach. From the Q-values and cross sections obtained, alpha emission reduced widths have been evaluated.

Neutron transmission experiments were made to obtain information on the spins and parities of the capture states in the case of Sm^{149}. The contribution of bound levels to the neutron capture cross section was confirmed for both Sm^{149} and Nd^{143}.

Bismillah ar-Rahman ar-Rahim.
(In the name of God, the Merciful, the Compassionate).

ACKNOWLEDGEMENTS

This work was begun at the suggestion of Dr. R. D. Macfarlane and was carried out under his direction. I feel highly indebted to Dr. Macfarlane for his keen interest, full devotion and guidance throughout the course of this research.

I would also like to express my thanks and gratitude to Dr. R. H. Tomlinson, Dr. T. J. Kennett, Dr. K. Fritze and Dr. G. W. King for their help and valuable suggestions.

I am indebted to N. S. Oakey for useful discussions and for the use of his equipment which was used in the study of Gd^{155} and Eu^{151} and the chemical effect on reaction cross section.

I am grateful to M. C. Gupta and M. A. Hakim for their help in writing the computer programme.

The staffs of the Reactor and Machine Shop have been most cooperative during all stages of the work and their help is gratefully acknowledged.

I would like to thank Mrs. Kennelly for her help in typing this thesis.

Above all, I would like to thank my wife, Nusrat, for her patience, optimism and encouragement when it was needed most.

I would also like to express my thanks to McMaster University for their financial support and the Pakistan Atomic Energy Commission for granting a leave of absence and for their continued interest in my work.

TABLE OF CONTENTS

LIST OF FIGURES

LIST OF TABLES

INTRODUCTION

(a) Scope of Thermal Neutron (n,α) Studies

The work described in this thesis deals with a study of the alpha decay properties of highly excited states of nuclei in the rare earth region populated by the capture of thermal neutrons. Alpha decay from these states is considerably enhanced relative to the ground state because of the large total energy available.

These studies in addition to their fundamental interest for the theory of alpha decay can give other useful information. For example, one can measure (n,α) reaction cross sections and obtain information on alpha-gamma branching ratios of excited states. Also, Q-values give information on atomic masses and nuclear binding energies. Further, since alpha transitions, in contrast to beta and gamma transitions are only mildly inhibited by angular momentum changes, one might expect to populate with reasonable intensity most of the low-lying states of the daughter nucleus. This process can therefore be useful in obtaining additional information on level schemes of nuclei which have been studied by beta-gamma spectroscopy. The relative population of these levels might also give information on the nature of the excited states.

The simple selection rules associated with these alpha transitions can further be used to derive information on the spins and parities of the excited states. Such studies can be complementary to the more elaborate techniques such as neutron-nuclei polarization or neutron resonance scattering for determining the spin of the capturing states in s-wave neutron capture.

Conditions for the appearance of the thermal neutron (n, α) reaction with a measurable cross section requires the consideration of two factors. Firstly, the reaction must be exothermic, that is, it must have a positive Q-value. The Q-value must be sufficiently high that the probability for the alpha particle to tunnel favourably through the Coulomb barrier be sufficiently large to compete significantly with the other possible decay modes. The probability of alpha emission from the capture state becomes increasingly small with increasing Coulomb barrier. The Coulomb barrier, in turn, depends on the atomic number, Z, of the element. Secondly, the total capture cross section must be large. This condition, as a result of an increase in the rate of capture events, enhances the possibility of alpha particle detection. The first condition is met, in general, by even-odd neutron deficient isotopes.

At present a number of examples of thermal neutron (n,α) reactions are known. Most of these are in the region of the

light elements where the Coulomb barrier is rather small and the probability of an alpha emission from the capture state is large. Often this is the major mode of decay in this region.

There are two other regions where the thermal neutron (n,α) reaction is favourable; near the 50 proton closed shell and in the rare earth region and above. These regions are of greater interest in the study of alpha decay theory compared to the low Z region because larger nuclei are involved and the concept of nuclear surface (where alpha formation is thought to occur) is more meaningful.

(b) Historical

Griffioen and Rasmussen[1] (1961) were the first to use the statistical model of the compound nucleus to predict thermal neutron (n,α) reaction cross sections for some favourable cases of the medium and medium-heavy regions. The first experimental evidence, however, came from the work of Macfarlane and Almodovar[2] (1962) at Berkeley, California and independently of Cheifetz, Gilat, Yavin and Cohen[3] (1962) in Israel on Sm^{149}. These researchers observed two distinct alpha groups in the energy spectrum obtained when Sm^{149} was irradiated by thermal neutrons. These alpha groups correspond to alpha transitions from the capture state of Sm^{150} compound nucleus to the ground and first excited states of the daughter

nucleus, Nd^{146}. Despite the higher energy available, the ground state transition was the less intense of the two.

The Israeli group, in addition, observed the thermal neutron (n,α) reactions in Sm^{147} and Nd^{143}. They obtained negative results for Nd^{145}, Gd^{155} and Gd^{157}. The results of Sm^{147} were very similar to those of Sm^{149}. Again, in this case the alpha particle energy spectrum was dominated by two well-defined groups corresponding to alpha transitions to the ground and first excited states of Nd^{144}. For Nd^{143}, only the transition to the ground state of Ce^{140} was observed.

Cresswell and Roy[4] (1962), using natural platinum targets, obtained evidence for thermal neutron (n,α) reactions. They observed three alpha groups and identified them as those resulting from Pt^{193}, Pt^{194} and Pt^{195} leading in each case to the ground state of the corresponding osmium isotopes.

Since 1962, considerable interest has developed in studying various aspects of the thermal neutron (n,α) reaction in several laboratories. Andreev and Sirotkin[5] (1965), have conducted a survey study of (n,α) reactions throughout the rare earth region and above. In addition to confirming the observations reported in references 2 and 3 they reported the existence of the (n,α) reaction in Eu^{151}. Some qualitative information about fine structure was also obtained by these workers in the alpha spectra of Nd^{143} and Sm^{149}. Ceulemans, Poortmans and coworkers[6,7] at Mol, Belgium, Kvitek and Popov[8] at Dubna, USSR and Dakowski et al[9] at

Warsaw, Poland have studied the spin and parity of the capture state of Sm^{150} to explain the ground state transition to Nd^{146}. Kvitek and Popov[10,11] have further extended their investigations to neodymium and samarium isotopes. Oakey and Macfarlane[12] have recently published a detailed study of fine structure in $Sm^{149}(n,\alpha)Nd^{146}$ reaction. The thermal neutron (n,α) reaction has also been reported recently in Te^{123} by Cheifetz and co-workers[13].

(c) Nature of Present Work

The present work was undertaken in 1963 with a view to making a thorough and detailed study on the thermal neutron (n,α) reaction for Sm^{147}, Sm^{149} and Nd^{143} with improved experimental techniques and to extend this work if possible to Gd^{155} and Eu^{151}. These nuclides provide interesting cases for study in the rare earth region. Because of the large thermal neutron capture cross sections and high Q-values (~8-10 MeV) they are the most favourable cases. The work undertaken has the following main objectives:

(i) To obtain precise values on the thermal neutron (n,α) reaction cross sections and compare these with those calculated using the statistical model.

(ii) To determine, accurately, the Q-values for (n,α) reactions and to compare them with those obtained from mass data.

(iii) To evaluate alpha emission reduced widths for the capture state transitions.

(iv) To obtain information on transitions to the excited states of the daughter nuclei.

(v) To obtain information on the spins and parities of the capturing states.

Chapter I contains a brief outline of the relevant alpha decay theory. Also included in this chapter is a review of the pertinent aspects of s-wave neutron capture. Chapter II contains a brief outline of the theory of measurement of effective (n,α) reaction cross sections. The details of the experimental set-up and the general discussion of the techniques used are given in Chapter III. Chapter IV contains a summary of the final results and their discussion. Chapter V has been devoted to a comparative study between experiment and theory. Chapter VI deals with a study of chemical effects on the reaction rate of the $Sm^{149}(n,\alpha)Nd^{146}$ reaction.

CHAPTER I

THEORY

(a) Alpha Decay and Alpha Clustering

The failure of classical mechanics to explain alpha emission in an alpha decay process led Gamow[14] and independently Condon and Gurney[15] in 1928 to adopt the quantum mechanical approach. Classically, an alpha particle confined to the interior of the decaying system can be emitted only if its energy exceeds the potential barrier height. Quantum mechanically, however, the Gamow-Condon-Gurney theory showed that there exists a small but finite probability that an alpha particle can penetrate through the potential barrier. According to this theory a pre-existing alpha particle is treated as a wave and its propagation through a potential barrier can be treated by solving the wave equation for the alpha particle of disintegration energy Q_{Eff}. If the barrier is assumed isotropic and the alpha wave involved be taken as having zero angular momentum (s-wave) the problem can be simplified. The wave equation can then be set in one dimensional form. The probability distribution for the alpha particle does not go to zero at the wall of the potential barrier but decreases sharply outside the radial distance R_i (see fig.1.1). By applying the boundary conditions that the wave function and its first derivative must be continuous at

Fig. 1.1. Potential energy of an s-wave alpha particle as a function of distance, r, from the centre of the nucleus. The solid curve represents the idealized potential energy. The dashed curve represents a more realistic rounded potential. Region I (Interior of Nucleus); potential energy in this region is less than alpha particle energy. Region II (Barrier Region); potential energy in this region is greater than alpha energy and $R_t > r > R_i$. Region III (Outer Region); potential energy in this region is less than alpha energy and $r > R_t$.

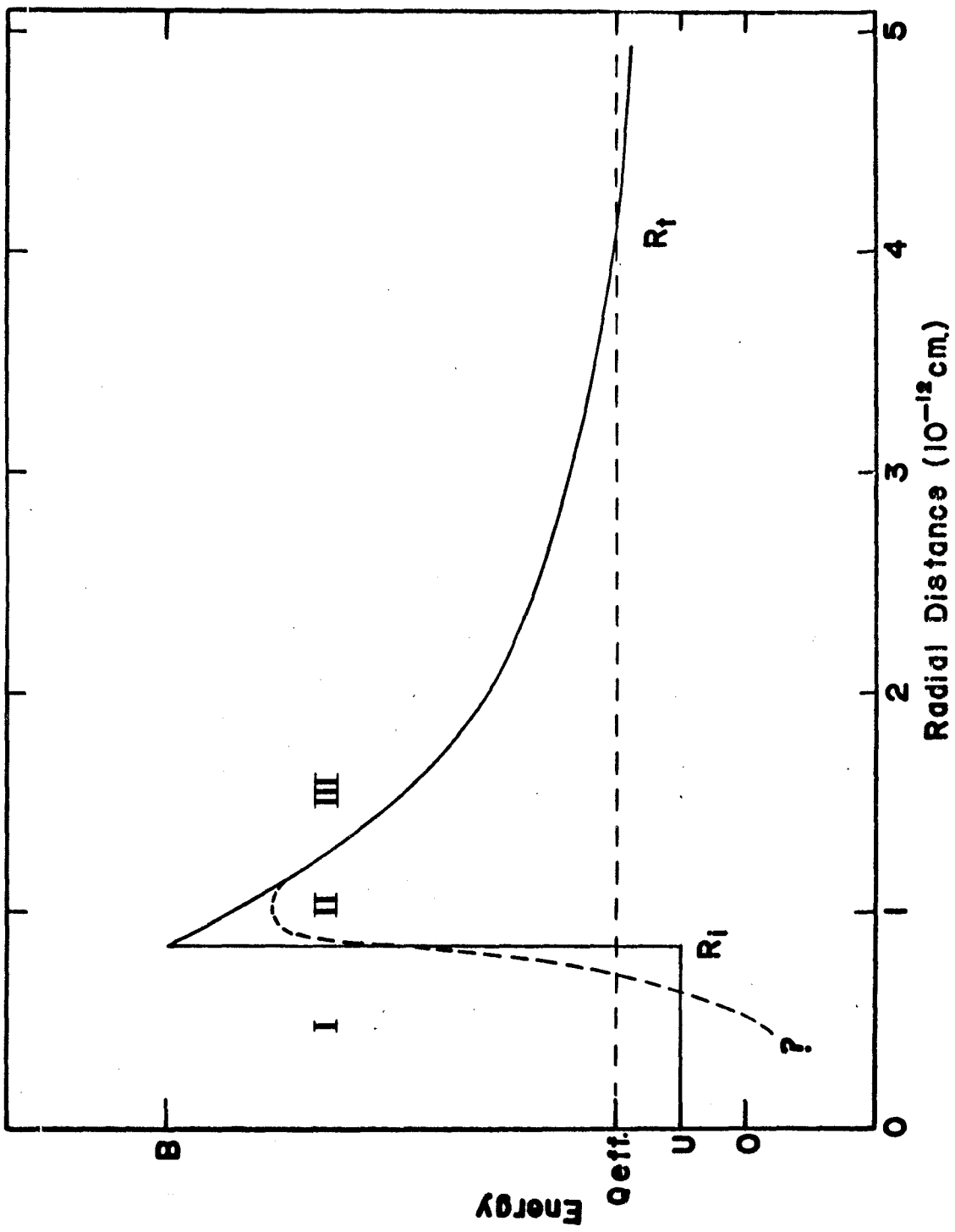
B
Qeff.
U
O
Energy
0
1
2
3
4
5
Radial Distance (10^{-12}cm.)
I
II
III
R_i
R_f
?

R_i and R_t one can solve the wave equation for the region between R_i and R_t, that is, inside the barrier where the potential energy is greater than the total alpha energy, Q_{eff}. A complete solution of the wave equation in the barrier and the interior regions can be obtained by the application of the WKB method[16].

The decay constant, λ, will be a simple product of two factors f and P. The factor f is related to the number of collisions per second which an alpha particle undergoes against the barrier wall; it is often called the frequency factor. Its order of magnitude is given by $v/2R_i$ where v is the velocity of the alpha particle. The factor P is the quantum mechanical penetration factor which accounts for the exponential dependence of the decay constant on energy. Using the WKB method[16] it can be obtained by the following expression.

$$P = \text{Exp}\left[-\frac{(8M)^{\frac{1}{2}}}{\hbar}\int_{R_i}^{R_t}(U(r) - Q_{Eff})^{\frac{1}{2}}dr\right] \qquad (1.1)$$

where R_i and R_t are the inner and outer turning points. Here $M = \frac{M_\alpha M_r}{M_\alpha + M_r}$ is the reduced mass of the system. U(r) is the potential barrier which is given by $U(r) = \frac{2Ze^2}{r}$; Ze being the charge of the daughter nucleus. Q_{Eff} is the total decay energy which is the sum of the alpha particle energy plus electron screening corrections[17], $E_{Sc} = (65.3(Z+2)^{7/2} - 80(Z+2)^{2/5}\text{eV})$

plus the recoil energy, $E_{rec} = \frac{E_\alpha M_\alpha}{M_r}$. It is clear from the above expression that the probability of penetration decreases with an increasing value of the integral in the exponent, that is, with increasing barrier height and width.

This simple one body theory of alpha decay has some limitations when more detailed aspects of the alpha decay problem are considered. The model assumes the pre-existence of the alpha particle in the nucleus whereas intra-nuclear alpha particle formation is now known to be quite a complex process.

Bethe[18], as early as 1937 pointed out that the alpha particle should not be thought of as existing independently within the nucleus a large fraction of time. It is only in recent years that this problem has received some serious study and numerous methods have been proposed for studying the effective alpha particle densities in nuclei.

Winslow[19] (1954) assumed that the alpha particle exists only in a narrow region on the nuclear surface and he proposed a surface-well potential with a repulsive potential in the interior. The decay probability obtained by him on applying a one body treatment to this system was higher than expected from the traditional one body model. He explained this by introducing a many body concept of an equilibrium between the nuclear configuration with the alpha particle in the surface well and the configuration with none in the well

but with constituent nucleons moving individually within the nucleus. The ratio of the probability of the former configuration to the total of configurations is designated as the formation factor. Winslow thus separated the decay probability into two factors, 'Formation factor' and 'Penetration factor'.

Brussaard and Tolhoek [20] (1958) formalized the problem of alpha particle formation at the nuclear surface by applying the shell model. They suggested that if the four nucleons, at the nuclear surface, are within a sphere of radius equivalent to that of an alpha particle, and, if the two neutrons and two protons are in singlet states they may be regarded as travelling together as an alpha particle. A pictorial representation of alpha clustering is given in fig. 2.1.

Mang[21-26] has made the most detailed theoretical study of the problem of alpha decay. He, too, adopted the shell model approach and developed a general expression for the calculation of the alpha decay constant, λ, which has the following form

$$\lambda = \frac{1}{\hbar} \sum_{j,\ell} P_\ell(E)\ \delta^2_{Jj\ell} \qquad (1.2)$$

where $P_\ell(E)$ is the penetrability factor for an alpha particle of energy, E, and an angular momentum ℓ. The $\delta^2_{Jj\ell}$ is a reduced width for the transition from state J to state j with the emis-

Fig. 1.2. Schematic diagram showing last Nilsson states to be filled in a spheroidal nucleus. Favoured alpha particle emission occurs when the encircled states are involved in alpha particle formation. For odd-A nuclei an unfavoured transition occurs if the alpha particle is formed from the nucleons 1,2,3,5.

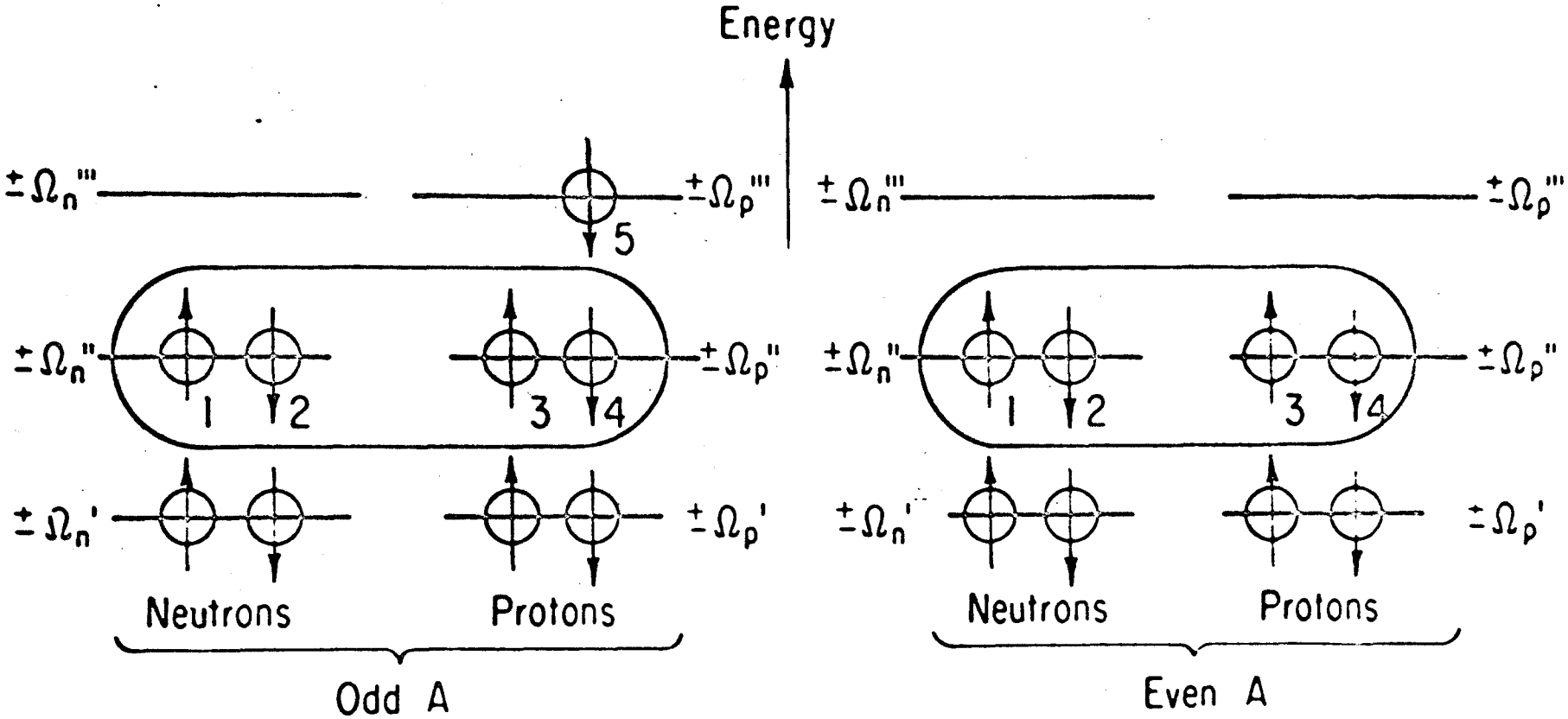
Energy
±Ωn'''
±Ωp'''
5
±Ωn''
±Ωp''
1
2
3
4
±Ωn'
±Ωp'
Neutrons
Protons
Odd A
±Ωn'''
±Ωp'''
±Ωn''
±Ωp''
1
2
3
4
±Ωn'
±Ωp'
Neutrons
Protons
Even A

sion of an alpha particle that has an angular momentum of $\ell\hbar$ units. This expression indicates that the alpha decay constants can be expressed as a sum of partial transition probabilities (the sum over all j and ℓ values). These partial transition probabilities consist of two factors. One represents the probability of formation of an alpha particle in the nuclear surface region, $\delta^2_{Jj\ell}$, the other represents the probability of penetration through the Coulomb barrier.

One of the important recent contributions to this study has been the attempt to determine experimentally the form of the alpha-nuclear interaction potential by measuring total alpha reaction cross sections and using the results to obtain the parameters of an optical model potential. This potential can be written as the sum of a real part and an imaginary part. The real part is involved in elastic scattering processes whereas the imaginary part takes account of the absorption of alpha particles. The best data for these potentials has been obtained by Igo[27] from an analysis of alpha particle scattering results, mostly in the region of 40 MeV. The real part is hoped to be close to the true potential seen by an alpha particle as it leaves the nucleus. This nuclear potential to which must be added the Coulomb and the centrifugal potential is:

$$V(r) = -1100\ \mathrm{Exp}\left[\frac{1.17A^{1/3} - r}{0.574}\right]\ (\mathrm{MeV}) \qquad (1.3)$$

where r is distance in fermis from the center of the daughter nucleus. This expression is valid in the region in which $V(r) \lesssim 10$ MeV and yields a potential barrier with a fairly sharp inner slope. When this potential is used in calculations of the alpha decay rate, it is possible to obtain a more complete separation of barrier transmission effects (which depend upon the form of the nuclear potential) from the alpha particle formation probability. The effect of the latter appears in the expression for the reduced width which Rasmussen[28] defined as:

$$\delta^2 = \frac{\lambda}{P} h \quad . \tag{1.4}$$

The symbol h, is Planck's constant and P is the penetrability as defined in equation (1.1). In this case, however, U(r) is replaced by V given by

$$V = [V(r) + \frac{2Ze^2}{r} + \frac{\hbar^2}{2Mr^2} \ell(\ell + 1)] \quad . \tag{1.5}$$

The symbol, ℓ, represents the angular momentum quantum number of the outgoing alpha particle and $\hbar = \frac{h}{2\pi}$. In equation 1.4, $\frac{\lambda}{P}$ represents the hypothetical decay rate in the absence of a barrier and is related to the alpha formation factor.

Rasmussen[28] has determined δ^2 for a number of heavy element alpha emitters and has obtained values in the neighbourhood of 0.1 MeV. Wilkinson[29] has pointed out that these values are orders of magnitude larger than one would expect if

nucleons were freely moving about within the nucleus independently of each other. This implies that there is a definite tendency for nucleons to cluster into aggregates, sometimes alpha particles. Poggenburg[30] has recently given an argument in favour of using a Woods-Saxon[31] type potential in place of the Igo potential for calculating the penetration factor, P. This potential can be represented as

$$V(r) = -74/\{1 + \exp(\frac{r-1.17A^{1/3}-1.6}{a})\} \quad . \qquad (1.6)$$

The symbol 'a' represents the surface diffuseness parameter. Use of this potential gives penetrability factors which are 34 to 48% lower than corresponding calculations made with Igo potential and consequently increasing the value of reduced widths. This results from a general thickening of the barrier with an inward shift of the inner turning point when the steep slope of the Igo potential is replaced by a more gradual slope of the Woods-Saxon form.

In the proposed research a study has been made of alpha decay from excited states of nuclei formed by thermal neutron capture. It is hoped that some useful information will be obtained from this study concerning alpha clustering within the nucleus. For the case of thermal neutron capture, it is possible to obtain a measure of δ^2 for the capture state if the width of the capturing state is known and the capture cross section and (n,α) reaction cross sections have been measured.

(b) Slow Neutron Resonances and Alpha Decay From Thermal Neutron Capture States .

When a thermal neutron interacts with a nucleus ${}_{Z}X^{A}$ belonging to the heavy region, the reaction is best described on the basis of the compound nucleus formation mechanism. According to this mechanism which was originally proposed by Bohr[32] (1936) a nuclear reaction may be considered as a two step process. In the first step there is a quick amalgamation of the incident neutron and the target nucleus to form a compound nucleus. In this process the energy of the incoming neutron is quickly shared among all the nucleons and the neutron loses its identity. The compound nucleus in this state, often called the capture state, constitutes a highly excited system having excitation energy $E_c=E_b+E$ where E_b is the binding energy (~ 6-10 MeV) and E is the kinetic energy of the absorbed neutron. For a target nucleus in the rare earth region the compound nucleus will usually have a high density of states at the energy of excitation. If E_c happens to coincide with an excited state of appropriate spin and parity, the probability for forming the compound nucleus is large and a resonance occurs in the neutron cross section at the corresponding kinetic energy, E. Such sharp resonances correspond to virtual levels in the compound nucleus. In the second step which may occur

within ~ 10^{-16} seconds[33] subsequent to its formation, the compound system loses its excitation energy in a variety of ways. It may emit a neutron, with a probability per unit time, $\Gamma_n/\hbar$, leaving the nucleus ${}_ZX^A$ in its ground state or it may emit electromagnetic radiations with a probability per unit time, $\Gamma_\gamma/\hbar$, leaving the nucleus ${}_ZX^{A+1}$ in its various bound states. Alpha particles may also be emitted from the compound system with a probability per unit time, $\Gamma_\alpha/\hbar$, to yield a nucleus ${}_{Z-2}X^{A-3}$ but due to Coulomb barrier effects this mode of decay is usually negligibly small. However, in some cases such as those selected for the present investigations, where alpha emission from the compound nucleus is exothermic by several MeV, this mode of decay may be detectable. The total probability per unit time, $\Gamma/\hbar$, for the decay of the compound nucleus is then given by

$$\Gamma/\hbar = \Gamma_n/\hbar + \Gamma_\gamma/\hbar + \Gamma_\alpha/\hbar + \text{----} \quad . \qquad (1.7)$$

According to the two step view of the nuclear reaction the cross section $\sigma(n,x)$ can be expressed as:

$$\sigma(n,x) = \sigma_c(n) \cdot \Gamma_x/\Gamma \qquad (1.8)$$

where the terms $\sigma_c(n)$ and Γ_x/Γ correspond to the cross section for the formation of the compound nucleus and the relative probability of emission for x respectively. In the particularly important case of resonance processes the cross section as a function of neutron energy, in terms of the levels parameters

as maximum cross section, neutron and radiation widths, is given by the Breit-Wigner[34] dispersion formula. The formula for an isolated resonance, in which the effect of all other neighbouring levels is neglected, is almost always sufficiently accurate in practice and is given as:

$$\sigma(n,x) = \frac{\lambda^2}{4\pi} g \frac{\Gamma_n \Gamma_x}{(E-E_o)^2+(\Gamma/2)^2} \qquad (1.9)$$

where λ = wavelength of the neutron at a neutron energy E,

E_o = neutron energy at resonance,

Γ_n = partial width for neutron emission ,

Γ_x = partial width for emission of x,

Γ = full width of resonance at half maximum,

$g = (2J+1)/(2I+1)(2S+1)$,

J = spin of the resonance,

I = spin of the target nucleus,

S = spin of the neutron $(\frac{1}{2})$,

Equation (1.9) is obviously a combination of three factors. The first factor which corresponds to the compound nucleus formation probability is proportional to λ^2. The second factor,

$$\frac{1}{(E-E_o)^2 + (\frac{\Gamma}{2})^2} ,$$

is called 'resonance factor' and has its largest value when $E = E_o$. For all other values of E this factor and hence the

cross section decreases. The third factor is the probability for specific types of decay of the compound nucleus and is expressed by the partial widths Γ_n, Γ_x. If $E_o >> E$, so that variation of the E does not greatly affect the resonance factor then the cross section approaches the well-known '1/v' law.

Implicit in the form of equation (1.9) is the assumption that only neutrons with $\ell=0$ (s-wave) may interact with appreciable cross section. This assumption is certainly valid for nuclei and neutron energies considered in this work. The ratio of the strength of resonances having $\ell=1$ (p-wave) to those having $\ell=0$ (s-wave) is of the order of 10^{-6} at energies of the order of 1 eV[35]. It is therefore valid to consider only $\ell=0$ (s-wave) resonances at thermal energies. As a consequence, the spins of the observed resonances are restricted to

$$J = I \pm \frac{1}{2} \qquad (1.10)$$

and the parity of the resonances is the same as that of the ground state of the target nucleus.

The two step concept of the compound nucleus, discussed earlier, was used by Weisskopf and coworkers[36] to develop a schematic theory of nuclear reactions. Using this theory it is possible to establish an order of magnitude value of the reaction cross section for any particular mode

of decay. In the remaining part of this section we will show how this theory can be used to evaluate the reaction cross section for the thermal neutron (n,x) reaction where x is a charged particle.

In a special case where the most predominant mode of decay is gamma emission, one can to a good approximation, replace $\sigma_c(n)$, the cross section for the formation of the compound nucleus and Γ, the total width of the resonance by the (n,γ) reaction cross section and the partial gamma width, Γ_γ, respectively. The equation (1.8) then becomes

$$\sigma(n,x) = \sigma(n,\gamma).\frac{\Gamma_x}{\Gamma_\gamma} . \qquad (1.11)$$

If $\sigma(n,\gamma)$ and the partial gamma width, Γ_γ, are known, $\sigma(n,x)$ can be evaluated provided the partial width for the emission of particle x can be calculated theoretically.

The Weisskopf[36] theory assumes that a nucleus is a sphere with radius R, $(R = r_o A^{1/3})$, which has a sharp and well-defined surface. When a neutron penetrates the nuclear surface, it finds itself suddenly in a region where its kinetic energy changes from E to $E' = E+\varepsilon$, where ε is the average kinetic energy of a nucleon inside the nucleus. Such a sudden change of kinetic energy results in a reflection of the neutron wave. The probability for penetration of the surface is given by

$$P_n = \frac{4k_n K_n}{(k_n+K_n)^2} \qquad (1.12)$$

where k_n and K_n are the wave numbers associated with the

neutron outside and inside the nucleus respectively.

$$k_n^2 = \frac{2ME}{\hbar^2} = \frac{1}{\lambda^2} \cdot$$

$$K_n^2 = \frac{2M(E+\epsilon)}{\hbar^2} = k_n^2 + K_o^2; \qquad K_o^2 = \frac{2M\epsilon}{\hbar^2} \cdot$$

The value of ϵ can be computed by applying Fermi-Dirac statistics. Segre[37] has obtained a value of ~20 MeV for $R = 1.5 \times 10^{-13} A^{1/3}$ cm. This gives a value for $K_o \cong 1 \times 10^{13}$ cm^{-1}. For slow neutrons $k_n << K_n \cong K_o$, hence equation (1.12) becomes

$$P_n = \frac{4k_n}{K_o} \cdot \qquad (1.13)$$

P_n is less than 1 because $K_o >> k_n$. A similar expression is valid for any particle. However, in the case of a charged particle this has to be multiplied by a factor G_x (Gamow factor) which takes into account the penetration of the Coulomb barrier (in the case of neutron emission this factor is unity). Therefore P_x is given by

$$P_x = \frac{4k_n}{K_o} G_x \cdot \qquad (1.14)$$

Since at the time of the formation of the compound nucleus, the excitation energy is quickly shared among many particles, the possibility of emission of the particle x depends on the concentration of sufficient energy on a single particle to allow its escape. Let T_x be the average time between such arrangements of the nuclear constituents as would permit the emission of particle,x. The frequency of emission of x

is given by the product of such favourable configurations, $1/T_x$, and the probability P_x that the particle x, given the required amount of energy can penetrate through the potential barrier

$$\Gamma_x/\hbar = P_x/T_x$$

or

$$\Gamma_x = (\hbar P_x)/T_x \qquad (1.15)$$

Weisskopf[36], on the assumption that energy levels of the compound nucleus are equally spaced showed that the periodicity, T_x, is given by

$$T_x = (2\pi\hbar)/D_x \qquad (1.16)$$

where D_x is the level spacing. When this value of T_x is substituted in equation (1.15) the expression for the partial width of x is reduced to a simpler form given by equation (1.17).

$$\Gamma_x = \frac{P_x D_x}{2\pi} \qquad (1.17)$$

Since, P_x can be evaluated by using the expression given in equation (1.1) with U(r) replaced by a more realistic form of potential such as one given in equation (1.5), Γ_x can be calculated if the value for D_x is known.

At the excitation energies of the order of the binding energy of the neutron, D_x can be taken equal to D_n where the subscript 'n' corresponds to neutron. In the literature D_n is c ten represented simply by D and its value can be determined either

experimentally from the analysis of the neutron excitation-function data[38] or can be calculated from an expression for Γ_n analogous to equation (1.17) as shown in equation (1.18).

$$\Gamma_n = (P_n D_n)/2\pi \qquad (1.18)$$

Γ_n and P_n in this equation can be substituted from equations (1.9) and (1.13) respectively.

(c) Spin and Parity of the Capturing State

The parity and the total angular momentum and its projection along an axis, should be the same for the final system as for the initial parent nucleus. Since the alpha particle is spinless and has even parity, the selection rules take an especially simple form. The orbital angular momentum of alpha decay is restricted to values between the sum and differences of initial and final spin.

$$|I_i - I_f| \leq \ell \leq |I_i + I_f| \qquad (1.19)$$

If the parity of the parent and daughter are the same only even values of ℓ are permitted; if opposite, then, only odd values of ℓ are permitted.

Although results obtained from the thermal neutron (n,α) reaction can not give directly the spin and parity of the capturing state it is often possible to distinguish between two possibilities. If the spin and parity of an even-odd target nucleus are J and π, the s-wave capturing state has spin $J \pm \frac{1}{2}$ and parity π. Since alpha decay proceeds

to an even-even nucleus whose ground state spin and parity are 0^+, one of the states $J + \frac{1}{2}$ or $J - \frac{1}{2}$ can not populate the ground state. Depending on whether alpha particles corresponding to the ground state are observed, the spin and parity of the capturing state can be deduced. If both $J + \frac{1}{2}$ and $J - \frac{1}{2}$ states contribute to the capture cross section, the contribution of both can be measured from the relative intensity of certain groups in the alpha particle spectrum.

A considerable effort is being put forth in other laboratories in the determination of the spin of neutron capture resonances by techniques such as those involving the transmission of polarized neutrons through aligned target nuclei or neutron resonance scattering techniques. A knowledge of the spins of these resonances is an important contribution to our understanding of the distribution of spins of excited states which has an effect on many nuclear processes. Results obtained in the course of this investigation have yielded information on the spin and parity of the capture states and have augmented the results of neutron polarization studies.

CHAPTER II

THEORY OF MEASUREMENTS

In this section the definitions of the various terms appearing in the section on 'Experimental Measurements' are introduced. In addition, a brief outline of the theory involved in the estimation of the effective neutron cross section has been included. The discussion has been, however, confined to reaction rates rather than those involving scattering or diffusion.

(a) Definition of Cross Section and Flux

Cross section is a quantity having the dimension of area (cm^2) which is used to describe quantitatively the rates of nuclear reactions. In a general way it can be defined by means of the equation

$$R = \sigma\phi \qquad (2.1)$$

where R is the rate of a particular reaction per unit atom irradiated

σ is the cross section (cm^2) for the reaction under study

ϕ is the flux (neutrons/cm^2/sec.) It is defined as the product of the neutron density, n(neutrons/cm^3) and the neutron velocity, v(cm/sec). If N is the total number of target atoms then the total rate of reaction,

R_T can be expressed as

$$R_T = N\sigma\phi \qquad (2.2)$$

(b) Variation of Flux with Energy

In a reactor the situation is, however, far more complex than implied in the simple definition given above. The cross section varies markedly with neutron energy. The reactor neutrons have a wide spread of energy from several MeV for the unmoderated fission neutrons down to a fraction of an eV for the neutrons in thermal equilibrium with the moderator. The typical energy dependence of σ shows a low energy region in which σ is at least approximately inversely proportional to neutron velocity and a high energy region with marked resonance structure. Some isotopes show good '1/v' or $(1/E^{\frac{1}{2}})$ dependence over all energies; others do not show this dependence even at low energies.

In cases where the '1/v' law applies, the situation is comparatively very simple. The cross section can be written in the form

$$\sigma = \sigma_o/v \qquad (2.3)$$

where σ_o is a constant representing the value of the cross section at unit velocity. When this value of σ is substituted in equation (2.2) after replacing ϕ by nv, this equation reduces to

$$R_T = N\sigma_o n \qquad (2.4)$$

which indicates that the rate is independent of neutron

velocity and depends only on N, σ_o, and the neutron density, n. It is not even necessary to know the cross section at unit velocity. Measurements are usually made relative to the known cross section of a standard (monitor). If the standard also has a '1/v' response, then if one uses the value of the cross section for the monitor at any chosen neutron velocity one can obtain the cross section for the unknown at the same neutron velocity. Thus in a more general form equation (2.3) can be written as

$$\sigma(v) = (\sigma_o v_o)/v \qquad (2.5)$$

where v_o represents some standard velocity and σ_o is now the cross section at that velocity. The equation for the total reaction rate then becomes

$$R_T = N\sigma_o v_o n \, . \qquad (2.6)$$

By convention v_o is taken as 2200 m/sec.

In treating the more general case where the '1/v' law does not apply, the theoretical approach is to consider the reactor neutron spectrum as consisting of two independent spectra. These are referred to as 'the thermal' and 'the epithermal' constituents of the spectrum.

The Thermal Spectrum

The thermal component is represented by a Maxwellian distribution which can be expressed in terms of energy as:

$$n(E)dE = \frac{2\pi n}{(\pi kT)^{3/2}} e^{-E/kT} E^{1/2} dE \qquad (2.7)$$

where $n(E)dE$ is the number of neutrons per cm^3 having energies between E(eV) and E + dE(eV).

n is the number of neutrons per unit volume (cm^3)

k is the Boltzmann constant (8.6166×10^{-5} eV/degree K)

T is the characteristic temperature of the distribution in degrees Kelvin.

This distribution would be valid if the neutrons were in thermal equilibrium with the moderator at some characteristic temperature, T. In using this distribution, one assumes that the moderator is a non-capturing medium, that neutron leakage is negligible and that the temperature T is the temperature of the neutrons in thermal equilibrium with the moderator. The peak of the distribution of the neutron energy spectrum occurs at an energy equal to kT. If this energy is taken as that corresponding to a neutron velocity of 2200 m/sec, then neutrons at the peak of the distribution have the following properties[39].

Neutron Energy 0.025298 eV

Temperature $293.59(7) \pm 0.01(4) K^{\circ}$

The Epithermal Spectrum

According to simple neutron diffusion theory the energies of neutrons which are being slowed down by collisions with a non-capturing medium (moderator) have a dE/E distribution, that is, the flux of neutrons in a unit energy interval dE is proportional to $1/E$ or $1/v^2$. The low

energy end of the epithermal component overlaps the thermal region. In treating the spectrum analytically a lower energy cut off is suitably chosen. The low energy cut off for the epithermal region is given by μkT. The parameter, μ, is chosen to give the best approximation to the true reactor spectrum.

(c) Effective Cross Section

Having defined the thermal and the epithermal spectra we can now proceed to describe the effective rate of reaction which is the sum of the rates from neutrons in the thermal and the epithermal regions. This treatment was developed by Westcott[40-42] and independently by Freemantle and Campbell[43]. No attempt will be made to go into the mathematical details of this treatment. Only its application to our study will be discussed here.

According to this convention a quantity 'r' is introduced which measures the relative intensities of the thermal and the epithermal components. The departure of the cross section from true '1/v' dependence is taken into account by the factors g and s; g applying to the thermal region and s to the epithermal region. These factors are contained in the effective cross section, $\hat{\sigma}$, which is defined by the equation

$$R_T = N\hat{\sigma}nv_o \cdot \qquad (2.8)$$

The quantity, n, is the total density of neutron of all energies, v_o is 2200 m/sec and R_T is the rate as discussed previously. The quantity nv_o is called the conventional flux or 2200 m/sec flux. It is the flux if all the neutrons had a velocity of 2200 m/sec. The effective cross section, $\hat{\sigma}$, can be expressed by the following relationship

$$\hat{\sigma} = \sigma_o(g + rs) \quad . \qquad (2.9)$$

The quantity, σ_o, is the 2200 m/sec cross section discussed above. The factor r, the epithermal index, is the same as defined above. This factor is characteristic of the neutron spectrum in the vicinity of the irradiation sample. For a pure Maxwellian spectrum, r = 0. The parameters, g and s , are factors which depend upon the departure of the cross section from '1/v' dependence in the thermal and the epithermal regions respectively. These factors are properties of the target nuclei. If the cross section for the nuclide of interest has a '1/v' response for neutrons in the thermal (Maxwellian) region but not for the epithermal region, then g = 1 and s ≠ 0. If the response is not '1/v' even at thermal energies, then g ≠ 1 and s ≠ 0. The effective cross section in a pure Maxwellian flux is therefore given by the product $g\sigma_o$. The factor, s, is defined by the equation

$$s = \frac{1}{\sigma_o} \left(\frac{4T}{\pi T_o}\right)^{\frac{1}{2}} \int_{E_1}^{\infty} \left[\sigma(E) - \frac{g\sigma_o v_o}{v}\right] \frac{dE}{E} \qquad (2.10)$$

where T is the characteristic temperature, T_o=293.6°K . The quantity $\sigma(E)$ represents the excitation function. E_1 is the low energy cut-off. In cases where the neutron temperature is not available a temperature independent factor s_o is introduced such that

$$s_o = s(T_o/T)^{\frac{1}{2}} \qquad (2.11)$$

where s_o is the value which 's' has when $T = T_o$. Equation (2.9) then becomes

$$\hat{\sigma} = \sigma_o\{g + r(T/T_o)^{\frac{1}{2}} \quad s_o\}. \qquad (2.12)$$

Westcott has shown that

$$s_o = \sqrt{\frac{4}{\pi}} \left(\frac{\lesssim}{\sigma_o} - \frac{4E_o}{E_{cd}}\right) \qquad (2.13)$$

where E_o is the value of kT_o which for T_o = 293.6°K is 0.025 eV. E_{cd} is the energy corresponding to the Cd cut-off, that is, 0.5 eV. σ_o is as before and $\lesssim$ is the resonance integral above the Cd cut-off to be discussed later.

Westcott has further shown that

$$r(T/T_o)^{\frac{1}{2}} \quad = \frac{1}{C(s_o+1/K)-s_o} \qquad (2.14)$$

where C is the cadmium ratio and K is a number which depends upon the thickness of cadmium used when measuring C.

(d) Cadmium Ratio and Resonance Integral

A study of the excitation function of cadmium[44] shows that the cross section increases rapidly with decreasing neutron energy in the region from 0.2 to 1.0 eV. If a sample

is irradiated inside a cadmium wrapping, only the neutrons with energies greater than about 0.5 eV can penetrate while the lower energy neutrons are absorbed by the cadmium filter. In this way one can separate the effects of thermal and epithermal neutrons. The ratio of the rate without cadmium to that with cadmium is called the cadmium ratio.

From the cadmium difference measurements the rates for the unknown and monitor with neutrons of less than 0.5 eV can be obtained. If both cross sections have a '1/v' response in this energy range the σ_o for the unknown can be directly determined relative to that of the monitor.

As far as the resonance region is concerned, there is little practical use in comparing cross sections at any given energy. A more useful quantity is the resonance integral, $\lesssim$, which for neutrons with a dE/E distribution is given by

$$\lesssim = \int_{0.5\ eV}^{\infty} \sigma(E)\ \frac{dE}{E} \ . \qquad (2.15)$$

Provided the spectrum has the assumed dE/E form above the cadmium cut-off, the rates measured with a cadmium cover will be proportional to the resonance integral evaluated from the cut-off to the maximum energy of the spectrum. Then from the cadmium covered measurements we can relate $\lesssim$ for the unknown to $\lesssim$ for this monitor.

CHAPTER III

EXPERIMENTAL

(a) Experimental Set-Up

The thermal column of the McMaster University Swimming Pool Research Reactor was used as a source for thermal neutrons. A schematic diagram of this column is shown in fig. 3.1. The graphite thermal column (21.6 cm x 21.6 cm x 376.7 cm) was divided into four equal cylindrical holes by means of a hollow lucite structure (not shown in the diagram). This structure provided facility for conducting, simultaneously, four different experiments. It also permitted easy movement of the target assemblies in and out of the column without striking the walls of the column. In addition, it served as a guide for reproducing the irradiation positions. Only one such hole was used for most of the present investigations. All other holes were kept filled with stringers of graphite. Except in the case of Gd^{155} and Eu^{151} all the measurements were conducted by irradiating the target assembly at a position in the thermal column separated from the face of the reactor core by about 1.7 meters. This position was achieved by taking out of the column one of the removable stringers. In the case of Gd^{155} and Eu^{151} the irradiations were carried out at about 0.8 meters

Fig. 3.1. A schematic diagram of the thermal column facility at McMaster Swimming Pool Research Reactor.

THERMAL COLUMN

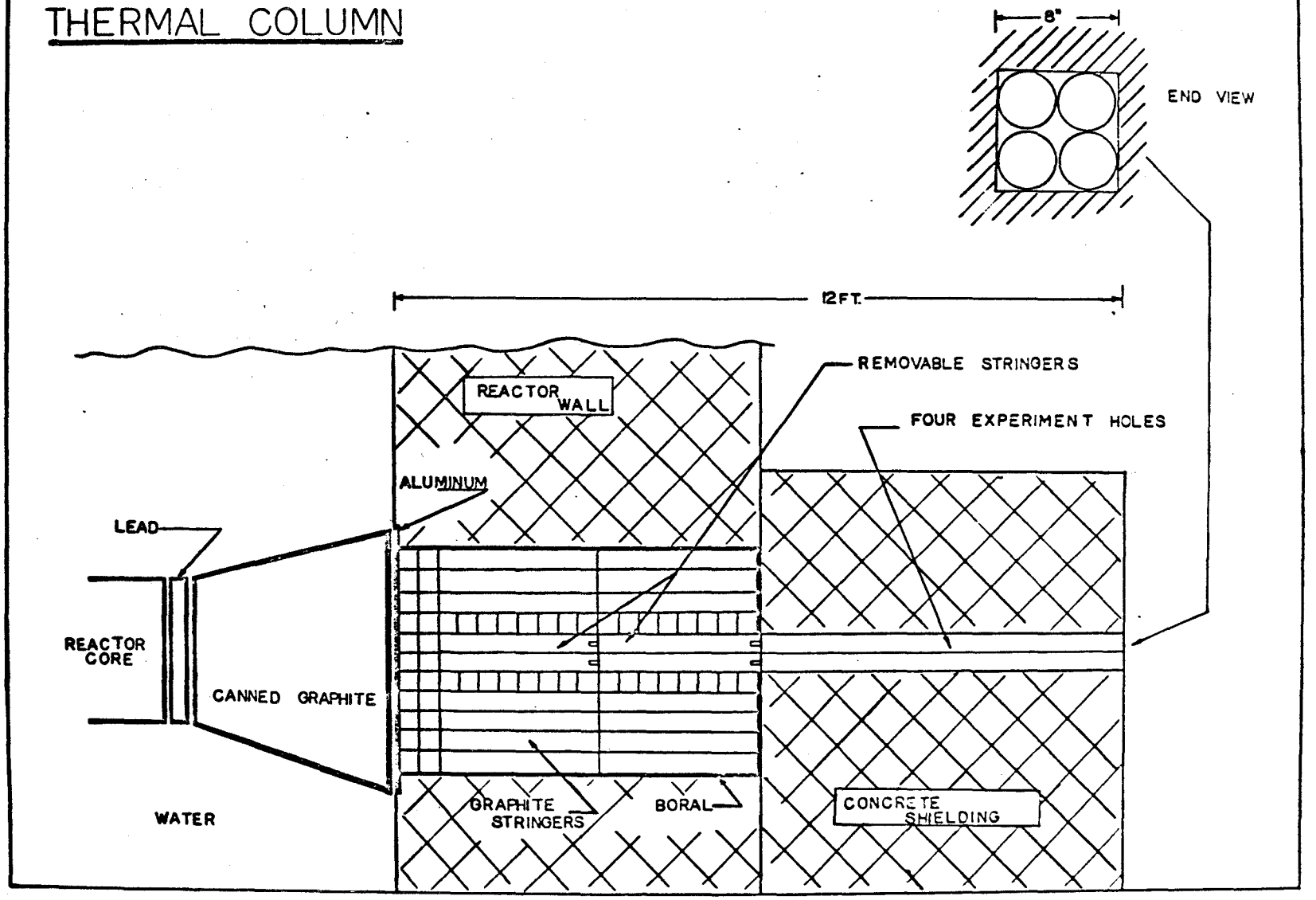

from the same position by removing both of the removable stringers. The cadmium ratio in the former position for a '1/v' detector was not measured but it should be much greater than 1000 on the basis of measurements at a similar position with the Livermore Pool Type Reactor (LPTR)[45]. In the latter position, however, the cadmium ratio was measured for an alloy of Fe-Mn-Mo (Fe = 85%, Mn = 13%, Mo = 2%) and was found to be about 100.

Most of the experimental work was done using a lucite target assembly in which the targets were mounted on a circular lucite disc fitted on the front end of this assembly. The target holder was connected to a drive shaft which extended outside the thermal column when the assembly was in its irradiation position. The drive shaft was manually driven to position different targets in front of the alpha-particle solid state detector while the reactor was in operation. All of these measurements were made under vacuum (< 1 mm Hg) with a separation of 3-6 mm between the target and the detector. The measurements in the case of Gd^{155} and Eu^{151} were, however, made by using'the electrostatic particle guide' developed by Oakey and Macfarlane[46]. This device was used at positions where the high neutron and gamma fluxes made the lucite assembly completely useless because of the fast deterioration of the

detector. The electrostatic particle guide (E.P.G.) operating at high voltages (20-40 kV) was capable of guiding the alpha particles, generated at the target, out of regions of high fluxes into one where they could be counted with improved resolution. A schematic diagram of this instrument is shown in Fig. 3.2.

The alpha particle spectra were obtained with n-type silicon gold surface barrier detectors connected to standard RIDL electronics and a 400-channel pulse-height analyzer. A schematic diagram representing this set up is shown in Fig. 3.3. The charge sensitive nuvistor preamplifier was placed adjacent to the detector for most of the experiments. In the last set of experiments involving neutron transmission measurements the preamplifier was located in the room separated by a long (~ 4.5 meters) low capacity (21.3 μμf/meter) coaxial cable (type Rg-114A/U). This improved the active lifetime of the preamplifier with very little change in resolution and noise. Any deterioration caused by the cable was compensated to a large extent by the operation of the preamplifier out of the radiation fields.

The alpha-detectors were either laboratory made or commercially available (ORTEC). Their resistivities varied between 800 and 1800 ohm-cm and their active surface area ranged from 0.3 cm^2-0.8 cm^2. They were normally operated with reverse bias voltages between 20 to 30 volts. The over

Fig. 3.2. A schematic diagram of 'The Electrostatic Particle Guide'. The target end is irradiated at a neutron flux of $\sim 10^{10}$ n/cm^2/sec. The alpha particles are guided towards the solid state detector by an electric field generated by two charged concentric cylinders, 6 meters in length with dia. 7.5 cm and 0.5 mm.

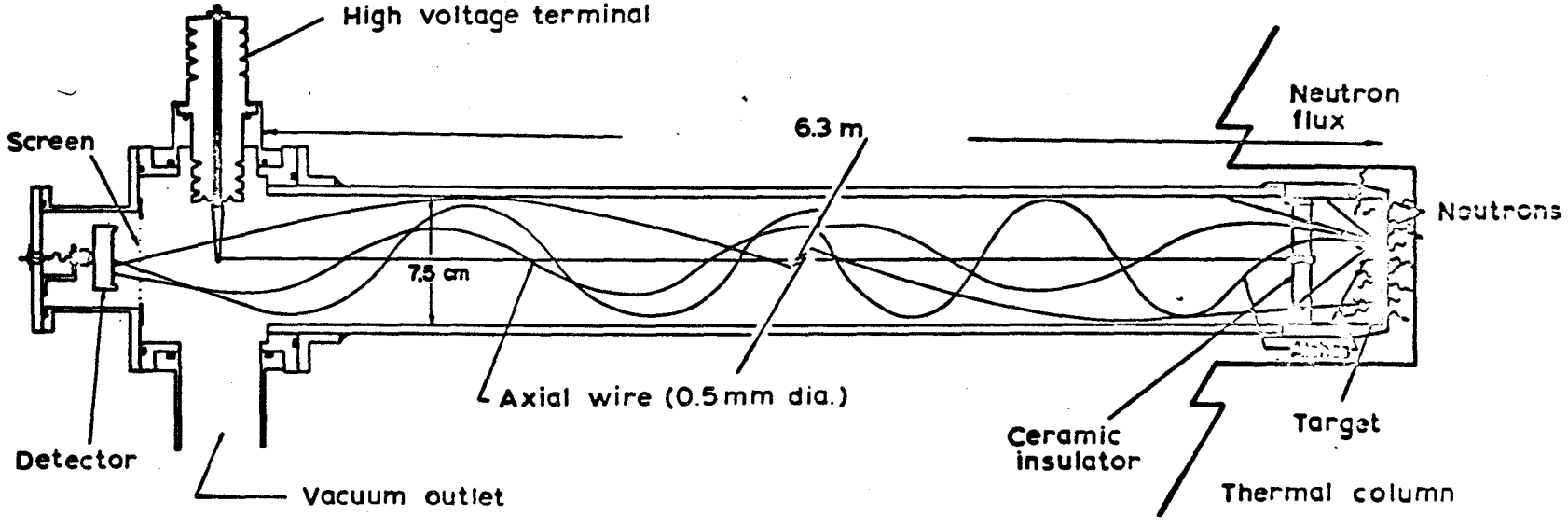
High voltage terminal
Screen
6.3 m
Neutron flux
Neutrons
7.5 cm
Axial wire (0.5mm dia.)
Detector
Vacuum outlet
Ceramic insulator
Target
Thermal column

Fig. 3.3. A schematic diagram of the lucite target assembly and the counting equipment.

TARGET ASSEMBLY

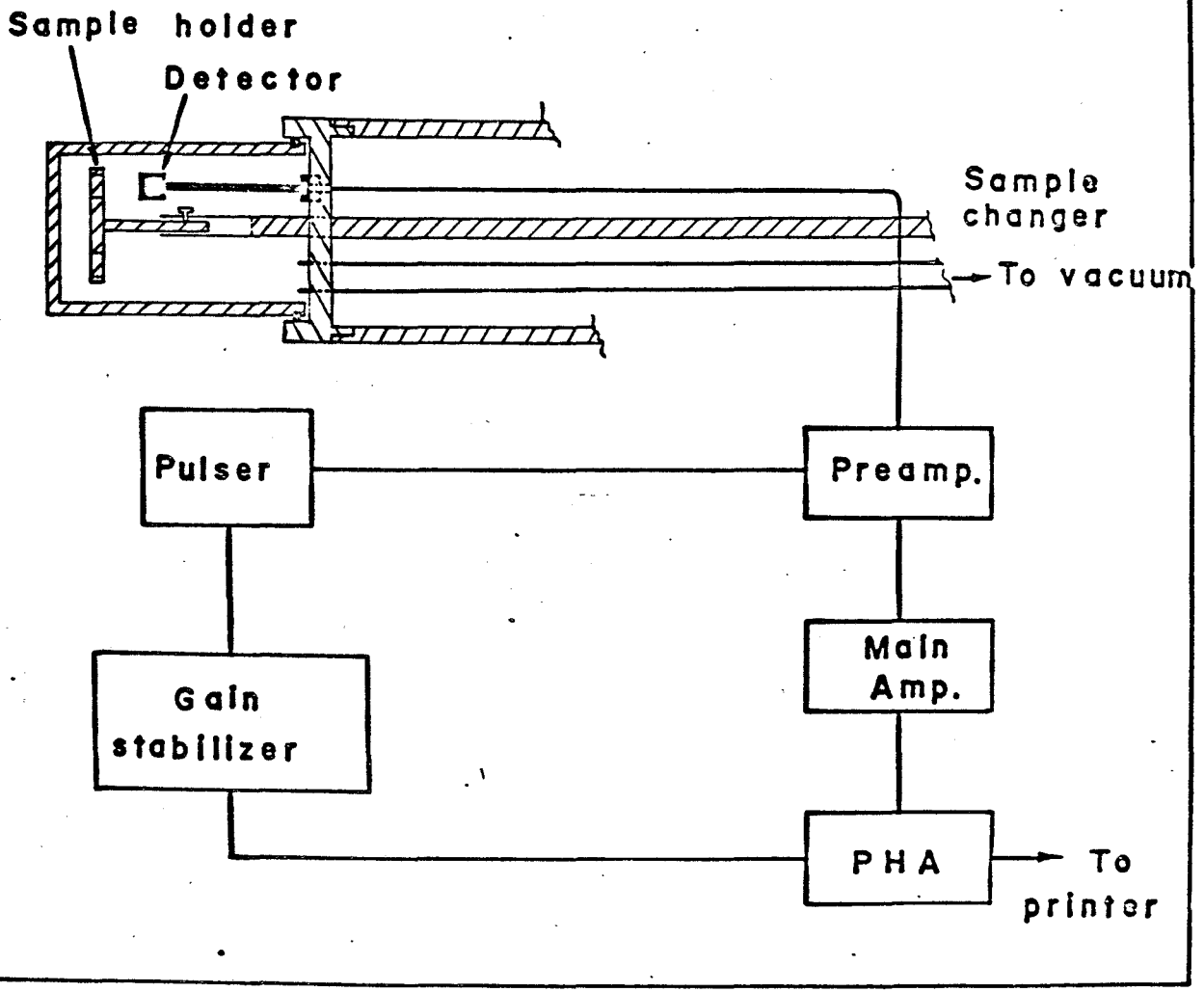

all resolutions obtained at ~ 8 MeV varied between 76 - 150 keV. In measurements with E.P.G. the overall resolution was 55 keV at ~ 8 MeV.

(b) Targets

The measurements for the determination of cross sections were made using targets of enriched samples of rare earths and Li^6(Li^7) isotopes. Li^6 was used as a standard while Li^7 was added to serve as a carrier for Li^6 in order to minimize losses due to exchange or diffusion processes occurring during the target preparations. Targets for energy measurements were also prepared from enriched samples of the rare earths but these contained carrier-free energy standards such as Am^{241} and decay products of Th^{228} and Ra^{226}. All of these isotopes were acquired from the Oak Ridge National Laboratory (U.S.A.). The rare earth isotopes were in the form of oxide while the Li^6 and the Li^7 isotopes were in the form of carbonate and metal respectively. The isotopic analysis of the stable isotopes are given in Tables 3.1-3.6. The oxide samples were heated for 2 hrs at 450°C in order to decompose any possible carbonate present in the sample and also to drive off the last traces of moisture. The carbonate samples were heated for 2 hrs at 120°C to remove traces of moisture. These samples were then cooled to room temperature in desiccators before they were finally weighed for the preparation of solutions. The Li^7 sample was converted to

its hydroxide by carefully dissolving the clean and dried metal pieces in water. All of these samples were subsequently converted into neutral nitrate solutions of known strength. The reagents used were of spectrographic grade and the water used was distilled deionized water. A stock solution of $Li^6(Li^7)$ was then prepared in a ratio of 1:300 (by weight) such that the resultant solution had a Li^6 concentration of 0.684 μg/ml.

Cross section measurements were made with mixed rare earth-$Li^6(Li^7)$ targets of thicknesses varying between 20-250 $\mu g/cm^2$ using known atomic ratios of rare earths and Li^6. The amount of $Li^6(Li^7)$ used was, however, kept constant and corresponded to 0.01 $\mu g/cm^2$ with respect to Li^6. In the case of Gd^{155} and Eu^{151}, Nd^{143} served as a secondary standard. Target thicknesses for the energy measurements were kept as low as convenient for counting. This was dependent on the cross section for the (n,α) reaction and the method of irradiation used. Table 3.7 gives information on target thicknesses.

Target preparations were done either by using a simple evaporation technique or by using a modified electrodeposition technique of 'Molecular Plating'[47].

Evaporation Technique

This technique was applied only for targets used in the cross section measurements. Desired aliquots of

solutions of the rare earth and Li^6(Li^7) isotopes were transferred to a small teflon container using microcapacity pipets. These pipets had been previously calibrated using doubly distilled Hg. To ensure complete transfer of solutions the pipets were rinsed thoroughly with three volumes of 10% HNO_3 into the teflon container. This solution was then evaporated to dryness by gentle heating under an infra-red lamp. The residue was subsequently dissolved in a small volume (~ .1 ml) of water and dried once again as described above. These steps were undertaken to remove excess HNO_3 and to allow thorough mixing of the sample. The glass container used in preliminary experiments was replaced by teflon in order to avoid losses of Li^6. Finally, the residue was dissolved in 0.05 ml of 50% alcoholic solution. This solution was then deposited homogeneously on a 1 mm thick aluminum backing disc (~ 1.3 cm dia). The deposit was first dried under an infra-red lamp and then heated in a furnace for one hour at 400°C to convert the nitrate into an adhering deposit of the oxynitrate. No analysis was made on the deposit to check the uniformity of the distribution of the rare earth/lithium ratio. Macfarlane and Almodovar[2] had previously observed no fluctuation in the ratio of Sm/Li in their samples prepared in a similar way.

Electrodeposition Technique

In experiments involving measurements of energy or the relative intensities of the adjacent peaks, thin uniform sample targets were prepared by electrodeposition. The technique of 'Molecular Plating' developed, originally, by Parker and Falk[47] was adopted after slight modification . A specially designed electrodepositing apparatus was used for preparation of the desired targets. This apparatus consisted of a polyethylene tube (~ 2 cm internal diameter) which held the aluminum backing disc on an aluminum base and served as the cell chamber when compressed against the disc using a bakelite block and a set of screws. A cross sectional view of this assembly is shown in fig. 3.4. The desired amounts (20-100 μg) of nitrate solutions of the materials to be deposited were evaporated to dryness and the residue was resolved in ~ 20 μl of deionized distilled water. This solution was then mixed thoroughly with 10 ml of spectrographic grade isopropyl alcohol and transferred into the cell chamber. The deposition was carried out by using a rotating platinum anode and the polished aluminum backing disc as the cathode.

A radio tracer technique was used in a set of preliminary experiments to investigate the efficiency of the deposited rare earth targets. Up to one milligram samples of Sm solutions (as nitrate) labelled with Sm^{153} were deposited

Fig. 3.4. Cross sectional view of 'Electrolytic Cell'. T is target on aluminum backing disc. E is electrolytic solution. P is Pt electrode and M is a D.C. motor to rotate the Pt electrode

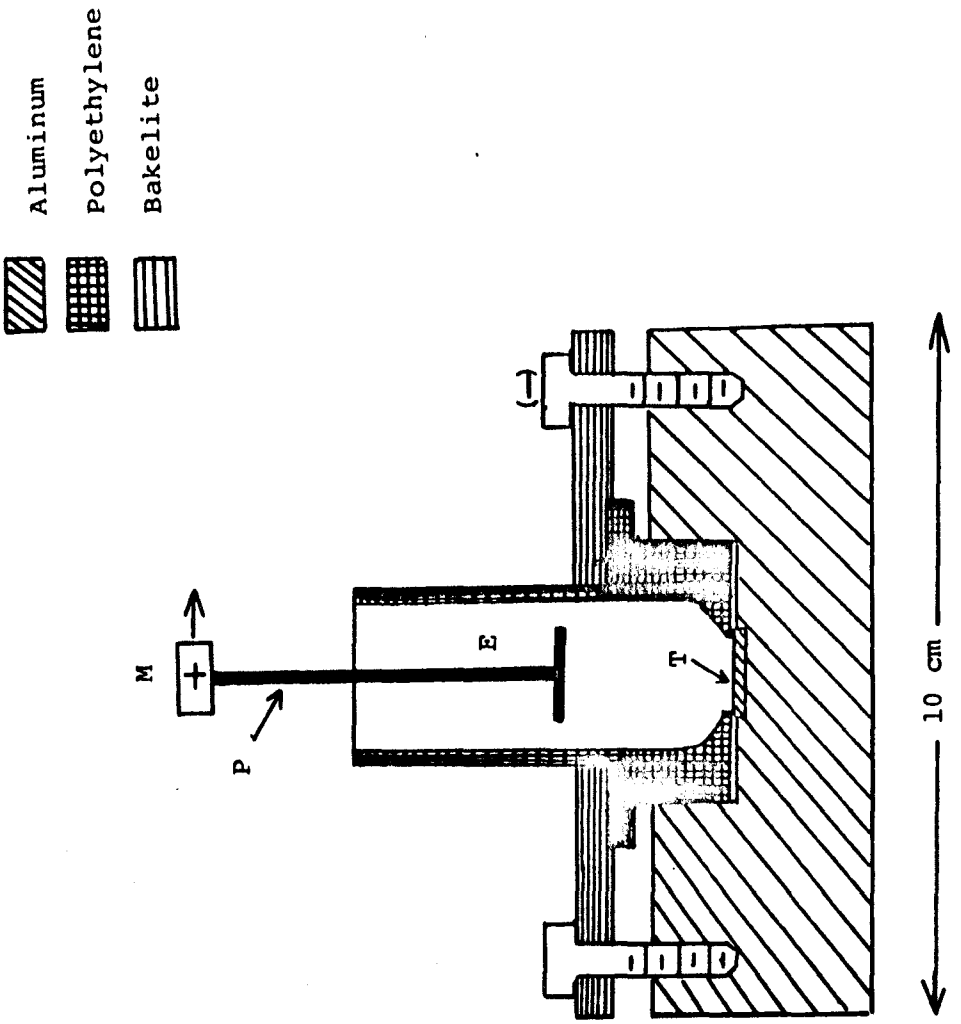
Aluminum
Polyethylene
Bakelite
M
P
E
T
10 cm

under varying conditions of deposition. The beta activity of the deposited samples was then compared with that of a standard using a proportional counter under identical conditions. Flame photometric technique was used to determine the efficiency of Li deposition. Weighings were also done to check these results. The optimum conditions established for the best performance of the deposition technique are given below. The efficiency of deposition under these conditions was 98 $\pm$ 2% at room temperature.

Voltage	200-250 V
Current	20-30 micro amps
Concentration	100 µg/10 ml
Duration	1-1.5 hrs.
pH	3-4
R.P.M. of Pt anode	< 60 R.P.M.
Water content	< 0.1 ml/10 ml isopropyl alcohol

In experiments involving the electrostatic particle guide, larger area targets (44 cm^2) were required. These targets were prepared by a similar technique using a larger cell described elsewhere[48].

Alpha spectra obtained with targets made by this technique showed a marked improvement in energy resolution (compare fig. 3.6 with fig. 3.5(a)).

(c) Background Measurements

Several independent measurements were performed in order to determine the contribution of background in the regions of interest, that is, 2.5-3.0 MeV and 6-10 MeV. These spectra were obtained at thermal neutron fluxes of ~10^8 n/cm^2/sec with pure Li_2O and R_2O_3 targets (R stands for the rare earth isotope used) with thicknesses comparable to those of the mixed Li-rare earth targets in actual measurements. Measurements were also made with a bare detector, a pure Al backing disc and rare earth targets but with the back of the Al disc facing the detector. Essentially no background was observed for any of these measurements above 6 MeV region. The background count rate in this region was less than 0.02 cpm. In the Li region, the background was less than 19 cpm and was mainly due to lithium contamination of the detector material. This constituted less than 3% of the total triton count rate recorded in this region. Alpha particle measurements with these targets at zero flux failed to show any contribution to the background from U or Th contamination of the samples.

(d) Cross-Section Measurements

The (n,α) standards (Li^6 or Nd^{143}) mixed with the rare earth target samples were used in the measurements of the effective thermal neutron (n,α) reaction cross sections without evaluating the counting geometry or neutron flux. The cross section measurements were made by comparing the

counting rates from the rare earth (n,α) reactions with those of the (n,α) reactions from the standards. $Li^6(Li^7)$ was used as a standard for measurements involving $Sm^{147,149}$ and Nd^{143} isotopes. Nd^{143} was then used for Gd^{155} and Eu^{151} as a secondary standard. For $Li^6(Li^7)$ the intensity of the 2.74 MeV triton peak from Li^6 $(n,\alpha)T^3$ was used in the analysis because the resolution of this peak was less affected by sample thickness than was that for the alpha peak (see fig. 3.6).

The counting rate of the two (n,α) reactions was obtained from the alpha-particle spectrum by integrating the counting rate over the peaks after appropriate corrections for background and contributions from adjacent peaks. The ratio of the integrated counts of the standard peak to the corresponding counts of the rare earth alpha peak needed for the evaluation of cross section was determined directly using the relationship

$$x = \frac{n}{E_s} \times E_r \qquad (3.1)$$

The quantity, x, is the number of channels to be integrated under the rare earth alpha peak at an energy E_r corresponding to the 'n' channels arbitrarily selected for integration under the standard peak having an energy E_s. The values of n were increased and the corresponding values of x were determined. The ratios of integrated counts in each n and x channels were then plotted against $1 - \frac{\Delta E}{E}$ (where ΔE is the energy correspon-

Fig. 3.5 (a) A typical alpha particle spectrum obtained from an evalprated Li-Sm mixed target (130 μ/cm^2). Resolution at 2.74 MeV is 136 keV.

(b) A plot of the ratio of integrated $(\frac{Li^6}{Sm^{149}_{2^+}})$ counts against $(1 - \frac{\Delta E}{E})$

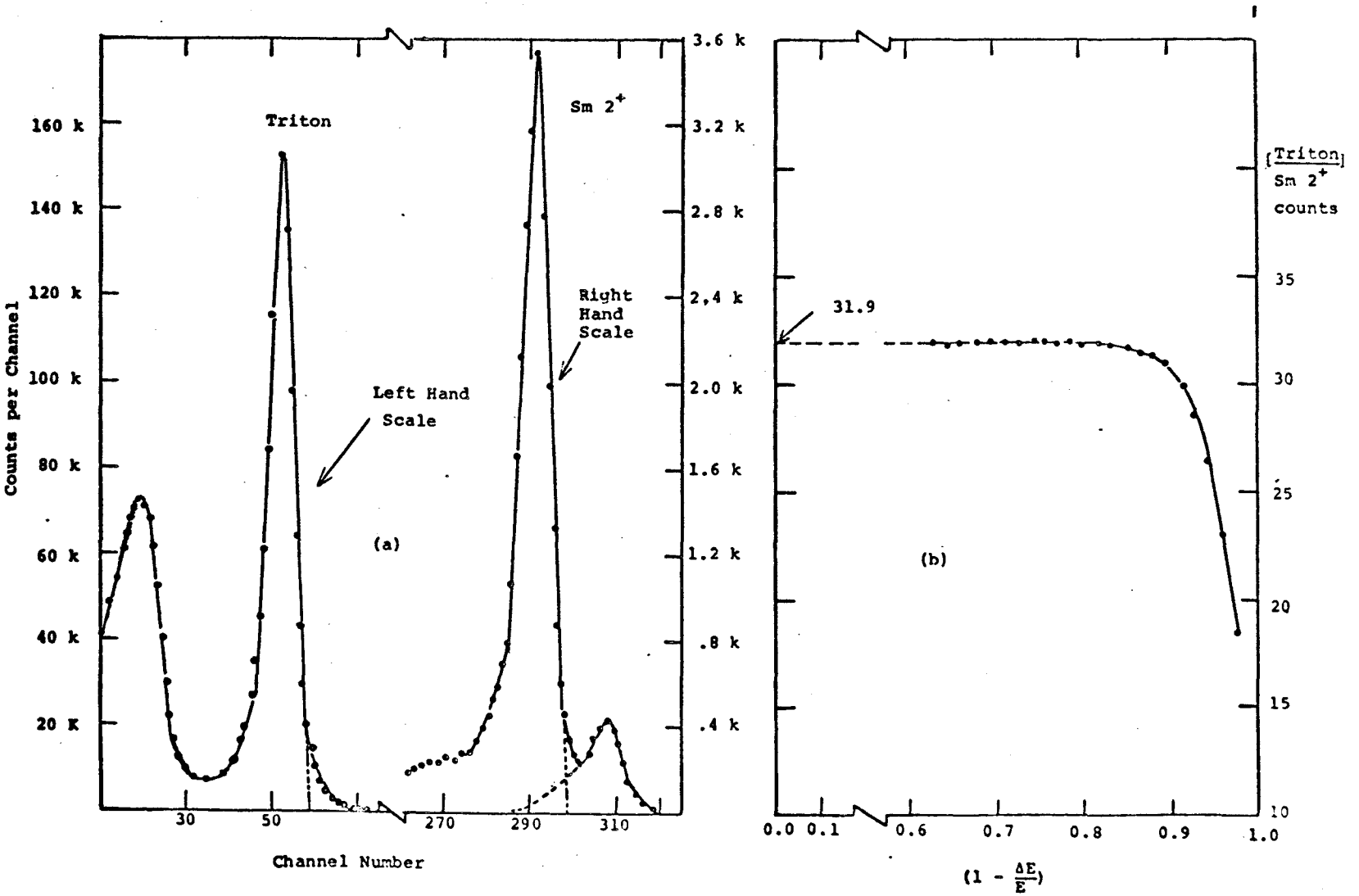
Counts per Channel
160 k
140 k
120 k
100 k
80 k
60 k
40 k
20 k
3.6 k
3.2 k
2.8 k
2.4 k
2.0 k
1.6 k
1.2 k
.8 k
.4 k
Triton
Sm 2+
Right Hand Scale
Left Hand Scale
(a)
30
50
270
290
310
Channel Number
31.9
(b)
[Triton / Sm 2+ counts]
35
30
25
20
15
10
0.0 0.1 0.6 0.7 0.8 0.9 1.0
(1 - ΔE/E)

ding to channels n or x). Finally the ratio of the total counts under the standard peak to the total counts under the rare earth peak was obtained by extrapolating it to zero value. A typical case for Sm^{149} is shown in fig. 3.5(b). The effective cross section of the rare earth alpha peak under study was obtained from the expression

$$\hat{\sigma}_{n,\alpha}(R) = \frac{A \times \hat{\sigma}_{n,\alpha}(S)}{c} \times f \qquad (3.2)$$

where $\hat{\sigma}_{n,\alpha}(R)$ is the effective thermal neutron (n,α) cross section for the rare earth peak under investigation.

$\hat{\sigma}_{n,\alpha}(S)$ is the effective (n,α) cross section for the standard peak; for Li^6 it is the same as the 2200 m/sec cross section (945 barns)[49].

c is the ratio of counts of the standard to the rare earth alpha peaks.

A is the standard to rare earth atomic ratio used.

f is the collection efficiency factor[46] (1 for the lucite assembly and is equal to the ratio of the energies of the rare earth to the standard alpha groups for the electrostatic particle guide.

In cases where more than one alpha group was present in the alpha spectrum the cross section for the highest intensity group was first determined as described above. This value was then used to evaluate the cross section for the

Fig. 3.6. A typical alpha particle spectrum obtained from electrodeposited Li-Sm mixed target.

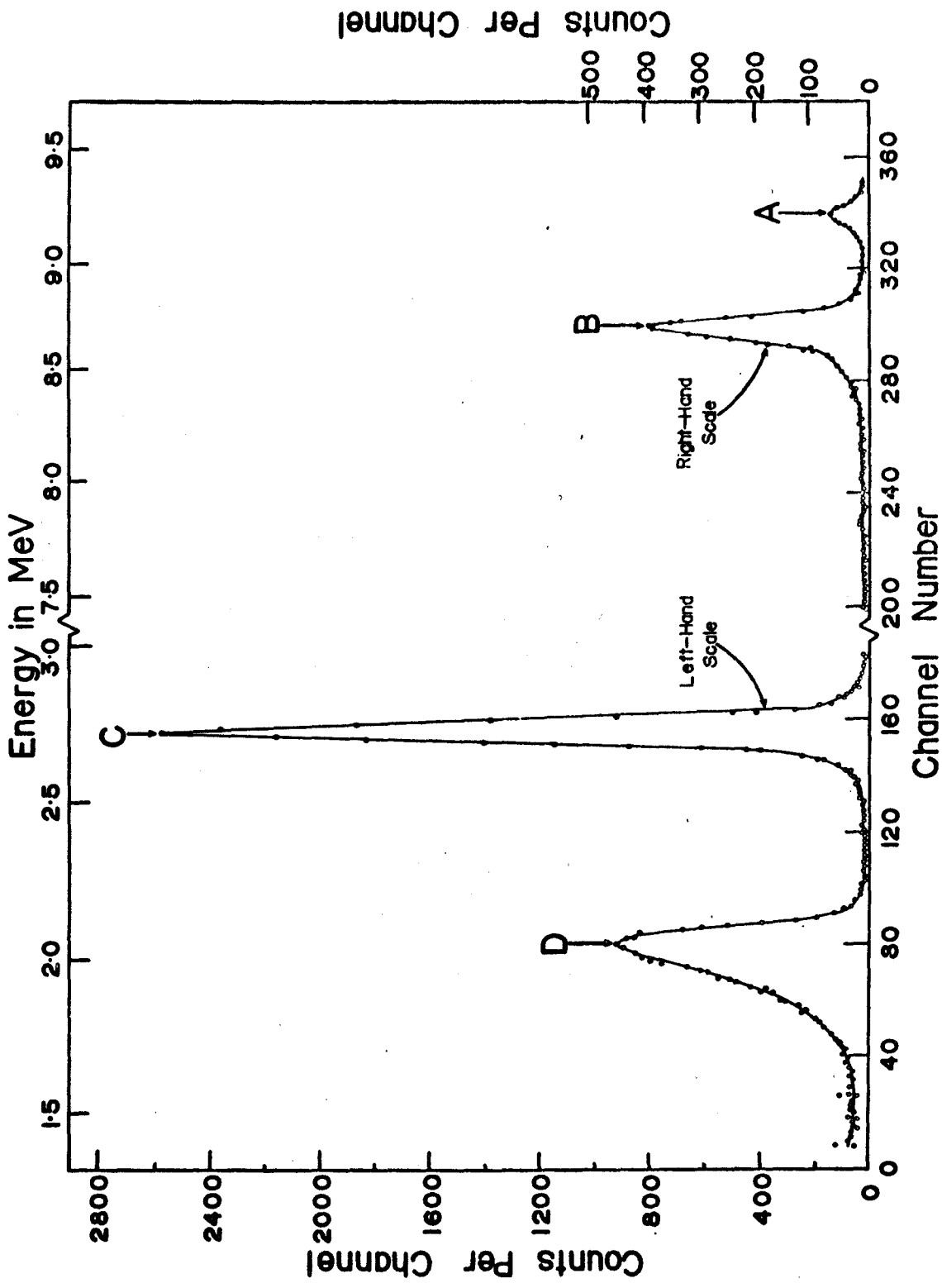
Counts Per Channel
500
400
300
200
100
0
A
B
C
D
Right-Hand Scale
Left-Hand Scale
Energy in MeV
1·5
2·0
2·5
3·0
7·5
8·0
8·5
9·0
9·5
Channel Number
0
40
80
120
160
200
240
280
320
360
Counts Per Channel
2800
2400
2000
1600
1200
800
400
0

other groups, using the following expression

$$\hat{\sigma}_{\ell} = \hat{\sigma}_{h} \times (I_{\ell}/I_{h}) \qquad (3.3)$$

where $\hat{\sigma}_{\ell}$ is the cross section of the low intensity group,

$\hat{\sigma}_{h}$ is the cross section of the highest intensity group ,

I_{ℓ}/I_{h} is the ratio of intensities of low to high intensity groups.

The relative intensities of these groups were measured in separate experiments using targets obtained by electrodeposition. These targets provided a much cleaner separation between the various alpha groups. An alpha spectrum obtained in this way with a Li^{6}-Sm^{149} target is shown in fig. 3.6.

(e) Alpha Particle Energy Measurements

Energy measurements involved the irradiation of the mixed rare earth-Th^{228}-Ra^{226} electrodeposited targets at neutron fluxes of ~10^{8} n/cm^{2}/sec using the lucite assembly. The use of the energy standards in this way eliminated the energy corrections for target thicknesses. A distance of about 6 mm was maintained between the detector and the target in order to make measurements with reasonably good counting geometry. The energy calibration of the system above 6 MeV was provided by alpha particle groups from the various energy standards present as decay products of Th^{228} and Ra^{226} in the target material. The alpha particle energies[50] used were

Po^{218}, 6000.0 ± 1.4 keV; Rn^{220}, 6288.4 ± 2.2 keV; Po^{216}, 6777.2 ± 1.6 keV; Po^{214}, 7688.4 ± 0.6 keV; Po^{212}, 8785.0 ± 0.8 keV. In order to establish a good calibration curve, extra points were obtained in the region from 6 MeV to 10 MeV with an RIDL precision pulse generator that was normalized with respect to the Po^{212} 8.785 MeV alpha group. The peak channel position for these alpha groups and the simulated pulser peaks were determined with a precision of better than 0.1 of a channel using a computer programme for a non linear least squares fit[51]. A second order polynomial ($Y = a + bX + cX^2$) was then fitted to these peak positions to establish the calibration curve. The contribution of the quadratic term was small but significant. From the computed positions of the various alpha groups resulting from the (n,α) reactions the energies of the alpha groups were obtained. In a typical case of Nd^{143}, for example, X(the position of α-group) was 328.41, and the values for the coefficients a,b,c were 5.524, 1.263×10^{-2} and -2.119×10^{-6} respectively, and the value for Y (alpha energy) was 9.444 MeV.

For Gd^{155} and Eu^{151} which were investigated using the electrostatic particle guide a similar procedure was adopted. The Nd^{143}(n,α) reaction, and Po^{216} and Po^{212} were used as standards together with various pulser peaks normalized to the 9.443 MeV alpha group from Nd^{143} to

establish the calibration curve.

(f) Neutron Transmission Measurements

These measurements were performed to study the effect of concentrations of various neutron absorbers (both '1/v' and resonance) on the relative intensities of the alpha (triton) peaks caused by the interaction of the transmitted neutrons with mixed Li^6-rare earth targets. The rare earth isotopes studied were Sm^{149} and Nd^{143} and the targets used were prepared by electrodeposition. The absorbers were aqueous chloride solutions of enriched Li^6 or Sm^{149} (in natural Sm)corresponding to 96.1% and 13.8% atomic abundances respectively. These solutions were obtained by diluting stock solutions of Li and Sm. These stock solutions corresponded to 0.0484 gm/cm^3 of Li^6 and 0.0292 gm/cm^3 of Sm^{149} respectively. For the transmission measurements the front end of the usual lucite assembly described previously was modified as shown in Fig. 3.7. A column of the absorber solution of the desired concentration was supported around the target-detector system in a narrow-necked, thin, double-walled spherical bulb. When in position the target which was housed on the detector was located at the centre of the bulb and was exposed mainly to the transmitted neutrons. Most of the experiments involving Li^6 absorbers were conducted with bulbs made of aluminum having an average column thickness of

about 0.5 cm. In preliminary experiments and especially in those where samarium absorbers were employed the bulbs used were made of lucite and had an average column thickness of 0.35 cm.

Fig. 3.7. Apparatus for neutron transmission measurements. A is a surface barrier silicon detector, B is a mixed Li-rare earth target and C is the double walled absorption bulb.

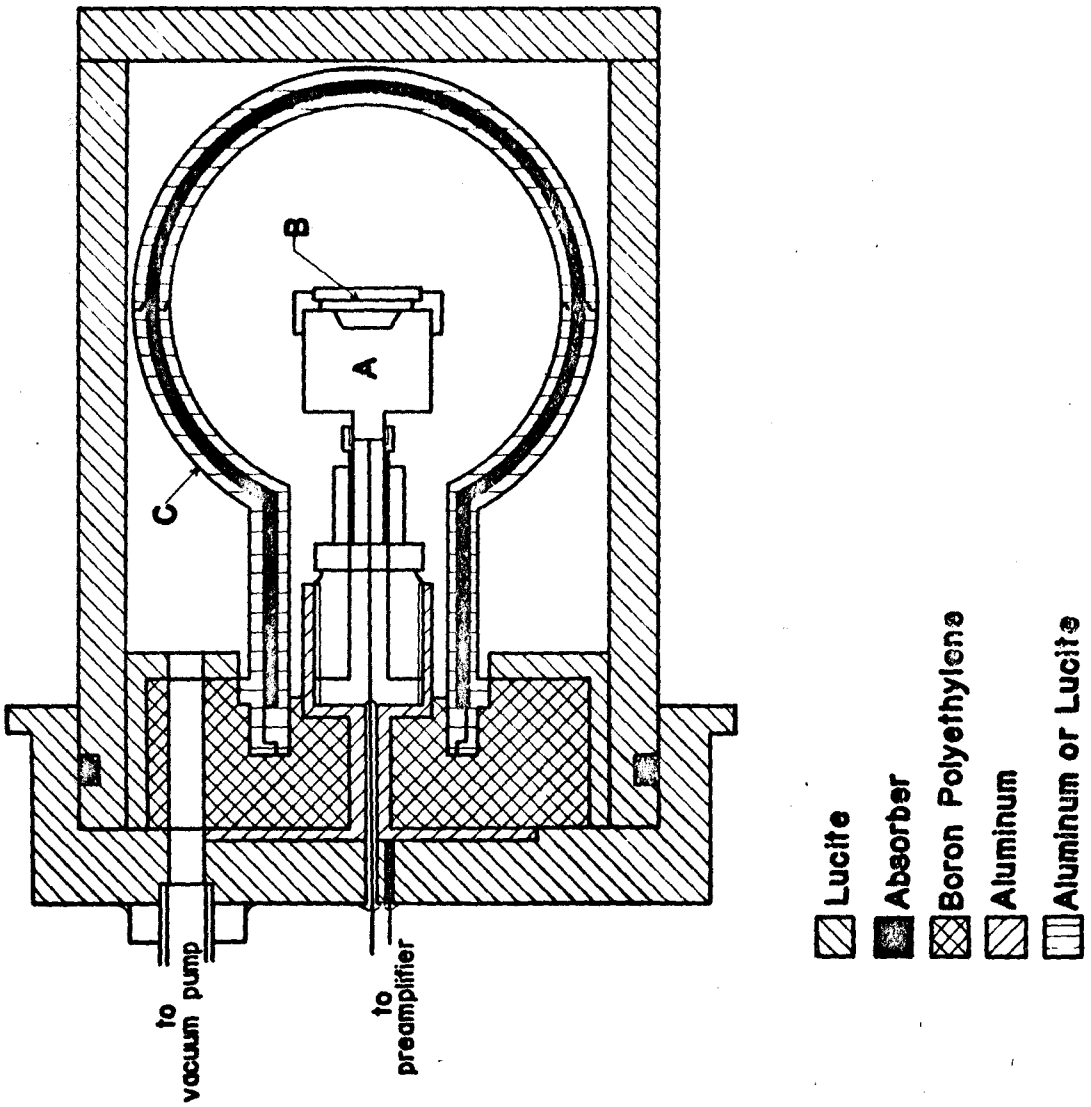
B
A
C
to vacuum pump
to preamplifier
Lucite
Absorber
Boron Polyethylene
Aluminum
Aluminum or Lucite

Table 3.1. Isotopic analysis of Sm^{147} sample

Isotope	Atomic Abundance %	Precision %
144	0.08	---
147	97.8	0.1
148	0.91	0.05
149	0.51	0.05
150	0.17	0.05
152	0.34	0.05
154	0.21	0.05

Table 3.2. Isotopic analysis of Sm^{149} sample

Isotope	Atomic Abundance %	Precision %
144	0.08	---
147	0.33	0.05
148	0.55	0.05
149	97.46	0.05
150	0.65	0.05
152	0.70	0.05
154	0.30	0.05

Table 3.3 Isotopic analysis of Nd^{143} sample

Isotope	Atomic Abundance %	Precision %
142	2.63	0.02
143	91.32	0.05
144	3.90	0.03
145	0.77	0.02
146	1.05	0.02
148	0.23	0.02
150	0.14	0.01

Table 3.4 Isotopic analysis of Gd^{155} sample

Isotope	Atomic Abundance %	Precision %
152	0.06	----
154	0.28	0.05
155	94.3	0.1
156	2.84	0.05
157	1.01	0.05
158	1.05	0.05
160	0.53	0.05

Table 3.5 Isotopic analysis of Eu^{151}

Isotope	Atomic Abundance %	Precision %
151	96.83	0.05
153	3.17	0.05

Table 3.6 Isotopic Analyses of Li^6 and Li^7 Samples

Sample	Isotope	Atomic Abundance %
Li^6	Li^6	96.1 ± 0.1
	Li^7	3.9 ± 0.1
Li^7	Li^7	99.99
	Li^6	0.01

Table 3.7 Targets for Energy Measurements of Alpha Particles

Target	Thickness $\mu g/cm^2$	Standards	Method of Measurement
Sm^{147}	100	Sm^{149} and Nd^{143} (n,α) reaction	Lucite assembly
Sm^{149}	20	Decay products of Th^{228} and Ra^{226}	Lucite assembly
Nd^{143}	50	Decay products of Th^{228} and Ra^{226}	Lucite Assembly
Gd^{155}	80	Decay products of Th^{228} and Nd^{143} (n,α) reaction	Electrostatic Particle Guide
Eu^{151}	155	Nd^{143} and Pulser	Electrostatic Particle Guide

CHAPTER IV

RESULTS AND DISCUSSION

During preliminary measurements several experiments were made with Nd^{143} and Sm^{149} targets of varying thicknesses in order to establish conditions for the accurate determination of effective (n,α) cross sections. These targets were prepared from enriched and natural isotopes as described in the previous chapter. The solutions in these experiments were however mixed in glass containers and no additional Li^7 was added. The Li^6 content of these targets was as low as ~ 0.1 μg. The irradiations were carried out at neutron fluxes up to $10^8 n/cm^2/sec$. The observed counting rate of $Li^6(n,\alpha)T^3$ reaction was too high to be recorded simultaneously with those resulting from the rare earth isotopes. The Li^6 was therefore counted in most cases for 1 hour before and 1 hour after the counting of the rare earth. This was done to reduce chances of errors in counting resulting from slight fluctuations in the neutron flux. Although the counting precision was maintained at < 1%, the results showed fluctuations of the order of ~ 15%. These fluctuations were later found to be mainly due to losses of Li^6 resulting possibly through exchange, diffusion and adsorption processes occurring

during the target preparations. In subsequent experiments the glass containers were therefore replaced by teflon. This helped in reducing considerably the largest source of fluctuation in results. However, the method in this form was used only in measurements involving Sm^{147}. For measurements with Sm^{149} and Nd^{143} the targets were prepared from solutions with considerably reduced Li^6 content (6.838×10^{-3} μg) but with an increased total Li content (~ 3 μg). This step permitted the rare earth and Li^6 to be counted simultaneously on the same spectrum and thereby eliminated the errors caused by possible variations in the neutron flux. In addition, the higher overall Li concentration coupled with the use of teflon containers for mixing of solutions almost completely eliminated the loss of Li^6 during target preparation.

Only the final set of results are presented in this chapter. The method used to obtain these results, unless otherwise mentioned, was the same as described in detail in the previous chapter. From the alpha energies and cross-sections it was possible to calculate directly the corresponding Q-values and the 2200/sec neutron cross sections.

(a) $Nd^{143}(n,\alpha)Ce^{140}$ Reaction

The neutron-induced alpha particle spectrum obtained in Nd^{143} consisted mainly of a single alpha group. A typical alpha particle spectrum obtained in cross section measurement is shown in fig. 4.1. The peak B in this spectrum corresponds

Fig. 4.1. Alpha particle spectrum from the mixed Nd^{143}-$Li^{6}(Li^{7})$ target. Thickness ~ 89 $\mu g/cm^2$; Time = 1000 minutes.

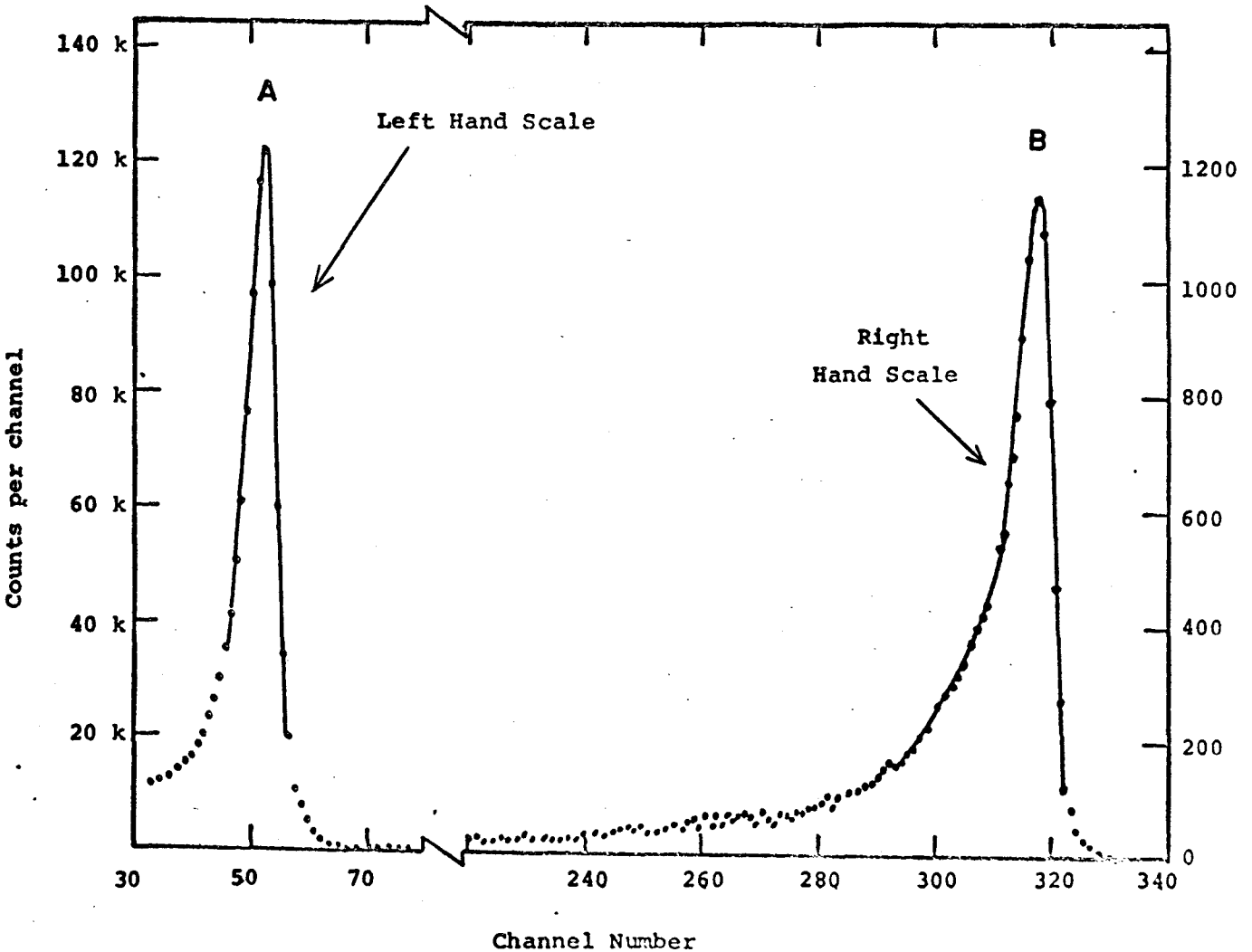
140 k
120 k
100 k
80 k
60 k
40 k
20 k
Counts per channel
A
Left Hand Scale
B
Right
Hand Scale
1200
1000
800
600
400
200
0
30
50
70
240
260
280
300
320
340
Channel Number

to an alpha particle group at 9.44 MeV. The peak A is the standard 2.74 MeV triton peak from the $Li^6(n,\alpha)T^3$ reaction. The results of six experiments with different target thicknesses are given in table 4.1. A final result of 21.28 ± 0.18 mb has been assigned for the effective cross section for this reaction. The irradiation of electrodeposited targets of pure Nd^{143} failed to show the existence of any fine structure. A spectrum covering a range of ~ 2 MeV below the main alpha group is shown in Fig. 4.2. The resolution of this peak (FWHM) is ~ 110 keV. The energy of this group was determined by making four independent measurements. A final value of 9.443 ± .005 MeV has been established.

The Q-value for the $Nd^{143}(n,\alpha)Ce^{140}$ reaction calculated from atomic mass differences is 9.732 ± 0.022 MeV[52]. This is in good agreement with our measured Q-value of 9.713 ± 0.005 MeV. This shows that most of the alpha decay takes place from the capturing state in the compound nucleus, Nd^{144}, and not from intermediate states populated by gamma transitions. The first excited state in the daughter nucleus, Ce^{140}, lies 1.596 MeV[53] above the ground state (0^+). No transition to this state was observed. A proposed decay scheme is given in Fig. 4.3.

The nuclide, Nd^{143}, in its ground state has a spin of 7/2[54]. It has an odd parity which is a consequence of

Table 4.1 Results of Cross Section Measurements For $Nd^{143}(n,\alpha)Ce^{140}$ Reaction

Target	Thickness ($\mu g/cm^2$)	Li^6/Nd^{143} (Atom Ratio) (A)	Li^6/Nd^{143} (Count Ratio) (c)	Effective Cross Section (mb) $\hat{\sigma} = (A/c) \times \hat{\sigma}Li^6$
33*	147	2.520×10^{-4}	11.06	21.53±0.43
84	30	4.337×10^{-3}	199.30	20.56±0.49
85	59	2.169×10^{-3}	95.10	21.55±0.48
86	89	1.446×10^{-3}	64.90	21.06±0.45
87	119	1.084×10^{-3}	48.60	21.08±0.43
88	148	8.675×10^{-4}	37.60	21.80±0.44
		Best value for Effective Cross Section (mb)		21.28±0.18

*Li^7 was not present in this measurement but solutions for target preparations were mixed in teflon container.

Fig. 4.2 Alpha spectrum from $Nd^{143}(n,\alpha)Ce^{140}$ obtained by irradiating electrodeposited target (~ 50 $\mu g/cm^2$) at $10^8/n/cm^2/sec$. T = 1000 min.

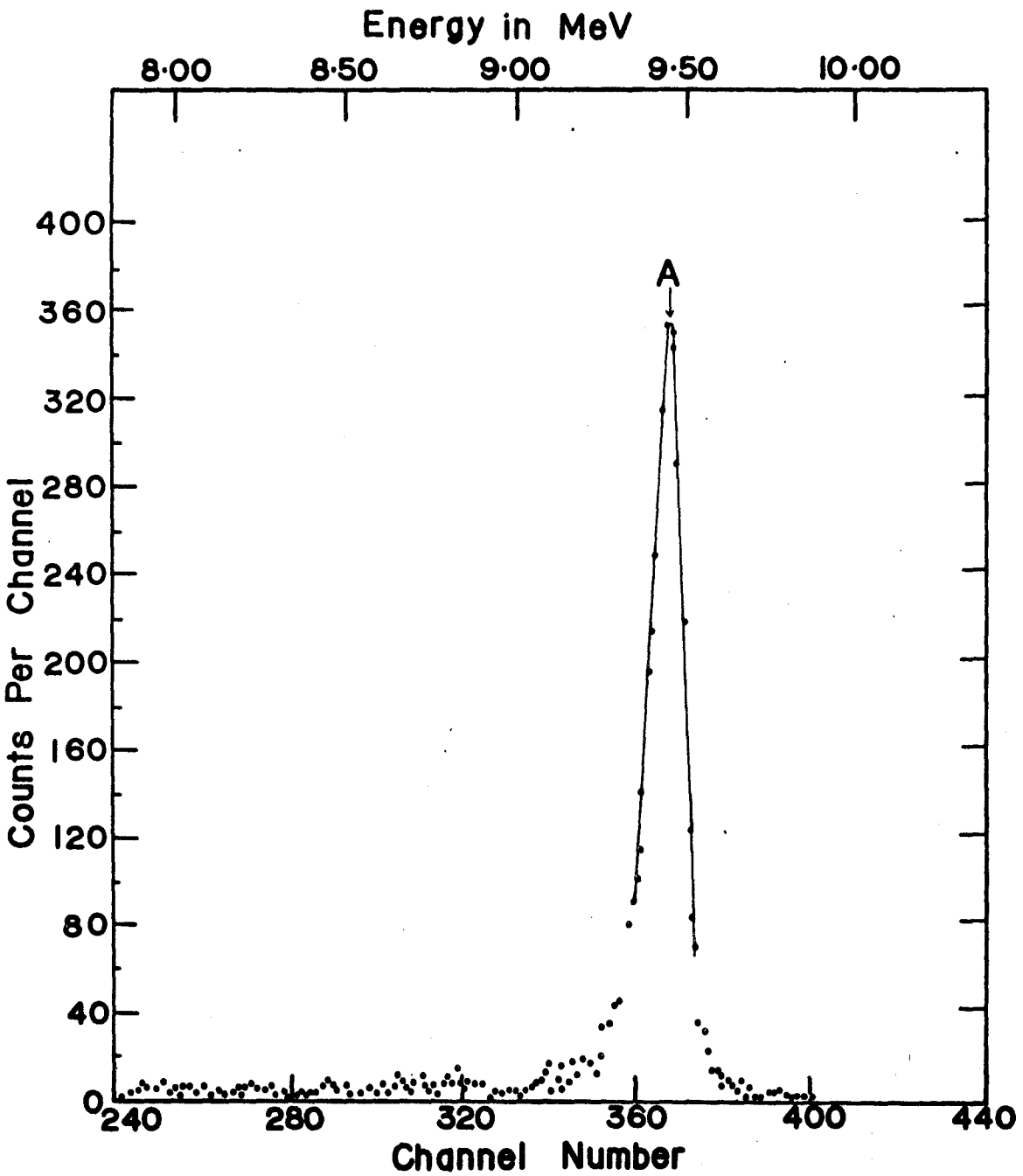
Energy in MeV
8·00
8·50
9·00
9·50
10·00
A
400
360
320
280
240
200
160
120
80
40
0
Counts Per Channel
240
280
320
360
400
440
Channel Number

Fig. 4.3. Proposed partial alpha decay scheme of the s-wave neutron capturing state of Nd^{144}.

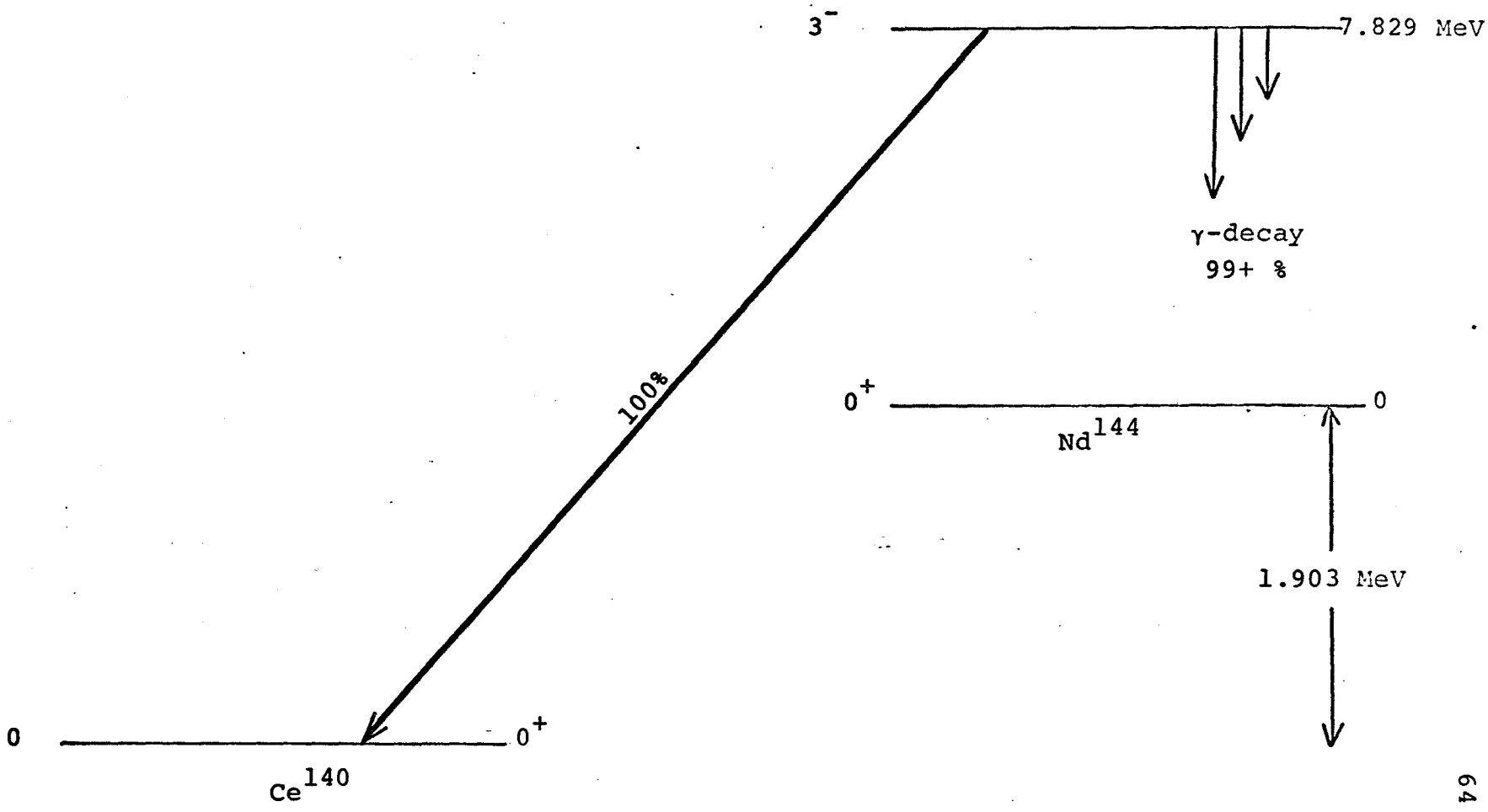
3⁻
7.829 MeV
γ-decay
99+ %
100%
0⁺
0
Nd144
1.903 MeV
0
0⁺
Ce140

the unpaired neutron of the target nucleus occupying the $f_{7/2}$ level. For an s-wave neutron absorption, the capturing state will have a spin 4 or 3 with odd parity. The contribution to the 2200 m/sec. neutron cross section for Nd^{143} is dominated by a resonance at -6 eV[55]. The first positive resonance is at 56 eV[56]. This, as well as the higher resonances, contributes only slightly to the 2200 m/sec cross section. The excitation function shows very nearly a '1/v' dependence . (The 2200 m/sec cross section is less than 1% higher than expected from a true '1/v' behaviour)[55]. The positive resonance at 56 eV has a spin of 4^-[57]. The alpha transition from this state to the ground state (0^+) in Ce^{140} is parity forbidden. A 3^- level[57] at 127 eV[56] can explain the alpha transition but its contribution is exceedingly small in the thermal neutron region. Cheifetz et al[3] have postulated that the -6 eV resonance reported by Hays[55] is a 3^-. Our results have confirmed this. Since the excitation function for the (n,γ) reaction shows essentially a '1/v' behaviour the alpha group observed should also exhibit a '1/v' behaviour. The results obtained in the neutron transmission measurements have confirmed this. These results will be discussed later. The failure to observe the 2^+ alpha transition which can occur by the emission of $\ell = 1,3,5$ wave alpha particles is the

result of the strong energy dependence of the alpha penetrability factor.

(b) $Sm^{149}(n,\alpha)Nd^{146}$ Reaction

The alpha particle spectrum obtained in the study of $Sm^{149}(n,\alpha)Nd^{146}$ reaction is dominated by two alpha groups; one at 8.73 MeV and the other at 9.17 MeV. The intensity of the low energy group is about 7 times that of the high energy group. An alpha particle spectrum obtained during cross section measurements is shown in Fig. 3.5. The cross section for the high intensity group was determined from several independent measurements using different target thicknesses. The final results based on 11 measurements are given in Table 4.2. A value of 38.70 ± 0.45 mb has been established for the effective cross section of 8.73 MeV alpha transition. The fluctuations observed in the results of individual measurements are, most probably, due to errors introduced while making corrections for the contributions from the highest energy group.

The effective cross section for the highest energy group was determined relative to the more intense group. Four independent irradiations were made with electrodeposited targets of varying thicknesses. The results of these measurements are summarized in Table 4.3. A value of 5.23 ± 0.17 mb has been established for the cross section of 9.17 MeV alpha group.

Table 4.2 Results of Cross Section Measurements of $Sm^{149}(n,\alpha)Nd^{146}$ Reaction for 8.73 MeV Alpha Group

Target	Thickness ($\mu g/cm^2$)	Li^6/Sm^{149} (Atom Ratio) (A)	Li^6/Sm^{149} (Count Ratio) (c)	Effective Cross Section (mb) $(A/c)\times\sigma_{Li^6}$
78	18	11.728×10^{-3}	289.00	38.34±0.48
79	18	7.818×10^{-3}	181.40	40.73±0.57
91	18	7.818×10^{-3}	180.60	40.91±0.39
92	18	7.818×10^{-3}	181.20	40.77±0.43
77	36	5.864×10^{-3}	152.40	36.36±0.54
80	36	3.909×10^{-3}	101.77	36.30±0.61
81	72	1.955×10^{-3}	38.40	38.40±0.44
89	72	1.955×10^{-3}	46.80	39.47±0.35
82	108	1.303×10^{-3}	31.90	38.60±0.19
83	144	9.773×10^{-4}	23.20	39.81±0.31
90	156	7.819×10^{-3}	20.20	36.57±0.26
		Best Value for Effective Cross Section (mb)		38.70±0.45

Four independent energy measurements were made and values of 8.734 ± 0.004 MeV and 9.177 ± 0.004 MeV were obtained.

A very thin target was irradiated for 72 hours in order to detect the presence of any fine structure in the spectrum. The spectrum from this experiment is shown in Fig. 4.4. In addition to the prominent 9.177 MeV(peak A) and 8.734 MeV (peak B) alpha groups two additional peaks were observed at 8.160 ± 0.010 MeV (peak C) and 8.000 ± 0.010 MeV(peak D). Their effective cross sections, determined from relative intensity measurements,are 0.61 ± 0.05 mb and 0.66 ± 0.06 mb respectively. These results have been confirmed in a recent high resolution study by Oakey et al[12]. The alpha group (D) has been resolved into components and several other peaks in the low energy region were observed.

Summing the contributions from each of the alpha groups, the total effective cross section for the $Sm^{149}(n,\alpha)Nd^{146}$ reaction is 45.20 ± 0.48 mb.

The Q-values of the four alpha groups (A,B,C and D) of Fig. 4.4 are 9.429 ± 0.004 MeV, 8.974 ± 0.004 MeV, 8.384 ± 0.010 MeV and 8.219 ± 0.010 MeV respectively. The Q-value for the $Sm^{149}(n,\alpha)Nd^{146}$ reaction obtained from mass table is 9.460 ± 0.020 MeV[52]. This means that the highest energy alpha group is associated with the transition to the ground state of the daughter nucleus Nd^{146}. The excited

Table 4.3 Results of Cross Section Measurements for the 9.17 MeV Alpha Group of the $Sm^{149}(n,\alpha)Nd^{146}$ Reaction

Target	Thickness ($\mu g/cm^2$)	Ratio of Alpha Intensities (R)	Effective Cross-section (mb)
6	36	7.24 ±0.37	5.34 ±0.28
2	72	7.81 ±0.45	4.96 ±0.29
7	108	7.24 ±0.37	5.34 ±0.28
4	144	7.40 ±0.27	5.23 ±0.20
		Best Value for Effective Cross Section (mb)	5.23 ±0.17

Fig. 4.4. Alpha particle spectrum from $Sm^{149}(n,\alpha)Nd^{146}$ reaction; T = 72 hours. Target Thickness $\sim 72\ \mu g/cm^2$.

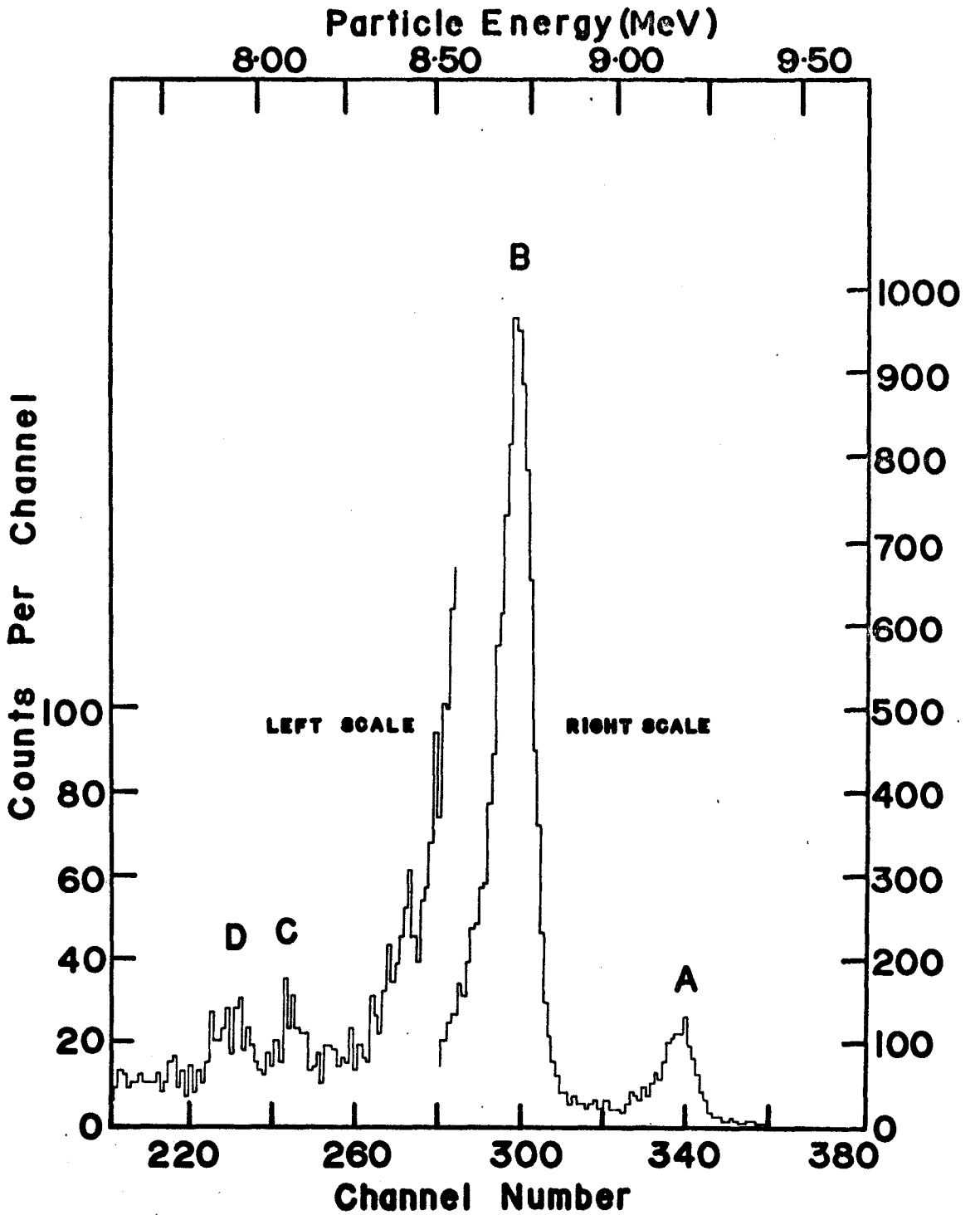
Particle Energy (MeV)
8·00
8·50
9·00
9·50
B
D
C
A
LEFT SCALE
RIGHT SCALE
Counts Per Channel
100
80
60
40
20
0
1000
900
800
700
600
500
400
300
200
100
0
220
260
300
340
380
Channel Number

states near the ground state are known to have spins and parities 2^+, 4^+ and 3^- lying 454 keV, 1043 keV and 1190 keV respectively[58] above the ground state. The experimental Q-values for the lower energy alpha groups are consistent with the known excitation energies of the 2^+, 4^+ and 3^- states in Nd^{146}. The agreement between the present work and previously reported work[58,59] based on decay scheme studies suggests that all of the alpha transitions result from the capture state and not from levels populated through its gamma decay. A proposed decay scheme is given in Fig. 4.5. As shown in Fig. 4.5, about 86% of the alpha decay leads to the first excited state and about 12% goes to the ground state. The weak intensities of the alpha transitions to the 4^+ and 3^- states are due to the effects of the alpha barrier penetrability which is strongly energy dependent. The relatively low intensity of the highest energy group is due to a different effect related to the spins and parities of the contributing states in the compound nucleus. This subject has received serious study in recent years and a good part of the present study has also been devoted to it.

The neutron absorption cross section in the region of thermal energies is dominated by a resonance at 0.0967 eV[60,61]. There is a resonance at 0.87 eV[61,64] but the contribution from this as well as from higher energy resonances

Fig. 4.5. Proposed partial alpha decay scheme of the s-wave neutron capturing state of Sm^{150} .

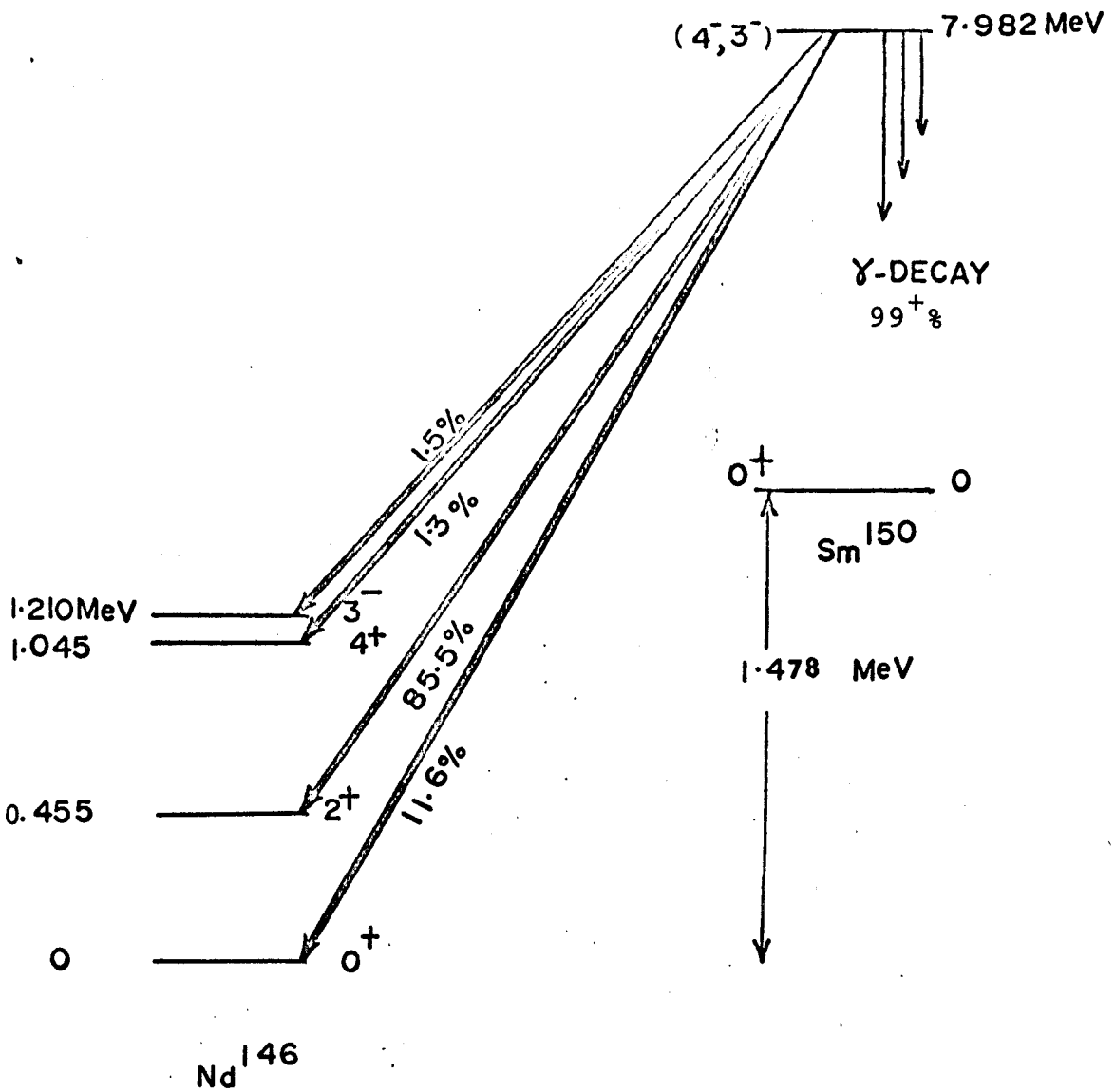
(4⁻,3⁻)
7·982 MeV
γ-DECAY
99⁺%
1·5%
1·3%
85·5%
11·6%
1·210MeV
1·045
0.455
0
3⁻
4⁺
2⁺
0⁺
Nd 146
0⁺
0
Sm 150
1·478 MeV

is negligible. The spin of the ground state of Sm^{149} is $7/2$[54] and the parity is odd. The spin and the parity of the capture states can be 3^- or 4^- for s-wave neutron absorption. The spin and parity of the 0.0967 eV resonance has long been thought to be 4^- [62,64]. Alpha decay from this state can lead to the first excited state (2^+) of Nd^{146} through $\ell = 3$ and $\ell = 5$ wave alpha emission. This state is therefore most presumably responsible for the major part of the (n,α) reaction cross section to the first excited state of Nd^{146}. The transition to the 0^+ state of Nd^{146} from the same resonance is, however, parity forbidden. The presence of the transition to the 0^+ ground state requires that there must be a 3^- bound state contributing to the neutron capture cross section. The 0.87 eV resonance has also been shown to be a 4^- level[64]. The probability for p-wave neutron interaction at thermal neutron energies is extremely low and can be ruled out as an explanation for the appearance of this transition. The only plausible explanation is the presence of a 3^- bound state close to the neutron separation energy. Macfarlane and Almodovar[2] and independently Cheifetz et al[3] postulated a contribution from a 3^- bound resonance. Since Pattenden[61] and Hohne[65] had previously reported the existence of an additional '1/v' component in the low energy tail of the 0.0967 eV resonance, Macfarlane et al suggested that the 0^+ transition might be associated with this component.

Shortly afterwards, Ceulemans et al[6] reported that 0.0967 eV and the 0.87 eV resonances both have spin parity (J^{π}) 3^- and not 4^- as originally considered by others. Dakowski et al[9] in recent studies of the (n,α) reaction on Sm^{149}, on the other hand, gave support to the interpretation of Macfarlane et al[2]. They compared their experimental cross sections with values calculated from the statistical model. They base their calculations on the possible combinations of spins (3^-,4^-), (3^-,3^-) and (4^-,3^-) for the bound and the 0.0967 eV resonances respectively. The values obtained using spin combinations (3^-,4^-) gave the best agreement with their experimental values. Their measured effective cross sections, however, are a factor of about 2 higher than those reported by others. This may be due to some confusion about the definition of the term "effective cross section". A comparison of these results is given in Table 5.1 of Chapter V. The only other value which is too high is that of Macfarlane et al[2] but this has since been found to be in error. Neutron transmission measurements conducted in the course of the present investigation showed that there is a 3^- bound state and that the 0.0967 eV resonance is definitely 4^-. Shortly after we reported our findings[66] Ceulemans et al[7] published their work on the (n,α) reaction which essentially refuted their earlier results and substantiated ours.

(c) $Sm^{147}(n,\alpha)Nd^{144}$ Reaction

Three prominent peaks at energies of 9.87 MeV, 9.19 MeV and 8.73 MeV were observed in the alpha particle spectrum obtained with the Sm^{147} target. A typical spectrum obtained in the cross section measurements is shown in Fig. 4.6. Peaks A and B belong to Sm^{147} and the peak C is the result of Sm^{149} present as an impurity. The 9.17 MeV peak due to Sm^{149} could not be resolved from peak B. The peak D corresponds to the 2.74 MeV triton peak from the $Li^6(n,\alpha)T^3$ reaction. Thicker targets (40 $\mu g/cm^2$-160 $\mu g/cm^2$) were irradiated at neutron fluxes of $10^8 n/cm^2/sec$ for durations of over 4000 minutes. This gave counting statistics better than 2%. Because of high tailing and relatively poor resolution the method used for the determination of cross sections in previous cases could not be directly applied to the analysis of these results. The method consisted of determining the total (n,α) cross section after subtracting the background and the contribution from Sm^{149}. The Sm^{149} contribution was calculated from the Sm^{149} content of the target and its total effective (n,α) reaction cross section. The remaining count rate in the energy region above 8 MeV was attributed to the $Sm^{147}(n,\alpha)Nd^{144}$ reaction. This count rate was then compared with that from the standard triton peak to determine the effective cross section. The integration of these spectra

Fig. 4.6. Alpha particle spectrum from the mixed Li^6-Sm^{147} target. Target thickness 120 $\mu g/cm^2$; Time for Sm^{147}=4000 minutes; Time for Li^6= 5 minutes.

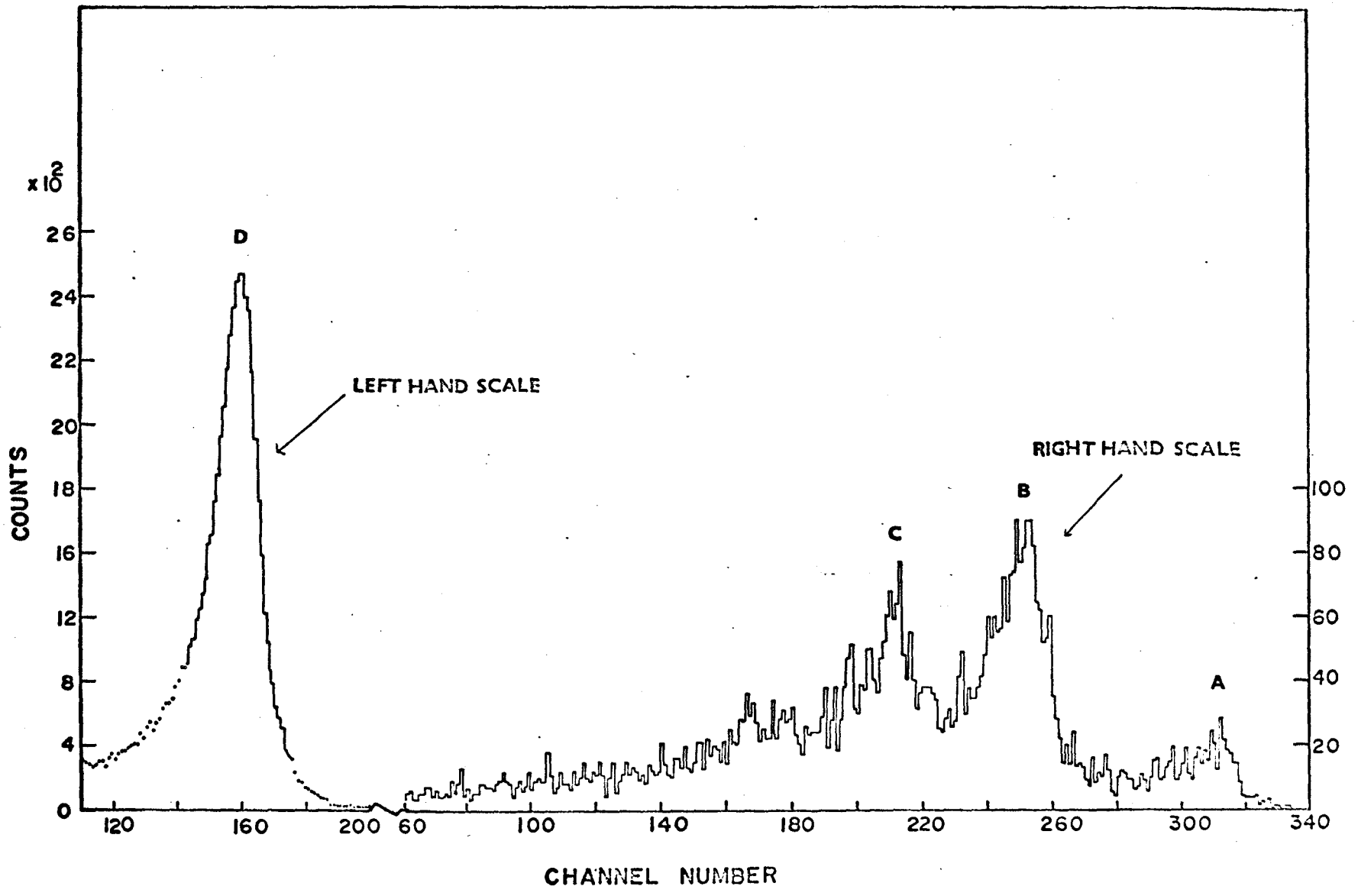
x 10²
26
24
22
20
18
16
12
8
4
0
COUNTS
D
LEFT HAND SCALE
C
B
RIGHT HAND SCALE
A
100
80
60
40
20
120
160
200
60
100
140
180
220
260
300
340
CHANNEL NUMBER

was terminated at an energy at which the counting rate was less than three percent of the peak height. The results of five independent measurements are summarized in Table 4.4. A final value of 0.894 ± 0.037 mb was obtained for the total cross section. Fig. 4.7 shows some evidence for fine structure in the low energy tail of the spectrum. In order to investigate the fine structure and to determine the relative contribution from each peak to the total (n,α) reaction cross section, an electrodeposited Sm^{147} target (~ 80 μg/cm^2) was irradiated for about 4000 minutes. The spectrum obtained in this case is shown in Fig. 4.7. It contains an additional peak D at 8.23 MeV. Peaks A, B, and C are the same as shown in 4.6. The relative intensities and cross sections as well as the energies of all the three peaks resulting from the $Sm^{147}(n,\alpha)Nd^{144}$ reaction are given in Table 4.5. The energies of peak A and B were evaluated from three independent measurements. The energy of D was obtained from the spectrum shown in Fig. 4.7. The energies of groups A and B correspond to Q-values of 10.143 ± 0.015 MeV and 9.452 ± 0.008 MeV respectively. The atomic mass difference calculations give a value of 10.143 ± 0.020 MeV[52] for the reaction $Sm^{147}(n,\alpha)Nd^{144}$. This is in excellent agreement with that corresponding to the highest energy alpha group. This means that the highest energy alpha group corresponds to the transition to the

Table 4.4 Results of Cross Section Measurements of $Sm^{147}(n,\alpha)Nd^{144}$ Reaction

Target	Thickness ($\mu g/cm^2$)	Li^6/Sm^{147} (Atom Ratio) (A)	Li^6/Sm^{147} (Count Ratio) (c)	Effective Cross Section (mb)
37	40	5.055×10^{-2}	55.390×10^{-3}	0.862±0.043
37	40	5.055×10^{-2}	54.007×10^{3}	0.883±0.046
36	80	2.527×10^{-2}	26.571×10^{3}	0.899±0.034
25	160	1.264×10^{-2}	12.938×10^{3}	0.923±0.017
21	120	1.685×10^{-2}	17.609×10^{3}	0.904±0.013
		Best Value for Effective Cross Section (mb)		0.894±0.037

Fig. 4.7. Alpha particle spectrum from electrodeposited Sm^{147} sample groups. T = 4000 minutes; Thickness ~ 80 $\mu g/cm^2$.

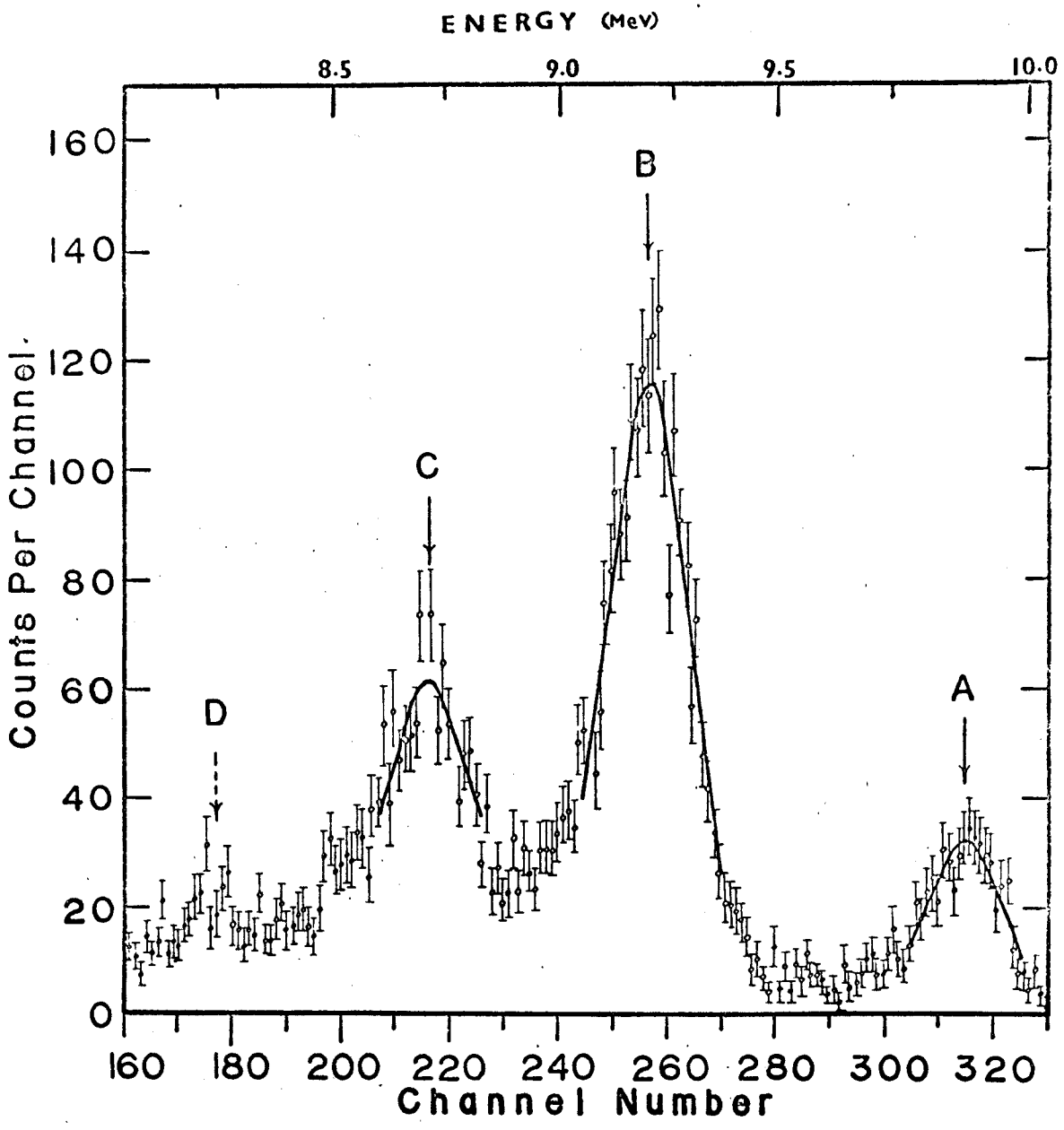
ENERGY (MeV)
8.5
9.0
9.5
10.0
160
140
120
100
80
60
40
20
0
Counts Per Channel
A
B
C
D
160
180
200
220
240
260
280
300
320
Channel Number

Table 4.5 Relative Intensities and Energies of Various Alpha Groups in $Sm^{147}(n,\alpha)Nd^{144}$ Reaction

Alpha Energy (MeV)	Relative Intensity of Alpha Group	Effective Cross Section (mb)
9.868 ± 0.015	20.6%	0.184 ± 0.012
9.196 ± 0.008	70.4%	0.629 ± 0.040
8.23 ± 0.02	9.0%	0.081 ± 0.067

ground state. Duckworth and coworkers[68] have reported a value of 10.109 ± 0.007 MeV for the same reaction from their most recent mass spectrometric studies. This value is significantly lower than our value.

The even-even daughter nucleus, Nd^{144}, has a 2^+ first excited state lying 696 keV above the ground state[69,70]. The measured Q-value for the lower energy group is consistent with the assignment of the alpha transition to this state. A decay scheme summarizing these results is shown in Fig. 4.8. Because of the large amount of tailing from higher energy alpha group, the alpha transition to the 4^+ state was not observed. The Q-value of the alpha group D(see Fig. 4.7) corresponds to an excitation energy of 1.68 MeV. No level is known at that energy which means that it can be populated by the (n,α) reaction but not by beta decay transitions. Further work with improved resolution and better counting statistics is required before any definite conclusion can be made concerning this group.

As in the case of Nd^{143} and Sm^{149}, the Sm^{147} nucleus also has a spin of 7/2 and an odd parity in its ground state[54]. The s-wave neutron interaction would therefore lead to a spin-parity $J^\pi = 4^-$ or 3^- for the capture state in Sm^{148} compound nucleus. The ground state alpha transition is parity forbidden from the 4^- states. The ground state transition is, however, observed and the situation is again very similar to that observed for Sm^{149}. Despite the

Fig. 4.8. Proposed partial alpha decay scheme of the s-wave neutron capturing state of Sm^{148}.

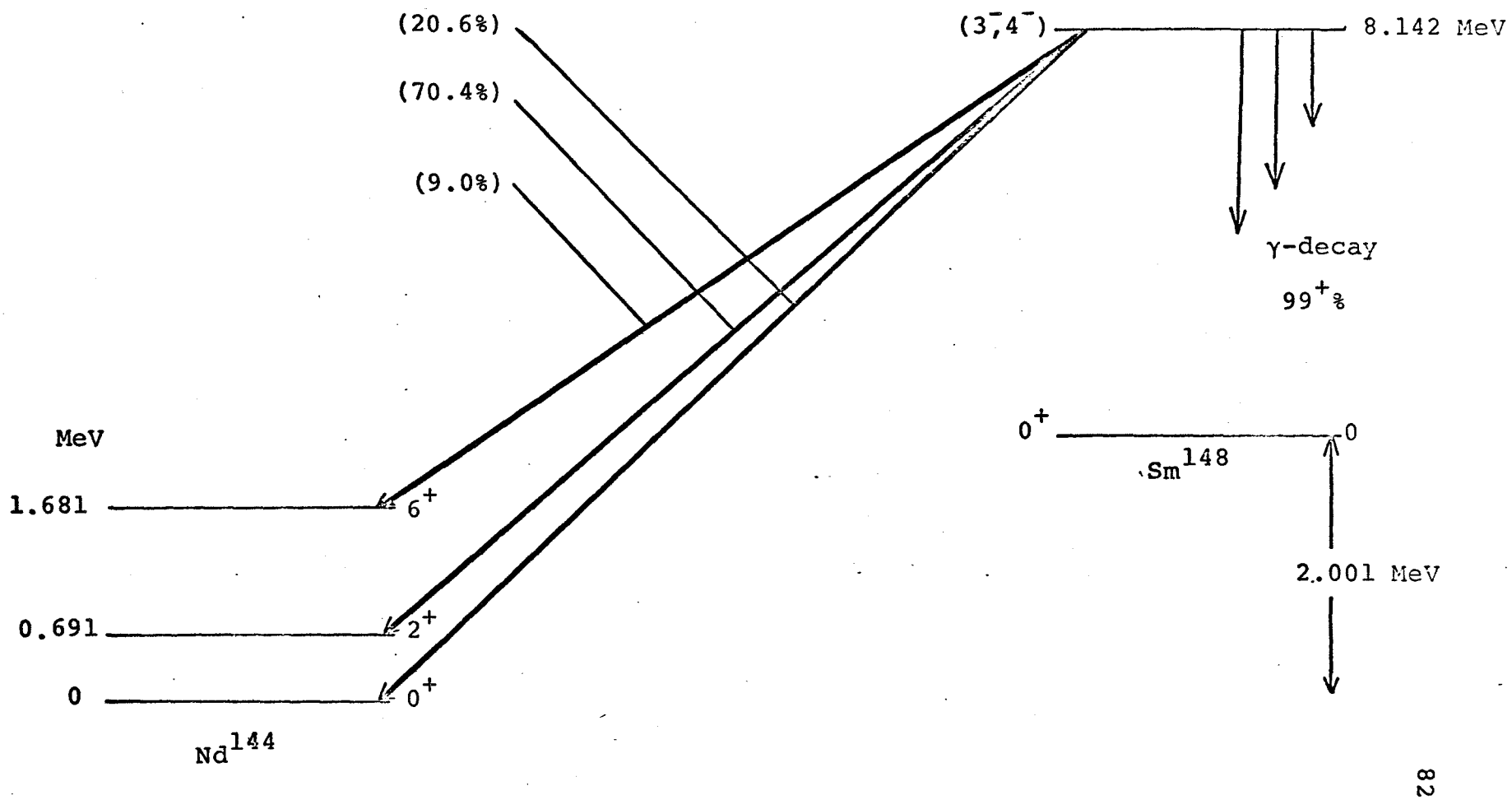
(20.6%)
(70.4%)
(9.0%)
(3⁻,4⁻)
8.142 MeV
γ-decay
99+%
MeV
1.681
6+
0.691
2+
0
0+
Nd144
0+
0
Sm148
2.001 MeV

high Q-value for this transition only 21% of the total alpha decay leads to this state. Cheifetz et al[3] explained this by postulating that the contributing resonances at 3.4 eV and 18.3 eV[56] have spins of 4^- and 3^- respectively. They did not consider the necessity of invoking the existence of a contributing bound resonance. At about the same time, however, Carpenter[71] from his study of capture gamma rays reported values of 3^- and 4^- respectively for the spins of these resonances. These values have been confirmed, more recently, by Poortmans et al[67] from neutron resonant scattering studies of Sm^{147}. The low intensity of the ground state alpha transition must then be due to some other effect.

The contribution of each resonance (3.4 eV and 18.3 eV) to the 2200 m/sec neutron absorption cross section can be calculated using the Breit Wigner formula and is found to be of the order of 5 barns. The total 2200 m/sec neutron absorption cross section is, however, 75 ± 11 barns[72]. The contribution of higher resonances is even smaller and can be disregarded. This means that a large contribution must arise from a negative resonance existing close to the neutron separation energy. The excitation function for neutron absorption in Sm^{147} has not been studied in detail and one can not entirely rule out the possibility of a contributing low energy positive resonance. The spin

of this resonance in any case must be 4^- to account for the high relative intensity of the 2^+ alpha transition. Neutron transmission measurements similar to those conducted forestablishing the existence of contributing resonances in $Nd^{143}(n,\alpha)Ce^{140}$ and $Sm^{149}(n,\alpha)Nd^{146}$ should be able to resolve this problem. Because of the low (n,α) reaction cross section, these measurements were not possible with the existing experimental set-up.

(d) $Gd^{155}(n,\alpha)Sm^{152}$ Reaction

The first positive evidence for the existence of this reaction was obtained in a set of preliminary experiments using the lucite irradiation assembly. Thick targets ($\sim$0.3 - $\sim$0.5 mg/cm^2) were irradiated for several days at neutron fluxes of the order of 10^8n/cm^2/sec. A poorly resolved alpha group was consistently observed at about 8 MeV in the alpha particle spectra obtained in these measurements. Final measurements were, however, made by using the electrostatic particle guide. In these measurements two electrodeposited mixed Nd^{143}-Gd^{155} targets with different Nd^{143}/Gd^{155} atom ratios were used. The target thickness in each case was about 80 µg/cm^2. The spectrum obtained in a 400 hour irradiation is shown in Fig. 4.9. It contains three peaks A, C and D. The peak A corresponds to the 9.443 MeV alpha group from the $Nd^{143}(n,\alpha)Ce^{140}$ reaction. The peak served as a standard both for energy and cross

Fig. 4.9. Alpha particle spectrum from Nd^{143}-Gd^{155} reaction. T = 400 hours, Thickness ~ 80 $\mu g/cm^2$.

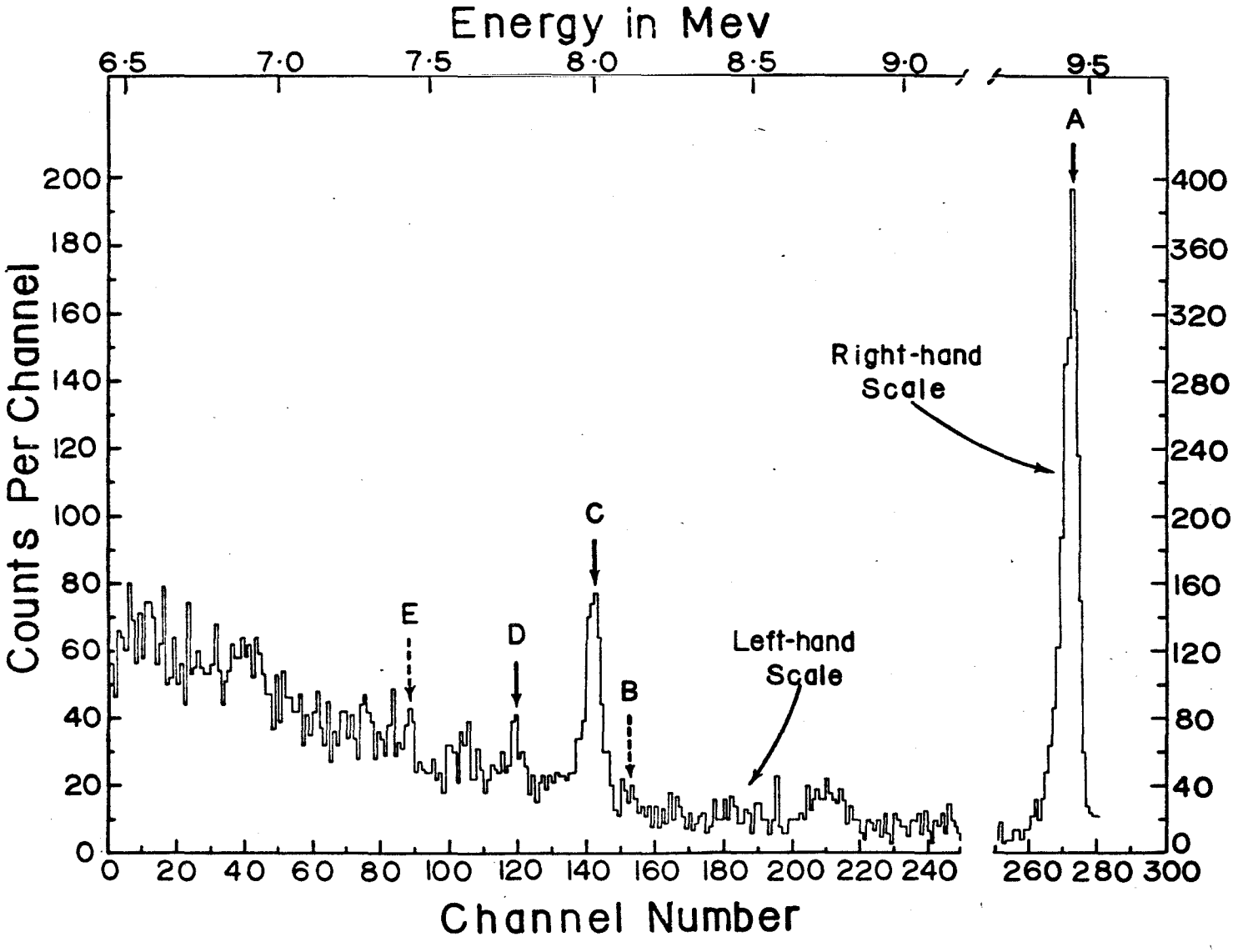
Energy in Mev
6·5
7·0
7·5
8·0
8·5
9·0
9·5
Counts Per Channel
Channel Number
A
B
C
D
E
Right-hand Scale
Left-hand Scale
0
20
40
60
80
100
120
140
160
180
200
220
240
260
280
300
360
400

section determinations. The peaks C and D are alpha groups from the $Gd^{155}(n,\alpha)Sm^{152}$ reaction. For cross section measurements it was assumed that the Gd^{155} and Nd^{143} isotopes are deposited with the same relative uniformity, and that the atom ratio remained unaffected during target preparation. The cross section for the group C was determined by comparing its integrated count rate with that of a standard peak, A. The cross section for group D was obtained from the relative intensities of peaks C and D. The results of the cross section measurements for peak C obtained in two determinations are given in Table 4.6. The average value for the cross section of this peak is 67 ± 7 microbarns. The final results for the effective cross sections and energies are given in Table 4.7. The positions B and E marked with the dotted arrow (Fig. 4.9) correspond to known levels of Sm^{152}. An upper limit for the cross section corresponding to position B has also been included in the same table.

The groups C and D have Q-values of 8.209 ± 0.006 MeV and 7.963 ± 0.009 MeV respectively. The Q-value for this reaction obtained from the atomic mass difference data is 8.355 ± 0.022 MeV[52]. This value is higher than the measured Q-value for the highest energy alpha group by 0.146 ± 0.023 MeV. The energy level diagram for Sm^{152} is well known[73]. The first excited state (2^+) lies 122 keV

Table 4.6 Results of Cross Section Measurements of Highest Intensity Peak (C) in $Gd^{155}(n,\alpha)Sm^{152}$ Reaction

Target	Thickness ($\mu g/cm^2$)	Irradiation (hrs)	Nd/Gd (Atom ratio)	Nd/Gd (Count ratio)	Effective Cross-section (μb)
G-1	80	400	16.826×10^{-3}	5.044	60±5
G-2	80	189	7.478×10^{-3}	1.806	74±8
			Average value of cross section		67±7

Table 4.7 Results of Energy and Cross Section Measurements for Various Alpha Groups in $Gd^{155}(n,\alpha)Sm^{152}$ Study

Alpha Group	Relative Intensity (%)	Particle Energy (MeV)	Effective (n,α) Cross Section (μb)
C	75.5	7.998±0.006	67±7
D	16.6	7.759±0.009	15±2
B	7.7	8.12	$\leq$ 7

above the ground state and the second excited state (4^+) is at 366 keV. If 122 keV is added to the measured Q-value for the highest energy alpha group a value of 8.331 ± 0.006 MeV is obtained. This value is in a very good agreement with the calculated Q-value for this reaction. This suggests that the highest energy alpha group, in fact, corresponds to the alpha transition to the first excited state. This is also consistent with the fact that the measured Q-value difference between the 2^+ and 4^+ states (246 ± 11 keV) is in agreement with the excitation-energy difference (244 keV) between these two levels. The values of 8.331 ± 0.006 MeV, is, therefore, associated with the alpha transition leading directly to the ground state of Sm^{152}. The alpha particle energy expected for this transition is indicated by position B in Fig. 4.9. Below the alpha group D in this figure the spectrum is too complex to obtain any information on other transitions. The position E corresponds to the alpha transition leading to the 6^+ state. A proposed decay scheme is given in Fig. 4.10.

The spin for the neutron capturing state in the compound nucleus, Gd^{156}, resulting from an s-wave interaction is 1^- or 2^-. (The Gd^{155} ground state has a spin and parity of $3/2$[54].) There exist three known resonances in the low neutron energy region at 0.0268 eV, 2.01 eV and 2.57 eV [79] and have spins 2^-, 1^- and 2^- respectively[75].

Fig. 4.10. Proposed partial alpha decay scheme of the s-wave neutron capturing state of Gd^{156}.

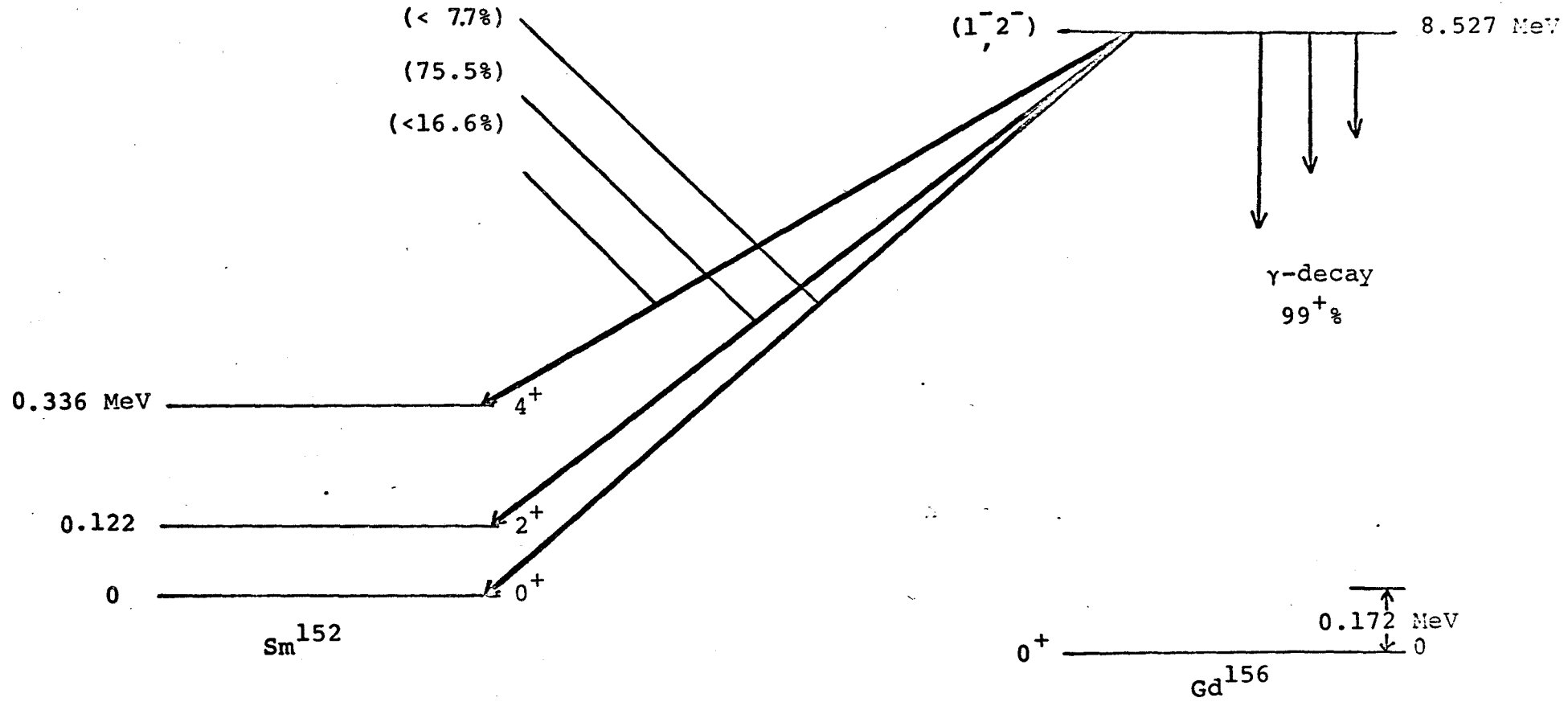
(< 7.7%)
(75.5%)
(<16.6%)
(1⁻,2⁻)
8.527 MeV
γ-decay
99⁺%
0.336 MeV
4⁺
0.122
2⁺
0
0⁺
Sm¹⁵²
0.172 MeV
0
0⁺
Gd¹⁵⁶

The 0.0268 eV resonance is the largest contributor to the 2200 m/sec neutron absorption cross section. This as well as the 2^- resonance at 2.57 eV can undergo alpha decay leading to the 2^+ state in the daughter nucleus, Sm^{152}, with alpha particles carrying $\ell = 1$ and $\ell = 3$ waves. The fact that no ground state transition was observed rules out any significant contribution from the 2.01 eV resonance or from any of the higher energy $J^\pi = 1^-$ resonances. The results obtained in the present investigation are therefore consistent with the reported spin assignment of the 0.0268 eV ($J^\pi = 2^-$) in Gd^{155}. Alpha particle emission from this capture state can also take place via $\ell = 3$ and $\ell = 5$ waves to the second excited state 4^+, in Sm^{152}.

A careful examination of the alpha particle spectrum at position B (Fig. 4.9) gives a slight indication of a ground state alpha transition. The counting statistics are too poor to make a positive identification. An upper limit of < 7 μb has been set for the magnitude of this transition.

(e) $\underline{Eu^{151}(n,\alpha)Pm^{148}}$ Reaction

The results for this reaction were based essentially on a single experiment involving the use of the electrostatic particle guide and an enriched electrodeposited mixed Nd^{143}-Eu^{151} target. The target thickness in this case corresponded to 150 μg/cm^2 deposited on a target area

of ~ 44 cm^2. The irradiation was conducted at a neutron flux of about 10^{10} $n/cm^2/sec$. The spectrum obtained after an irradiation of 170 hours is shown in Fig. 4.11. The peak A is 9.443 MeV alpha group from $Nd^{143}(n,\alpha)Ce^{140}$ reaction while peak B corresponds to an alpha group from the $Eu^{151}(n,\alpha)Pm^{148}$ reaction. The cross section corresponding to the peak intensity has been estimated to be 25 μb. The energy of this group is 7.610 ± 0.020 MeV and it corresponds to a Q-value of 7.815 ± 0.015 MeV. The Q-value for the $Eu^{151}(n,\alpha)Pm^{148}$ reaction calculated from the mass table[52] is 7.897 ± 0.031 MeV. This is considerably higher than the measured value and suggests that the observed alpha group corresponds to the first excited state. If the excitation energy of the first excited state (75 keV)[73] of the daughter nucleus, Pm^{148}, is added to the measured Q-value, a value of 7.890 ± 0.020 is obtained. This is in good agreement with the calculated Q-value. The appearance of the ground state transition is not apparent from the study of the alpha particle spectrum. The corresponding alpha group would be expected to fall at position C in the spectrum. The energy corresponding to this position is 7.680 ± 0.020 MeV. Because of a high background no information could be obtained in the lower energy region. From [illegible] of the spectrum at position C an upper limit of [illegible] for the ground state alpha transition. [illegible] is shown in Fig. 4.12.

Fig. 4.11. Alpha particle spectrum from mixed Nd^{143}-Eu^{151} target. Nd/Eu atom ratio = 3.922×10^{-3}; Nd/Eu count ratio = 2.667; Time ≃ 170 hours and target thickness ≃ 155 $\mu g/cm^2$.

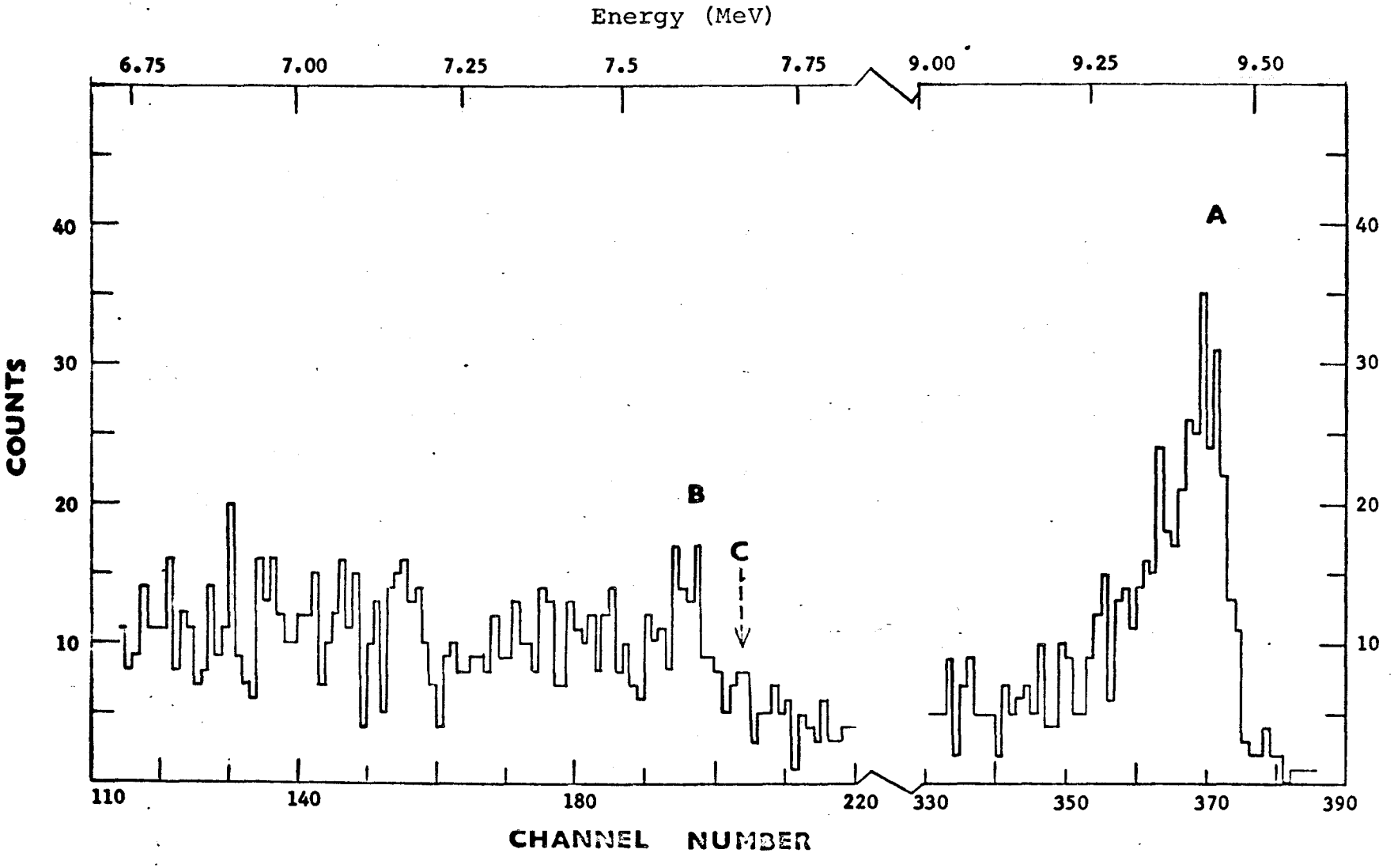
Energy (MeV)
6.75
7.00
7.25
7.5
7.75
9.00
9.25
9.50
40
30
20
10
COUNTS
A
B
C
110
140
180
220
330
350
370
390
CHANNEL NUMBER

Fig. 4.12. Proposed partial alpha decay scheme of the s-wave neutron capturing state of Eu^{152}.

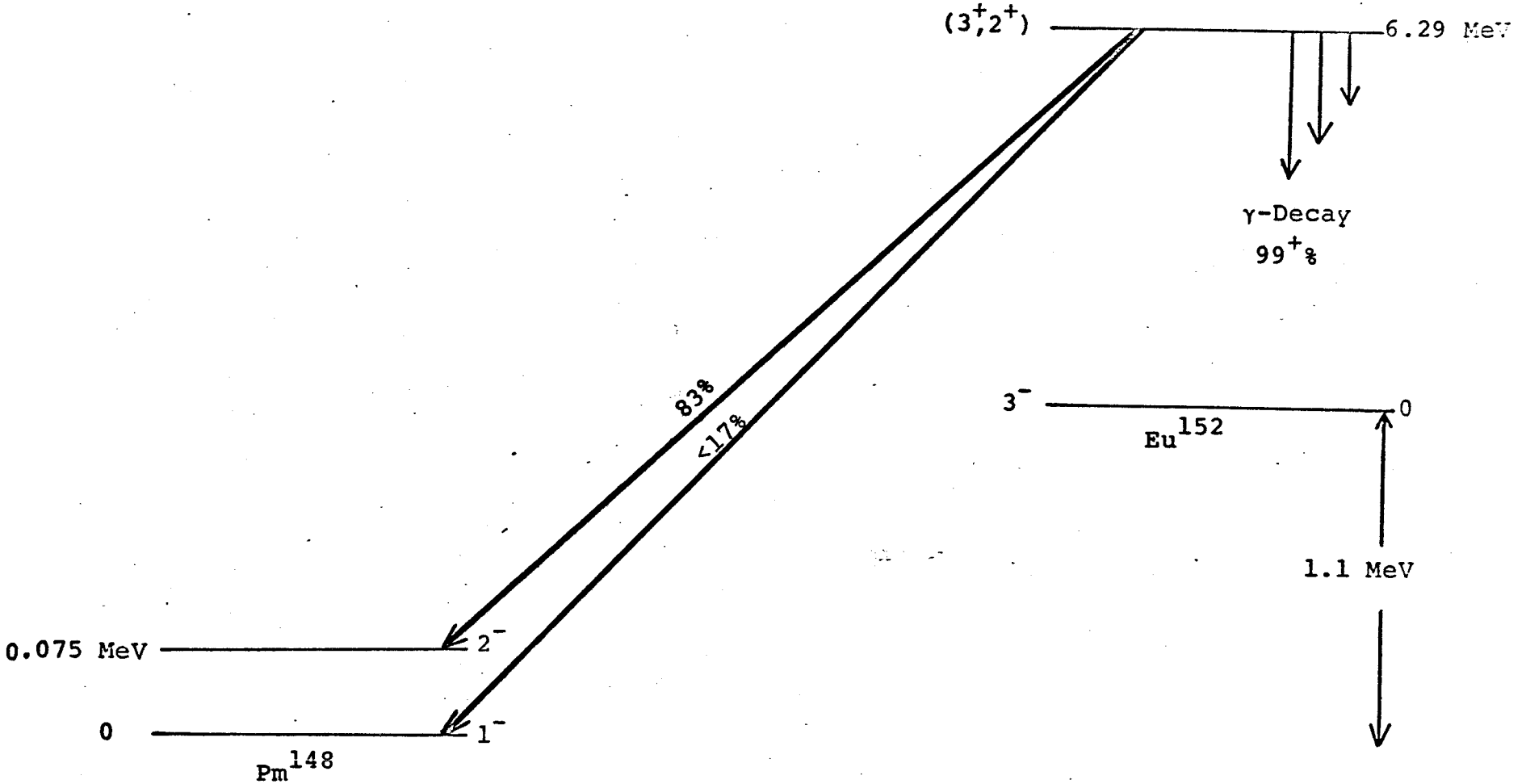
$(3^+,2^+)$
6.29 MeV
γ-Decay
$99^+\%$
3^-
0
Eu^{152}
1.1 MeV
83%
<17%
0.075 MeV
2^-
0
1^-
Pm^{148}

The spin of Eu^{151} in its ground state is 5/2[54] and its parity is even. The s-wave neutron capture will give rise to capturing states with spins of 2^+ and 3^+. The level structure of the daughter nucleus, Pm^{148}, is not well known. Its ground state spin and parity have recently been found to be 1^-[76]. The spin and parity of the first excited state is either 1^- or 2^-[81]. The main contributions to the 2200 m/sec neutron absorption cross section of Eu^{151} arise from resonances at neutron energies 0.32 eV, 0.46 eV, 1.06 eV and 3.37 eV[77,78]. In addition, a large contribution also results from a bound resonance[79] existing close to the neutron binding energy. The contribution from the 3.37 eV resonance is expected to be very small in the region of thermal energies. The spins and parities of the negative and the first three positive resonances are 3^+[75]. The high relative intensity of the alpha transition to the first excited state is more consistent with a spin of 2^- rather than 1^-. Alpha decay to this state would be more enhanced from angular momentum considerations. Alpha decay from the 3^+ capture state to the 2^- state in the daughter nucleus is possible with $\ell = 1,3$ and 5 alpha waves while only $\ell = 3$ would be possible if the spin of this state was 1^-.

CHAPTER V

COMPARISON OF EXPERIMENT AND THEORY

(a) Cross Sections and Reduced Widths

The main objective in this section is to make a comparative study between the measured and the calculated values of (n,α) cross sections and the alpha emission reduced widths, as well as to compare the measured Q_α and the cross section values with those obtained by other workers.

The experimental results on Q_α and cross section values obtained by other workers have been compared with the present results in Table 5.1. Only those values from other works are included for which data have been obtained in the present work. Except for Gd^{155} and Eu^{151}, the experimental values for Q_α and cross sections agree with the older work and are generally more precise. The most recent high resolution work by Oakey (ref e) has confirmed the results of our fine structure study in Sm^{149}. The (n,α) reaction in Gd^{155} has been observed for the first time and there is only one previous value for $Eu^{151}(n,\alpha)Pm^{148}$ reaction[5]. Our results do not agree with theirs and further work is needed to resolve this discrepancy. The last column of Table 5.1 includes the Q-values for the different (n,α) reactions obtained from the mass difference data[52]. In the same column

Table 5.1 Experimental Results on (n,α) Cross Sections

Target	State of Daughter	Q_α(MeV) (n,α) work	$\hat{\sigma}_{eff}$ (mb)	Ref.	Q_α(MeV) from Mass Data
Nd^{143}	0^+	9.71 ± 0.06	16 ± 4	b	
		9.7	23 + 5	c	9.732 + 0.022
		9.713± 0.005	21.28± 0.18	f	(9.714 ± 0.010)
Sm^{149}	0^+	9.38 ± 0.04	22 ± 10	a	
		9.45 + 0.07	5 ± 1.5	b	
		9.6	7 ± 3	c	9.460 ± 0.020
		9.40	8.5 ± 1.5	d	(9.426 ± 0.005)
		9.429± 0.004	5.29± 0.005	e	
		9.429± 0.004	5.23± 0.17	f	
	2^+	8.96 ± 0.04	211 ± 22	a	
		-	37 ± 10	b	
		9.1	48 ± 10	c	
		-	46 ± 10	d	
		8.974± 0.004	38.70± 0.45	f	
	4^+	8.385± 0.006	0.67± 0.04	e	
		8.384± 0.010	0.61± 0.05	f	
	3^-	8.238± 0.006	0.81± 0.005	e	
		8.219± 0.010	0.66 ± 0.006	f	

Table.5.1 Experimental Results on (n,α) Cross Sections (cont'd)

Target	State of Daughter	Q_α (MeV) (n,α) work	$\hat{\sigma}_{eff}$ (mb)	Ref.	Q_α from Mass Data
Sm^{147}		10.09 ± 0.006	0.16 ± 0.05	b	
	0^+	10.1	-	c	10.143 ± 0.020
		10.143± 0.015	0.184± 0.012	f	(10.109 ± 0.007)
	2^+	9.40	0.53 ± 0.15	b	
		9.452 ± 0.008	0.629± 0.04	f	
	6^+ (?)	8.46 ± 0.02	0.081± 0.067	f	
Gd^{155}	0^+	8.331 ± 0.006	<0.007	f	8.355 ± 0.022
	2^+	8.209 ± 0.006	0.067± 0.007	f	
	4^+	7.963 ± 0.009	0.015± 0.002	f	
Eu^{151}	1^-	7.890 ± 0.020	<0.005	f	7.897 ± 0.031
	2^-	7.815 ± 0.015	0.025+ 0.003	f	
		7.9	0.009± 0.002	c†	

a. R.D. Macfarlane and I. Almodovar; Phys. Rev. 127, 1665 (1962).
b. E. Cheifetz et al; Phys. Letters 1, 289 (1962).
c. V. N. Andreev et al; Jaderna Fizika 1,252 (1965).
d. M. Dakowski et al; Nucl. Phys. A97, 187 (1967).
e. N. S. Oakey, Ph.D. Thesis, McMaster University (1967).
f. Present work

† This is the total for all transitions in the neighbourhood.

Note: Work on Nd and Sm isotopes was completed before the results of ref. c,d, and e became available.

the parenthesized values are those obtained most recently by Duckworth and his colleagues[68] from mass spectrometric measurements. While our Q-values for Nd^{143} and Sm^{149} show excellent agreement with those of Duckworth and coworkers the Sm^{147} result is significantly different from their value. However, the results of Sm^{147}, Eu^{151} and Gd^{155} are in good agreement with the mass table data[52].

The calculations for the (n,α) reaction cross sections are based on the statistical model approach. The results of these calculations have been compared with the measured values under the individual isotope headings.

The basis for calculations of the effective (n,α) reaction cross section ($\hat{\sigma}$) has been discussed earler in part (b) of Chapter I. The equation (1.11) which was used in these calculations was extended to include the various ℓ-values associated with the emitted α-particles. The method used here is essentially the one adopted by Macfarlane and Almodovar[2]. The effective (n,α) cross section, $\hat{\sigma}_I^J(n,\alpha)$, for the alpha decay from the capture state J to the daughter state I was calculated from the following expression

$$\hat{\sigma}_I^J(n,\alpha) = \frac{\sum \Gamma_\alpha{}^J(I,\ell)}{\Gamma_\gamma(J)} \times \hat{\sigma}^J(n,\gamma) \qquad (5.1)$$

$\Gamma_\alpha{}^J(I,\ell)$ and $\Gamma_\gamma(J)$ are the partial widths for alpha and gamma emission respectively and $\hat{\sigma}^J(n,\gamma)$ is the effective n,γ reaction cross section. For the present calculations we

assumed that the neutrons in the thermal column follow a true Maxwellian distribution (T = 300°K). Under this condition the value for $\hat{\sigma}^J(n,\gamma)$ was obtained by taking a product of the 2200 m/sec neutron absorption cross section ($\sigma_o{}^J$) and the temperature dependent parameter, g, (see Chapter II). The value for $\Gamma_\alpha{}^J(I,\ell)$ was obtained from equation (5.2)

$$\Gamma_\alpha{}^J(I,\ell) = \frac{D}{2\pi} P_\ell \qquad (5.2)$$

P_ℓ is the barrier penetrability factor for an ℓ-wave α particle of energy E and D is the average level spacing for levels with the same spin and parity near the capturing state. The penetrability factor has been defined earlier in Chapter I (equation (1.1). Its values for different ℓ-waves were calculated by using the method of Rasmussen[28]. Once the $\Gamma_\alpha{}^J(I,\ell)$ values for the various alpha transitions were obtained the evaluation of the $\hat{\sigma}_I^J(n,\alpha)$ was straightforward. However, in cases where more than one resonance contributed to the total 2200 m/sec neutron absorption cross section it was necessary to treat the contribution from each state separately. In cases where these contributions were not available in the literature, the Breit Wigner single level formula was used to determine these contributions. The resonances which do not contribute significantly were neglected.

In order to determine the values for the various alpha reduced widths, δ^2_{exp}, equation (1.4) was used in a simplified

form as given below.

$$\delta^2_{exp} = \frac{2\pi\Gamma_\gamma}{\sum_\ell P_\ell} \times \frac{\hat{\sigma}^J_I(n,\alpha)}{\hat{\sigma}^J(n,\gamma)} \qquad (5.3)$$

The symbols appearing in this equation have the same significance as defined previously. In cases where both types of spin states (resulting from the s-wave neutron capture) contribute, equation (5.3) must be modified. The nuclides Sm^{149} and Sm^{147} provide examples of such cases. In these cases the transitions to the excited states in the corresponding daughter nuclei Nd^{146} and Nd^{144} result both from the 4^- and the 3^- capture states of Sm^{150} and Nd^{148} compound nuclei respectively. The reduced width in these cases was obtained from the following expression

$$\delta^2_{exp} = 2\pi\hat{\sigma}_I(n,\alpha) \left[\frac{\sigma^{3-}(n,\gamma)}{\Gamma_\gamma(3^-)} \sum_\ell P_\ell + \frac{\sigma^{4-}(n,\gamma)}{\Gamma_\gamma(4^-)} \sum_\ell P_\ell\right]^{-1} \qquad (5.4)$$

In these calculations it was assumed that $\Gamma_\gamma 3^-) = \Gamma_\gamma(4^-) \simeq \Gamma$.

(1) Neodymium-143. The theory for the calculation of (n,α) reaction cross section in its simplified form, as described above, can not be applied for this isotope. Its total 2200 m/sec neutron cross section is 410 barns of which 75 barns is due to neutron scattering. The scattering cross section is obviously too large to be ignored relative to the (n,γ) cross section. The approximation that the partial gamma width $\Gamma_\gamma(J)$ is very nearly

equal to the total width, Γ, is no longer valid. We have therefore used the relationship

$$\hat{\sigma}_I^J(n,\alpha) = \left[\hat{\sigma}^J(n,n) + \hat{\sigma}^J(n,\gamma)\right] \frac{\sum_\ell \Gamma_\alpha^J(I,\ell)}{\Gamma_\gamma(J)+\Gamma_n(J)} \qquad (5.5)$$

The values for the partial widths, $\Gamma_\gamma(J)$, $\Gamma_n(J)$ and σ_o^J were taken from reference (55). The value for the g factor required to convert the σ_o^J value to the effective cross section was taken from reference (61). Its value at 300^oK is 0.981. The σ_o has its main contribution from the bound state[55]. The first positive resonance is at 56 eV[49] and its contribution is negligibly small. The results of these calculations have been summarized in Tables 5.2 and 5.4. Table 5.2 presents the calculated values for P_ℓ and $\Gamma_\alpha^J(I,\ell)$. In order to calculate $\Gamma_\alpha^J(I,\ell)$ a value of 33 eV[80] was used for D. Since the spin-parity of the contributing state is 3^-, only $\ell=3$ wave alpha particles are possible for the ground state (0^+) alpha transition. Table 5.3 compares the calculated effective (n,α) cross section values with the corresponding measured values. The agreement between them is satisfactory.

(a) Samarium-149. The 2200 m/sec neutron absorption cross section (σ_o = 39900 barns)[61] for this isotope has its major contributions from two resonances, one negative[61,65] and the other positive (0.0967 eV)[61]. The largest contribution results from the positive energy resonance ($J^\pi = 4^-$). A relatively smaller contribution with a '1/v' behaviour comes from the negative resonance ($J^\pi = 3^-$)[61,65]. According

Table 5.2 Alpha Penetrability and Partial Width for $Nd^{143}(n,\alpha)Ce^{140}$ Reaction

Q_α (MeV)	Alpha Particle ℓ-wave	Penetrability (P_ℓ)	$\Gamma_\alpha^J(I,\ell)$ (eV)	$\frac{\Gamma_\alpha^J(I,\ell)}{\Gamma_\gamma(J)}$
9.713	3	2.79×10^{-6}	14.65×10^{-6}	15.10×10^{-5}

Table 5.3 Effective Cross Sections and Reduced Widths for $Nd^{143}(n,\alpha)Ce^{140}$ Reaction

Transition	(total) (barns)	$\hat{\sigma}_I(n,\alpha)$		δ^2_{Expt} (eV)
		Calc.	Exp.	
$3^- \rightarrow 0^+$	402	60.7	21.28 ± 0.18	11.5

to Pattenden its value is 4800 barns[61]. From Hohne's work, however, its value is only 2200 barns [65]. Since the ground state alpha transition results only from the 3^- bound state the smaller contribution is quite important for the present calculations. Both these values for the capture cross section from this state have been used for the evaluation of the (n,α) reaction cross sections and the alpha emission reduced widths. Since Hohne's value for the total absorption cross section does not differ very significantly from the value given by Pattenden, only Pattenden's value (39900 barns)[61] for the total cross section was used for these calculations. The alpha transitions leading to the 2^+, 4^+ and 3^- states of the daughter nucleus can originate from both the 3^- and 4^- states. The various possible ℓ-values and the corresponding calculated alpha particle penetrability, P_ℓ, for all of the four observed alpha transitions are given in Table 5.4 From these values of P_ℓ, $\Gamma_\alpha^J(I,\ell)$ were calculated from equation (5.2) using a value for D = 6.6 eV[38]. These values as well as the values for the ratios between these and the partial gamma widths $\Gamma_\gamma(J)$ have also been included in Table 5.4 It was assumed that $\Gamma_\gamma(3^-) = \Gamma_\gamma(4^-) = \Gamma_\gamma(J)$. Its value (0.058 eV) was taken from reference (61). These numbers were those used to evaluate the effective (n,α) reaction cross sections and the alpha emission reduced widths. In order to calculate

Table 5.4 Penetrabilities and Partial Widths for α-Transitions in $Sm^{149}(n,\alpha)Nd^{146}$ Reaction

Q_α(MeV)	α-particle ℓ-wave	Penetrability (P_ℓ)	$\Gamma_\alpha^J(I,\ell)$ (eV)	$\frac{\Gamma_\alpha(I,\ell)}{\Gamma_\gamma{}^J(J)}$
9.429	3	3.58×10^{-7}	3.77×10^{-7}	6.49×10^{-6}
8.974	1	1.72×10^{-7}	1.81×10^{-7}	3.12×10^{-6}
8.974	3	6.71×10^{-8}	7.05×10^{-8}	1.21×10^{-6}
8.974	5	1.26×10^{-8}	1.32×10^{-8}	2.28×10^{-7}
8.384	1	1.60×10^{-8}	1.68×10^{-8}	2.89×10^{-7}
8.384	3	6.08×10^{-9}	6.38×10^{-9}	1.10×10^{-7}
8.384	5	1.09×10^{-9}	1.15×10^{-9}	1.98×10^{-8}
8.384	7	9.60×10^{-11}	1.01×10^{-10}	1.74×10^{-9}
8.219	0	9.51×10^{-9}	9.98×10^{-9}	1.72×10^{-7}
8.219	2	5.29×10^{-9}	5.56×10^{-9}	9.58×10^{-8}
8.219	4	1.37×10^{-9}	1.44×10^{-9}	2.47×10^{-8}
8.219	6	1.69×10^{-10}	1.77×10^{-10}	3.05×10^{-9}

the reaction cross sections, the σ_o^J values from both contributing states were converted to their corresponding effective cross section values. The g factor used for the contribution from the 3^- state was taken as 1. Its value for the 4^- resonance at 300^oK is 1.72[61]. The reduced widths were calculated using equations (5.3) and (5.4) the results of these calculations are shown in Tables 5.5 and 5.6. Table 5.5 summarizes the calculated effective n,α reaction cross sections corresponding to different ℓ-values of the alpha transitions resulting from both the states, 3^- and 4^-. The total calculated effective (n,α) reaction cross sections for the different α-transitions have been compared with the corresponding experimental values in the same table. In Table 5.6 are the experimental values for the reduced widths (δ^2_{expt}). The columns marked (1) and (2) in both the tables 5.6 and 5.7 correspond to calculations using 4800 barns[61] and 2200 barns[65] respectively for the neutron capture cross section (σ_o^J) from the $J = 3^-$ resonance.

The calculated values for the effective (n,α) reaction cross sections are, in general, an order or two higher magnitude than those obtained experimentally and no definite trend appears to exist. It is interesting, however, to note that the calculated value for $\sigma_{2^+}/\sigma_{o^+}$ agrees well with the experimental value. The agreement between theory and experiment is good when the calculations were based on Höhne's value for σ_o^J (2200 barns) from the 3^- resonance. These results are shown below. The values marked (1) and (2)

Table 5.5 Cross Sections for α-transitions in $Sm^{149}(n,\alpha)Sm^{146}$ Reaction

Transition	ℓ	$\hat{\sigma}^{(1)}_{n,\gamma}$(a) (barns)	$\hat{\sigma}^{(1)}_{n,\alpha}$(a) (mb)	$\hat{\sigma}^{(2)}_{n,\gamma}$(b) (barns)	$\hat{\sigma}^{(2)}_{n,\alpha}$(b) (mb)	$\hat{\sigma}_{n,\alpha}$(Exp) (mb)
$3^- \rightarrow 0^+$	3	4800	31.2	2200	14.3	
Total to 0^+ (σ_{0^+})			31.2		14.3	5.23
$4^- \rightarrow 2^+$	3	60372	73.3	64844	78.8	
	5	60372	13.7	64844	14.8	
$3^- \rightarrow 2^+$	1	4800	14.9	2200	6.8	
	3	4800	5.8	2200	2.6	
	5	4800	1.1	2200	0.5	
Total to 2^+ (σ_{2^+})			108.8		103.5	38.7
$4^- \rightarrow 4^+$	1	60372	17.4	64844	18.7	
	3	60372	6.6	64844	7.1	
	5	60372	1.2	64844	1.3	
	7	60372	0.1	64844	0.1	
$3^- \rightarrow 4^+$	1	4800	1.4	2200	0.6	
	3	4800	0.5	2200	0.2	
	5	4800	0.1	2200	0.04	
	7	4800	0.01	2200	0.004	
Total to 4^+ (σ_{4^+})			27.3		29.0	0.61
$4^- \rightarrow 3^-$	2	60372	5.8	64844	6.2	
	4	60372	5.8	64844	6.2	
	6	60372	1.5	64844	1.2	
$3^- \rightarrow 3^-$	0	4800	0.8	2200	0.4	
	2	4800	0.4	2200	0.2	
	4	4800	0.1	2200	0.04	
	6	4800	0.01	2200	0.004	
Total to 3^- (σ_{3^-})			8.8		8.64	0.66

Table 5.6 Reduced Widths for α-transitions in $Sm^{149}(n,\alpha)Nd^{146}$ Reactions

Q (MeV)	State of Daughter Nucleus	δ^2_{Expt} (eV)	
		(1)	(2)
9.429	0^+	1.11	2.42
8.974	2^+	2.34	2.40
8.384	4^+	0.15	0.14
8.219	3^-	0.49	0.50

correspond to σ_o^J values 4800 barns and 2200 barns respectively.

$\sigma_{2^+}/\sigma_{o^+}$		
Calc		Expt.
(1)	(2)	
3.5	7.2	7.4

A general discussion of the reduced width will be left until the end of this chapter after the results of the studies of other isotopes have been presented.

(3) Samarium-147. It was mentioned earlier in section (c) of Chapter IV that in addition to the known resonances at 3.4 eV ($J^\pi = 3^-$) and 18.3 eV ($J^\pi = 4^-$)[67,71] the contribution of a negative energy resonance ($J^\pi = 4^-$) near the neutron separation energy must be assumed to explain the relative intensities of the α-transitions observed in the $Sm^{147}(n,\alpha)Nd^{144}$ reaction. It was also pointed out that the σ_o^J values for the (n,γ) reaction from these resonances should be ~65, 5 and 5 barns for the negative and the positive resonances respectively. Using these values for the (n,γ) cross sections and the spin parity combination as given above, we have calculated the (n,α) reaction cross sections and reduced widths for the various α-transitions. These results have been compared with the corresponding experimental values.

In order to calculate $\hat{\sigma}_I^J(n,\alpha)$ values (equation 5.1) the factor g was required to convert the $\sigma_o^J(n,\gamma)$ values to the corresponding $\hat{\sigma}^J(n,\gamma)$ values. For these calculations, it was assumed to be unity. This value should not be very different from the true value, since the excitation function near the thermal region has very nearly a 1/v behaviour. It was also assumed that the gamma widths for all the three resonances are equal and a value 0.063 eV[56] was used. The calculated P_ℓ values are shown in Table 5.8. Using these P_ℓ values and a value of 14 eV[38] for the level spacing, D, $\Gamma_\alpha^J(I,\ell)$ values for the different α-transitions were evaluated. These values as well as the ratios between them and the partial gamma width $\Gamma_\gamma(J)$ have been included in the same table. The spin and parity of the state in the daughter nucleus, Nd^{144}, populated by the lowest energy α-transition (Q_α = 8.46 MeV) is not known. For the present calculations this was taken as 6^+. The contributions from ℓ-values of 7 and 9 were ignored in this case, since they are exceedingly small. Table 5.8 compares the calculated cross sections for the three α-transitions with their experimental values. The reduced widths, δ^2_{exp} are also included in the same table. The calculated cross section values are higher than the measured values except for the lowest energy group. The assumption of the spin and parity of the lowest energy group however, is probably not a good one. The situation for the first excited

Table 5.7 Penetrabilities and Partial Widths for α-Transitions in $Sm^{147}(n,\alpha)Nd^{144}$ Reaction

Q_α (MeV)	Alpha Particle ℓ-wave	Penetrability (P_ℓ)	$\Gamma_\alpha(I,\ell)$ (eV)	$\frac{\Gamma_\alpha(I,\ell)}{\Gamma_\gamma(J)}$
10.143	3	3.49×10^{-6}	1.56×10^{-5}	24.71×10^{-5}
9.452	1	9.00×10^{-7}	4.01×10^{-6}	63.68×10^{-6}
9.452	3	3.56×10^{-7}	1.59×10^{-6}	25.21×10^{-6}
9.452	5	6.86×10^{-8}	3.06×10^{-7}	48.52×10^{-7}
8.46	3	7.76×10^{-9}	1.73×10^{-8}	27.45×10^{-8}
8.46	5	1.39×10^{-9}	3.11×10^{-9}	49.30×10^{-9}
8.46	7	1.23×10^{-10}	2.73×10^{-10}	43.36×10^{-10}
8.46	9	5.51×10^{-12}	-	-

Table 5.8 Cross Sections and Reduced Widths for α-transitions in the $Sm^{147}(n,\alpha)Nd^{144}$ Reaction

Transition	Resonance	α-particle ℓ-wave	$\hat{\sigma}^J(n,\alpha)$ barns	$\hat{\sigma}(n,\alpha)$ (mb) Calc.	Expt.	δ^2_{Expt} (eV)
$3^- \rightarrow 0^+$	unbound	3	5	1.230		
Total to 0^+				1.230	0.184	4.17
$4^- \rightarrow 2^+$	bound	3	65	1.630		
		5	65	0.320		
$3^- \rightarrow 2^+$	unbound	1	5	0.318		
		3	5	0.126		
		5	5	0.024		
$4^- \rightarrow 2^+$	unbound	3	5	0.126		
		5	5	0.024		
Total to 2^+				2.573	0.629	6.85
$4^- \rightarrow 6^+$	bound	3	65	0.020		
		5	65	0.003		
$3^- \rightarrow 6^+$	unbound	3	5	0.001		
$4^- \rightarrow 6^+$	unbound	3	5	0.001		
Total to 6^+				0.025	.081	4.6

state and the ground state appears to be similar to that observed in Sm^{149}. The calculated value for the ratio $\sigma_{2^+}/\sigma_{o^+}$ is 2.1. This is consistent with the experimental value of 3.4 for this measurement.

(4) Gadolinium-155. The main contribution to the 2200 m/sec neutron cross section for this isotope comes from a 0.0268 eV resonance[74] ($J^\pi = 2^-$)[75]. The Breit-Wigner calculation using the resonance parameters for this level gives a value of 60916 ± 500 barns which is essentially the total 2200 m/sec neutron cross section value. Similar calculations yield only ~ 10 barns for the σ_o^J value from the 2.01 eV resonance[74] ($J^\pi = 1^-$). The contributions from higher resonances are negligible.

In order to calculate the effective (n,α) reaction cross sections, the values for D, g, $\Gamma_\gamma(J)$ used were 4.2 eV, 0.85 and 0.108 eV respectively (references 38, 61 and 74). Table 5.9 gives the results of calculations for P_ℓ, $\Gamma_\alpha^J(I,\ell)$ and $\Gamma_\alpha^J(I,\ell)/\Gamma_\gamma(J)$ for α-transitions leading to the 2^+ and 4^+ states in Sm^{152} nucleus. The calculated values for the effective (n,α) reaction cross sections are summarized in Table 5.10 which also includes experimental values.

The calculated cross sections for the 2^+ and 4^+ transitions are higher than the corresponding experimental values. This trend is similar to the one observed in all

Table 5.9. Penetrabilities and Partial Widths for α-transitions in $Gd^{155}(n,\alpha)Sm^{152}$ Reaction

Q_α (MeV)	α-particle ℓ wave	Penetrability (P_ℓ)	$\Gamma_\alpha^J(I,\ell)$ (eV)	$\frac{\Gamma_\alpha^J(I,\ell)}{\Gamma_\gamma(J)}$
8.209	1	1.98×10^{-9}	1.32×10^{-9}	1.22×10^{-8}
8.209	3	7.75×10^{-9}	5.06×10^{-9}	4.68×10^{-9}
7.963	3	2.35×10^{-10}	5.06×10^{-10}	1.45×10^{-9}
7.963	5	4.20×10^{-11}	2.81×10^{-11}	2.59×10^{-10}

Table 5.10 Cross Section and Reduced Widths for α-transitions in $Gd^{155}(n,\alpha)Sm^{152}$ Reaction

Transition	Alpha Particle ℓ-wave	$\hat{\sigma}_I(n,\alpha)$ (μb) Calc	Expt.	δ^2_{Expt} (eV)
$2^- \longrightarrow 2^+$	1	688		
	3	263		
total to 2^+		951	67±5	0.31
$2^- \longrightarrow 4^+$	3	82		
	5	14		
total to 4^+		96	15±2	0.70

previous cases. The calculations give a value of ~ 10 for the ratio of σ_{2+}/σ_{4+} while the experimental value is ~ 5.

An examination of the results presented in this section show that the calculated values for the (n,α) reaction cross section are within an order of magnitude of the experimental values. The calculated values are in general higher than the corresponding experimental values. The results indicate that the statistical model approach, based on a number of simplified assumptions can predict (n,α) cross sections only very crudely. It is, however, interesting to note that the ratios between the calculated values of cross sections for different α-transitions are comparable with those obtained experimentally.

The experimental alpha reduced widths obtained in the present work are orders of magnitude smaller than those expected from the ground state to ground state α-transitions. This reflects the very complex nature of the capture states. Except for Nd^{143} where the transition to the ground state has relatively large reduced width, the general trend in all cases, nevertheless, is similar. The large reduced width for the ground state transition in Nd^{143}, is most likely related to the large level spacing which arises from the effect of the 82 neutron closed shell.

(b) Neutron Transmission Measurements

The neutron transmission measurements were performed to learn something about the spins of the contributing resonances in the Sm^{149} thermal neutron capture cross section. We also wished to establish the origin of the ground state alpha transitions both in the $Sm^{149}(n,\alpha)Nd^{146}$ and the $Nd^{143}(n,\alpha)Ce^{140}$ reactions. The experimental details have already been outlined in part (f) of Chapter III. Here we intend to show how the results obtained in these measurements, supported by the theoretical calculations, have established that the 0^+ alpha transitions observed both in Sm^{149} and Nd^{143} result mainly from the bound 3^- states and that the 2^+ alpha transition in Sm^{149} has its origin mainly in the 0.0967 eV positive 4^- resonance.

As outlined in Chapter III, we used both Li^6 and natural Sm absorbers for the Sm^{149} work and only Li^6 absorbers for Nd^{143}. The basis of these experiments was to study the effect of perturbing the flux distribution on the relative intensities of the various alpha and triton groups observed for the mixed rare earth and Li^6 targets. The overall effect of the '1/v' and resonance absorbers is a preferential depression in the flux distribution for the lower neutron energies and the resonance energy regions respectively.

Let us first consider the case of Sm^{149}. If we assume for the purposes of discussion that the '1/v' compo-

nent not associated with the 0.0967 eV resonance, comes from the negative resonance we can at least predict the effect of perturbing the flux on the relative intensities of the two main alpha transitions in Sm^{149}. In our first measurement using an enriched Sm^{149} target we observed an increase in the ratio of α-intensities, I_{2^+}/I_{o^+} from 7.7 with no absorber to 9.9 with a Li^6 absorber and a decrease to 5.9 with a Sm absorber. These observations are consistent with the postulate that the 0.0967 eV resonance is a 4^- and that a 3^- negative resonance does exist. The results of a more detailed investigation using Li^6 absorvers of varying concentration and an electrodeposited Li^6-Sm^{149} target (~ 72 μg/cm^2) have been given in Table (5.11).This table contains the measured values for the ratios of intensities of the triton group (I_T) from $Li^6(n,\alpha)$ reaction and the 0^+ α-transition (I_{o^+}) and the 2^+ α-transition (I_{2^+}) both from the $Sm^{149}(n,\alpha)Nd^{146}$ reaction. These results show an increase in I_{2^+}/I_{o^+}, a decrease in I_T/I_{2^+} and no change in I_T/I_{o^+} with an increasing concentration of the Li^6 absorber. They also show that the alpha group corresponding to the ground state transition follows the same behaviour as the triton and therefore is associated with a '1/v' cross section. Fig. 5.1 shows the effect of Li^6 absorbers of two different concentrations on the particle spectrum. The results of three independent measurements with the Sm absorber using the same absorber concentrations are given

Table 5.11 Li^6-Absorbers and Relative Intensities of Triton -Alpha Peaks in Transmission Measurements Using Sm^{149}-Li^6 Target

Experiment	Concentration of Absorber (mg/cc)	Relative Intensities of Peaks		
		I_{2^+}/I_{o^+}	I_T/I_{2^+}	I_T/I_{o^+}
1	Blank	7.97±.53	77.2±1.8	548.9±33.5
2	2.90	7.68±.61	67.6±1.6	498.4±60.0
3	5.80	7.64±.58	74.3±1.7	586.0±38.0
4	11.60	8.92±.65	61.7±1.5	545.5±40.0
5	23.20	9.12±.93	71.7±2.4	565.0±49.0
6	27.38	9.45±1.20	55.5±2.1	536.7±63.0
7	32.48	9.56±1.0	54.9±3.2	628.0±123.0
8	37.12	9.40±1.10	62.9±2.3	577.0±63.0
9	43.15	12.9 ±1.2	49.6±1.7	640.0±76.0
*10	46.40	11.6 ±1.3	---	---
*11	18.56	9.30±.71	---	---

*I_T/I_{2^+} and I_T/I_{o^+} could not be determined because the detector became contaminated with Li^6 in these experiments.

Fig. 5.1. Alpha particle spectra with different Li^6 absorber concentration from Li^6-Sm^{149} target. A and B are from $Sm^{149}(n,\alpha)Nd^{146}$ and C is the triton peak from the $Li^6(n,\alpha)T^3$ reaction. □ Li^6 absorber containing 2.9 mg/cc; Δ-Li^6 absorber containing 43.15 mg/cc.

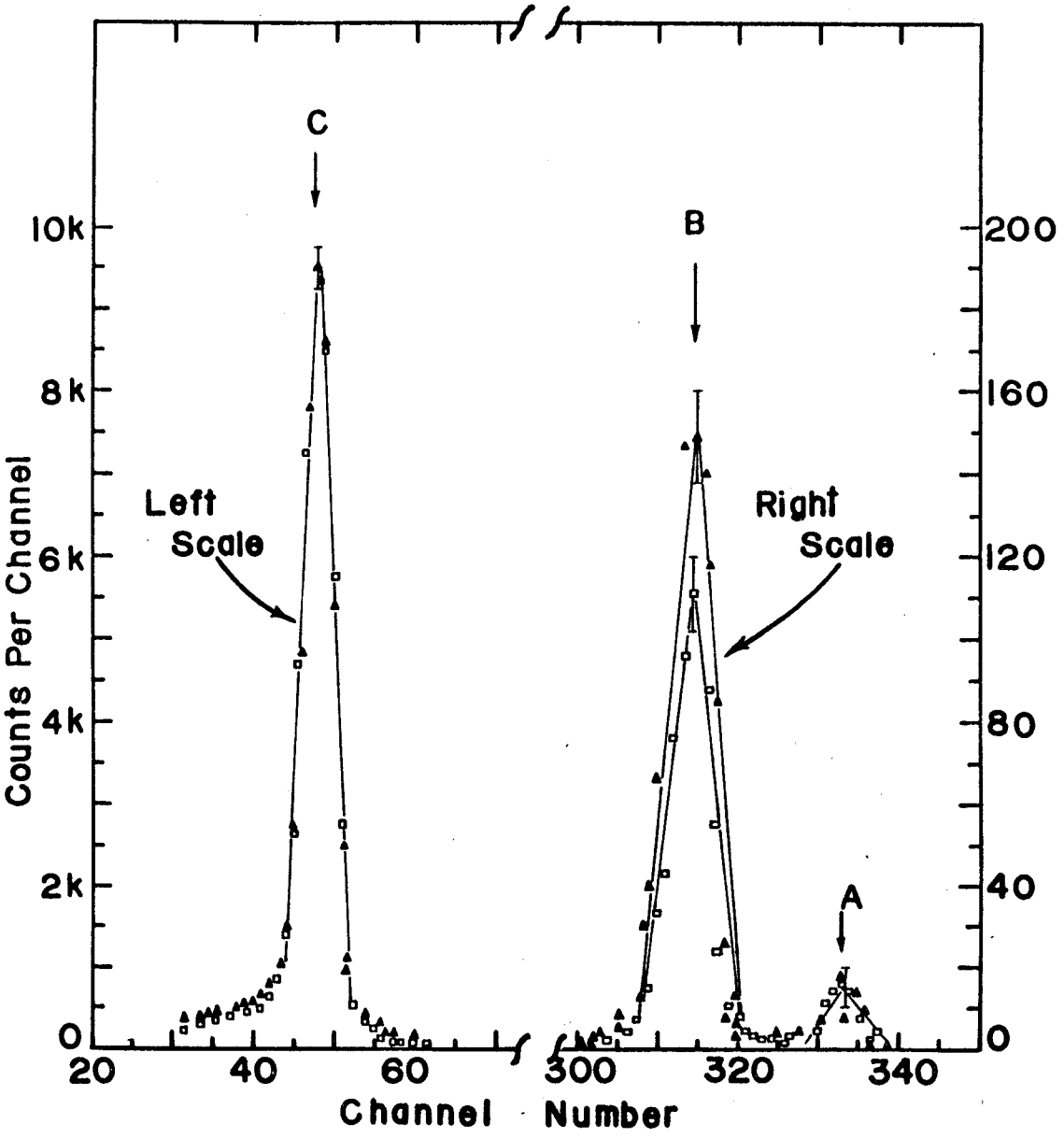
C
B
A
Left Scale
Right Scale
10k
8k
6k
4k
2k
0
200
160
120
80
40
0
20
40
60
300
320
340
Counts Per Channel
Channel Number

in Table 5.12. These measurements were made with a Sm^{149} target ($\sim$ 72 $\mu g/cm^2$) containing no Li. The Table 5.12 therefore shows ratios for I_{2^+}/I_{o^+} only. Fig. 5.2 shows the effect of the Sm absorbers on the alpha-particle spectrum from Sm^{149}. The spectrum has been normalized with respect to the higher energy alpha group obtained with no absorber. Because of the low counting rate large statistical errors were associated with these measurements. The general trend is, however, unmistakable. Because of difficulties associated with the hydrolysis of Sm solutions, measurements with other concentrations were not done.

The neutron transmission experiments for the $Nd^{143}(n,\alpha)C^{140}$ reaction were made using the Li^6 (1/v) absorbers only. The results, which are summarized in Table 5.13 clearly show that the $Li^6(n,\alpha)/Nd^{143}(n,\alpha)$ rate ratio is independent of the absorber concentration. The effect on the spectrum is shown in Fig. 5.3 . This means that the $Nd^{143}(n,\alpha)$ cross section also has a '1/v' dependence in the region of thermal neutron energies.

(c) Comparison of Experiment with Theory in the Neutron Transmission Experiments

Calculations were made to determine theoretically the effect of neutron flux perturbation on the particle spectra from the mixed Li-rare earth target. The following

Fig.5.2 Alpha particle spectra from the $Sm^{149}(n,\alpha)Nd^{146}$ reaction obtained with and without Sm absorber. □ -zero absorber strength (blank); Δ-Sm absorber containing 0.0146 g/cc Sm^{149}.

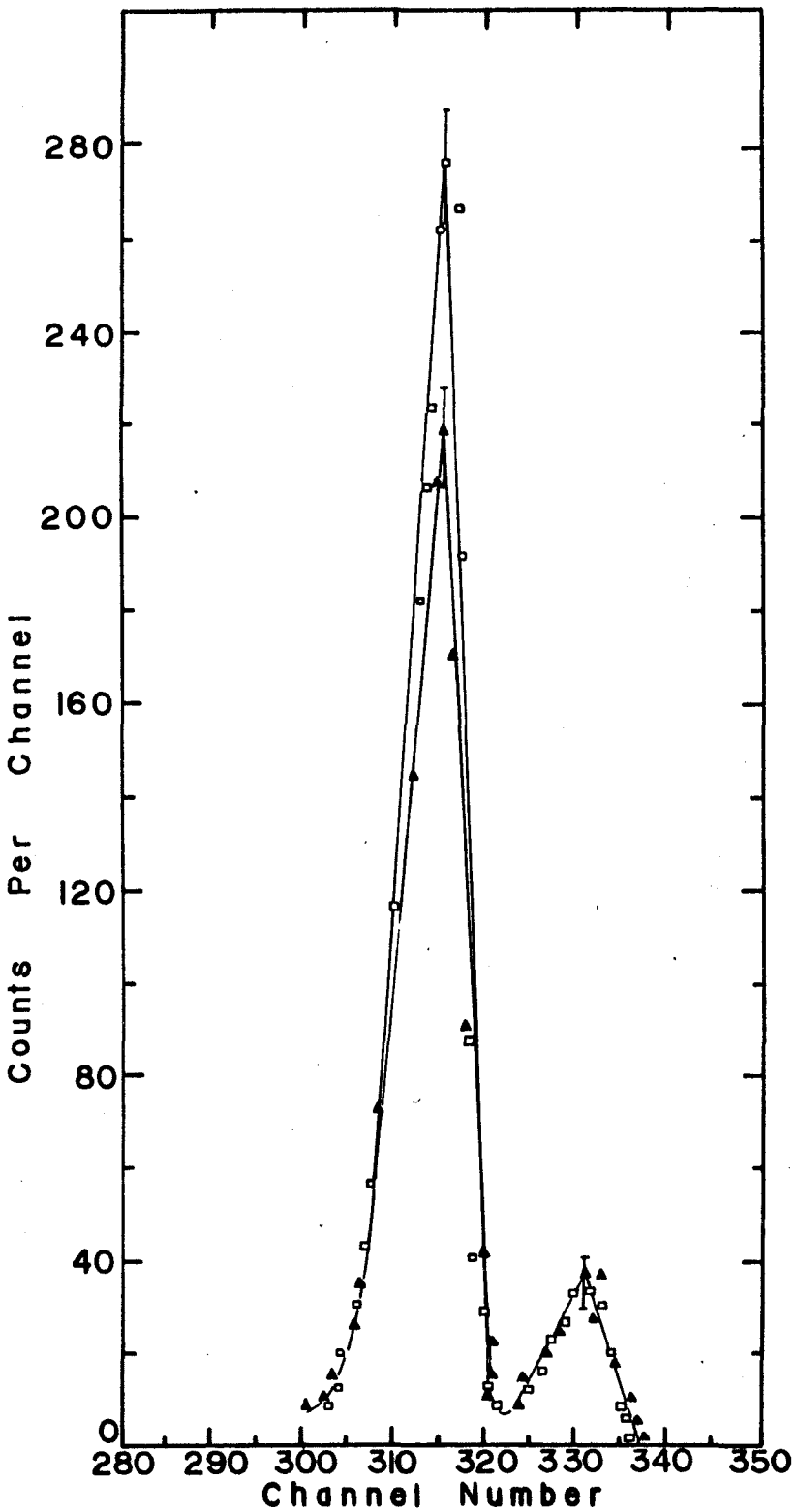
280
240
200
160
120
80
40
0
Counts Per Channel
280 290 300 310 320 330 340 350
Channel Number

Table 5.12 Results of Neutron Transmission Measurements Using Sm-Absorbers and Sm^{149} Target

Experiment	Sm^{149} Strength In Absorber (mg/cc)	Ratio of Alpha Intensities (I_{2+}/I_{o+})
1	Blank	7.85 ± .48
2	14.6	5.88 ± .23
3	14.6	5.77 ± .57
4	14.6	5.98 ± .39
	Best value of Experiments 2,3,4.	5.88 ± .24

Table 5.13 Relative Intensities of Triton-Alpha Peaks in Neutron Transmission Experiments on the $Nd^{143}(n,\alpha)Ce^{140}$ Reaction

Experiment number	Absorber Concentration (mg/cc)	$\frac{(Li^6\text{-Triton})}{(Nd^{143}\text{-Alpha}}$ Counts (I_T/I_{o^+})
1	Blank	3863 ± 103
2	15.2	4384 ± 300
3	30.2	3803 ± 285
4	40.8	4244 ± 293

Fig. 5.3. Alpha particle spectra from mixed Li^6-Nd^{143} target (~ 100 μg/cm^2) and without Li^6 absorber. A is triton peak from Li^6 and B is the alpha peak from Nd^{143}. ⊙-blank; ×-Li^6 absorber (40.8 mg/cc)

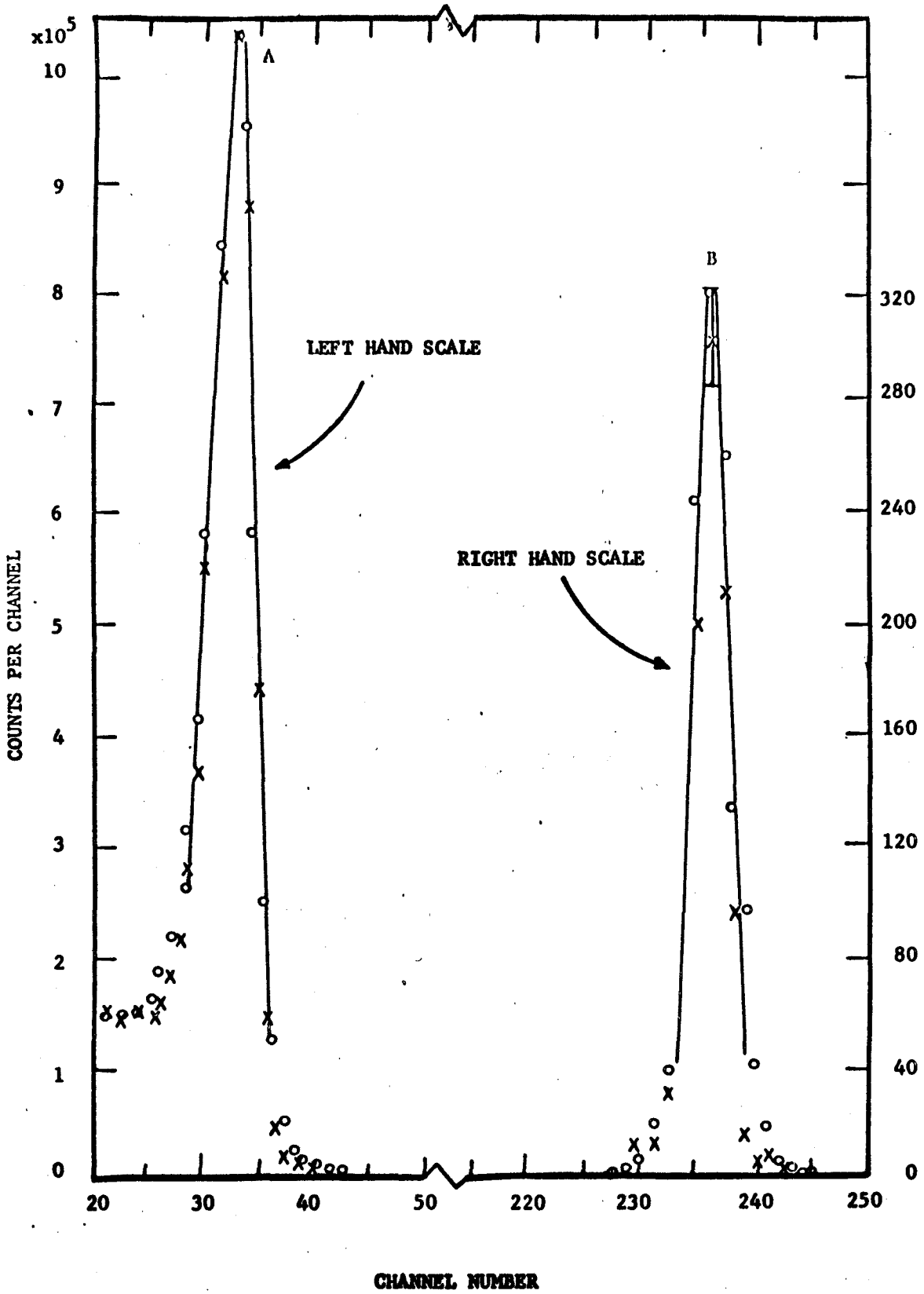
x10^5
10
9
8
7
6
5
4
3
2
1
0
A
B
LEFT HAND SCALE
RIGHT HAND SCALE
COUNTS PER CHANNEL
320
280
240
200
160
120
80
40
0
20
30
40
50
220
230
240
250
CHANNEL NUMBER

assumptions were made.

(i) The flux distribution in the thermal column is a pure Maxwellian with a temperature of $300^{o}K$.

(ii) The excitation function for the (n,α) reaction has the same shape as that observed for the (n,γ) reaction.

(iii) The effects of all other factors such as those due to scattering, absorption by all other isotopes present or higher resonances in Sm^{149} are negligible.

(iv) The cross sections for the ground state alpha transitions in Sm^{149} and Nd^{143} n,α reactions result purely from negative resonances and have a '1/v' cross section behaviour.

(v) The cross section for the 2^{+} alpha transition in $Sm^{149}(n,\alpha)$ study results mainly from the 0.0967 eV resonance and can be described by the Breit-Wigner single level formula.

With these assumptions we first evaluated the perturbed flux distribution for various neutron absorbers using the following general expression

$$\phi'(E) = \phi(E) \ [Exp- \{Nx\sigma(E)\}] \qquad (5.6)$$

$\phi(E)$ represents the energy dependent unperturbed neutron flux given by a Maxwellian distribution at $300^{o}K$.

$\phi'(E)$ represents the perturbed flux distribution.

N is the absorber atom density

x is the thickness of the absorber column

$\sigma(E)$ represents the excitation function of the absorber used. For Li^6 it follows a 1/v law and is represented by $\frac{149.41}{\sqrt{Eev}}$ barns[49]. For Sm^{149} it consists of two terms; one arises from the 1/v component from the bound level, the other from the unbound resonance. The total excitation function in this case can therefore be expressed as

$$\sigma(E)_{Sm^{149}} = \frac{C}{\sqrt{E}} + \pi\lambda^2 \frac{g\Gamma_n\Gamma_\gamma}{(E-E_o)^2+(\Gamma/2)^2} \qquad (5.7)$$

The value for the constants appearing in this formula were taken from reference (61). Fig. 5.4 shows the calculated excitation functions for Sm^{149} (curve A) and Li^6 (curve B). Using these excitation functions the perturbed flux distributions were evaluated for various absorber concentrations. A typical example of an unperturbed and perturbed flux distribution is given in Fig. 5.5. The curve A in this figure corresponds to pure Maxwellian distribution at $T = 300^oK$; curves B and C represent perturbed flux distributions calculated at the highest concentrations used for Sm^{149} and Li^6 absorbers respectively. Using these flux distributions the rates of the (n,α) reactions as a function of neutron energy were evaluated for the prominent alpha and triton groups detected using a mixed rare earth-Li^6 target. The total rate, R_T, for a particular reaction was obtained by taking a sum of rates calculated at energy inter-

Fig. 5.4. Calculated excitation functions for Sm^{149} (curve A) and Li^{6} (curve B).

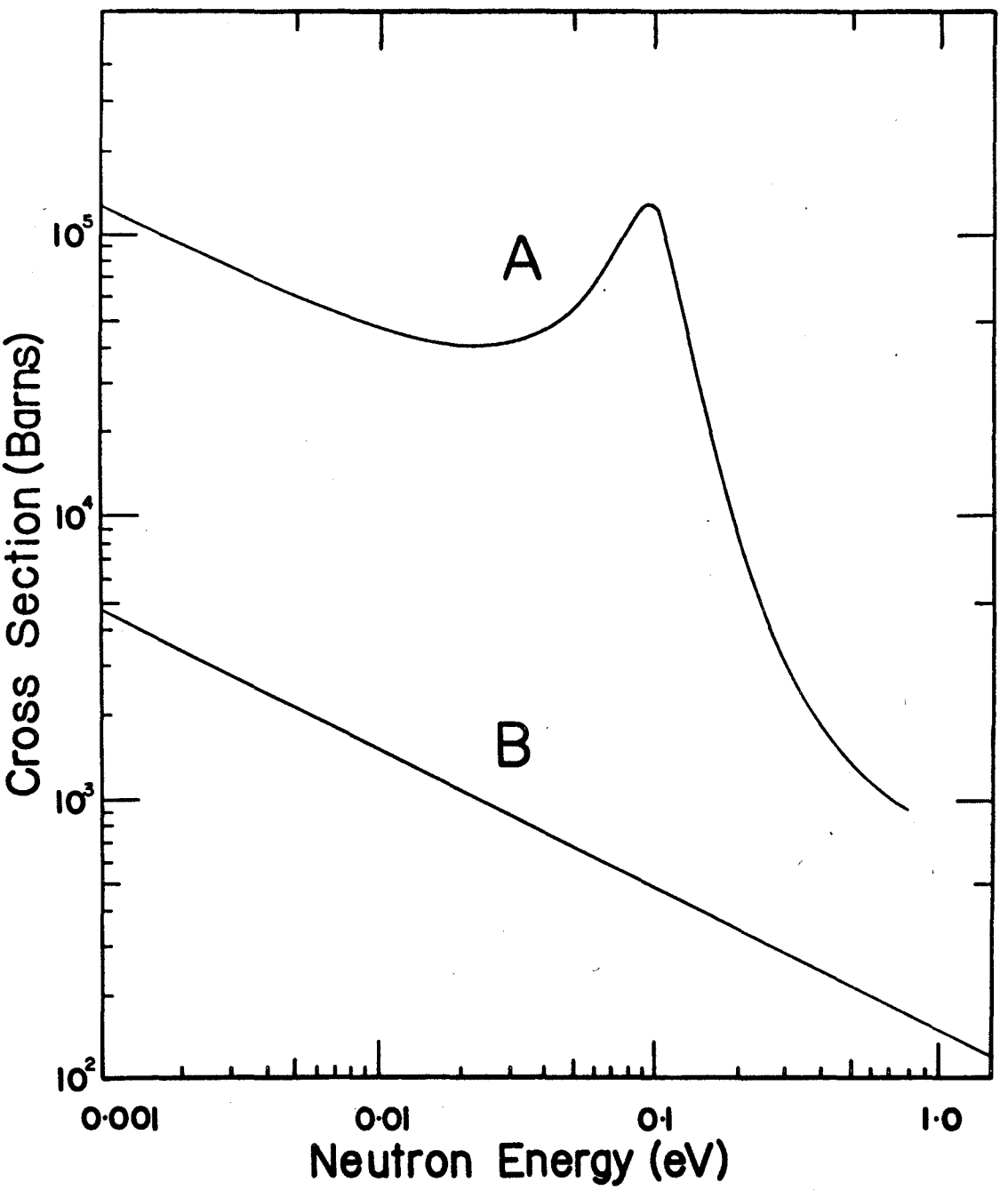
A
B
10^5
10^4
10^3
10^2
Cross Section (Barns)
0·001
0·01
0·1
1·0
Neutron Energy (eV)

Fig. 5.5. Calculated neutron flux distributions

Curve A - with no absorber

Curve B - with Sm absorber

Curve C - with Li^6 absorber

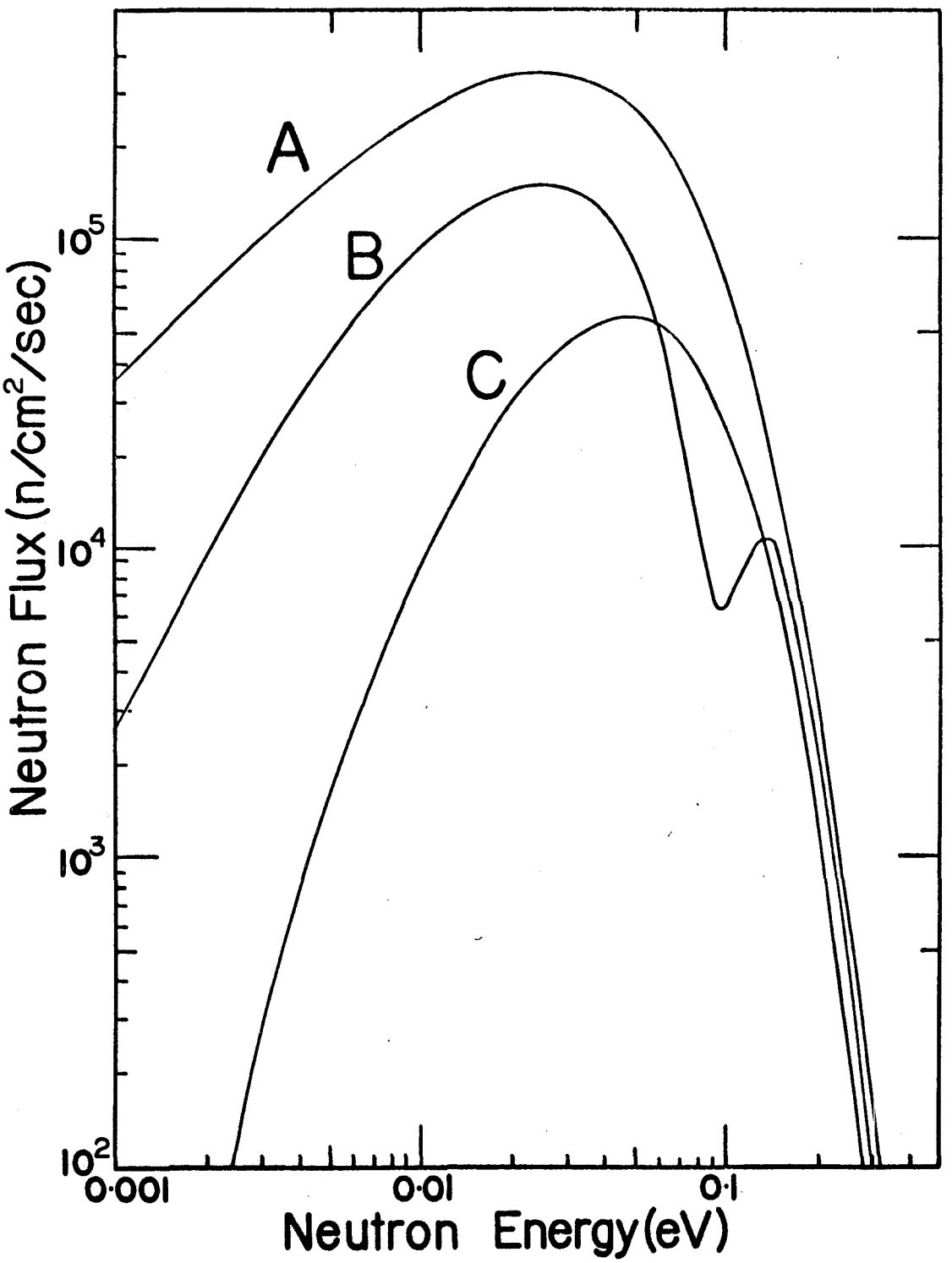
A
B
C
10^5
10^4
10^3
10^2
Neutron Flux (n/cm²/sec)
0·001
0·01
0·1
Neutron Energy (eV)

vals of 0.001 eV over an energy range of 0.001 eV - 0.5 eV using the following expression.

$$R_T \simeq \sum R(E) = N\sum \phi(E)\sigma(E) \qquad (5.8)$$

R(E) is the rate of a particular reaction at energy E. The excitation functions for evaluating these rates were obtained from measured values of the effective cross sections. Since the ground state transitions resulting both from $Sm^{149}(n,\alpha)Nd^{146}$ and $Nd^{143}(n,\alpha)Ce^{140}$ reaction follow the 1/v law the experimental values for their effective cross sections will be the same as their values for the 2200 m/sec neutron cross section. These values therefore directly give expressions for the evaluation of the excitation functions for these reactions. The expression for the evaluating of the excitation function for the 2^+ alpha transitions in $Sm^{149}(n,\alpha)Nd^{146}$ reaction was obtained in the following manner. The experimental value for the effective cross section (38.70 mb) was first divided by a factor, g, to obtain the 2200 m/sec neutron cross section (σ_o). As a first order approximation the total contribution to this transition was assumed to come only from the 0.0967 eV resonance and σ_o is equal to 22.5 mb. Using this value for the (n,α) reaction cross section and substituting for $E_o = 0.0967$ eV, $E = 0.025$ eV and $\Gamma \simeq \Gamma_\gamma = 0.058$ eV[61], the value for the energy dependent factor, $(g\,\Gamma_n\,\Gamma_\alpha)$, was evaluated from the general Breit-Wigner formula for the (n,α)

reaction. This value was then used to obtain an expression for the excitation function in the format of the Breit-Wigner formula. The mathematical form for the excitation function for the 0^+ transition in the $Sm^{149}(n,\alpha)Nd^{146}$ reaction was obtained using a value of 5.275 mb for the 2200 m/sec cross section obtained by taking a weighted average of the cross section (5.23 ± .17 mb) from this work and a more precise value (5.29 ± 0.05 mb) recently obtained by Oakey[48] from the fine structure studies of this reaction. The excitation function for the $Nd^{143}(n,\alpha)Ce^{140}$ reaction was based on the 2200 m/sec cross section value (21.28 mb) obtained in this study.

The rates for the (n,α) reactions were then calculated as a function of energy using these excitation functions and the calculated flux distributions obtained as above. The reaction rates over the entire energy range were summed to obtain the total rate, R_T, for each reaction. The ratio of the total rates were then taken for a comparison with the experimental values.

The assumption that the 0.0967 eV positive resonance is the only contributing resonance to the 2^+ alpha transition is , however, an over simplification. The negative 3^- resonance is also expected to contribute a small amount to this transition but it is much less than the contribution from the unbound 4^- level. We cannot measure its contributions directly but we can estimate it assuming $\delta^2_{0^+} = \delta^2_{2^+}$. This

gives a value of 0.7 for $\sigma_{2^+}/\sigma_{o^+}$ from the bound 3^- level. Since this cross section has a 1/v behaviour the total expression for the excitation function for the 2^+ α-transition becomes a sum of two terms; a contribution from the bound state (3.689 mb) and one from the unbound level (35.0 mb). Substituting these values into the expression for the total excitation function for the transition to the 2^+ level, the rate calculation was then repeated (see appendix A for the programme used). The results of these calculations are shown in Fig. 5.6. The solid lines represent the calculated values and the individual points the experimental values. The absorber concentrations have been expressed as percent of the most concentrated solutions used. For the Li^6 absorbers, 100 percent concentration corresponds to 46.4 mg/cm^3 with respect to Li^6. For Sm absorbers it corresponds to 29.2 mg/cm^3 with respect to Sm^{149}. The plots A, B and C give I_T/I_{o^+}, I_T/I_{2^+} and I_{2^+}/I_{o^+} for the Li^6 absorbers while plot D gives I_{2^+}/I_{o^+} for the Sm absorbers. For curve C there are two curves marked (1) and (2). The curve marked (1) represents the results of calculations based on the assumption that the 0.0967 eV resonance is the only source for the 2^+ alpha transition. The curve marked (2) includes the contribution from the 3^- negative resonance. For the $Nd^{143}(n,\alpha)Nd^{146}$ reaction the observations are similar to that for the ground state transition in the $Sn^{149}(n,\alpha)Nd^{146}$ reaction. The results are shown in Fig. 5.7.

Fig. 5.6. Effect of Li and Sm (absorber) concentrations on relative intensities of α-groups from mixed Li^{6}-Sm^{149} target.

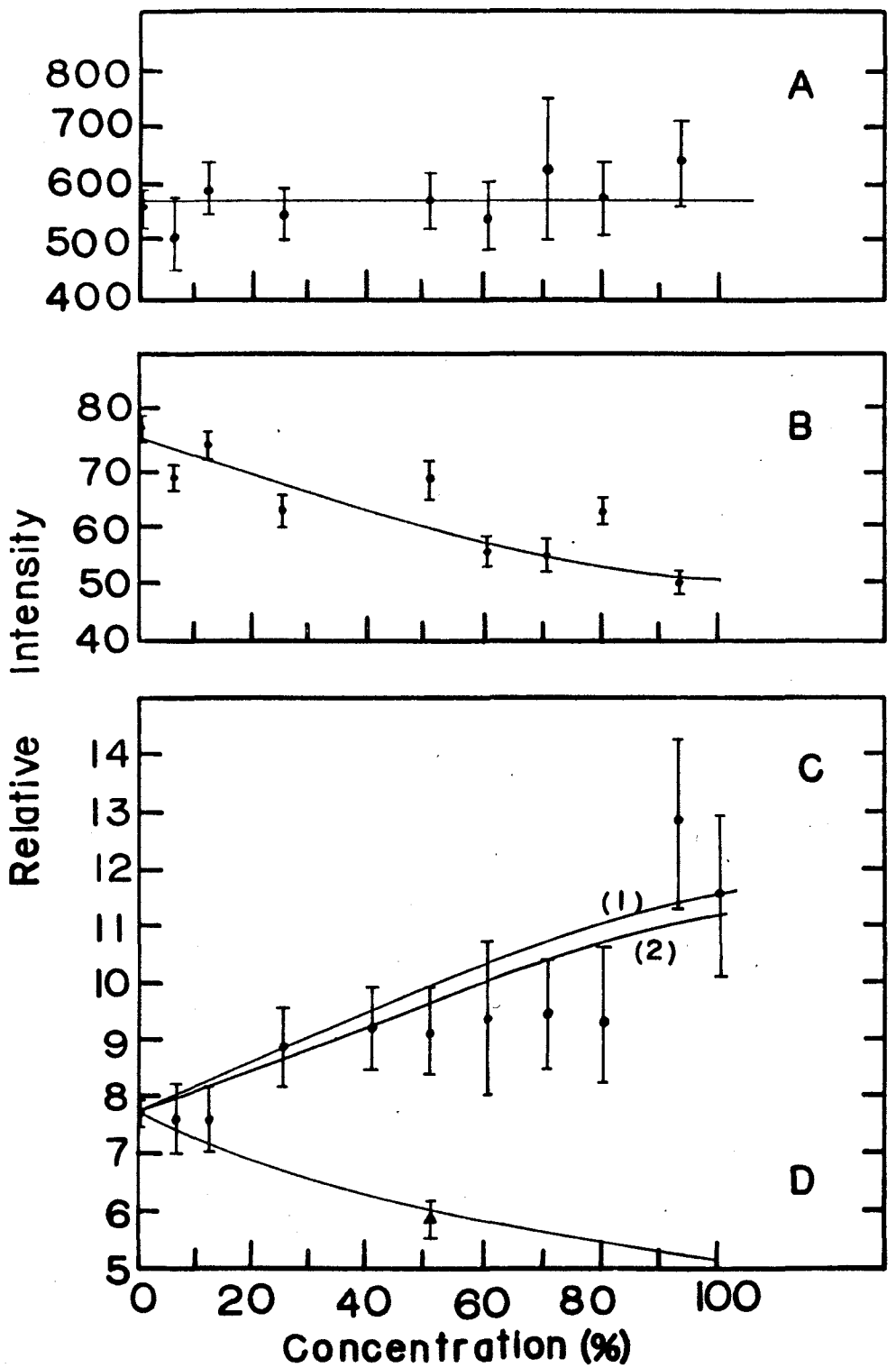
800
700
600
500
400
A
80
70
60
50
40
B
Intensity
Relative
14
13
12
11
10
9
8
7
6
5
C
D
(1)
(2)
0
20
40
60
80
100
Concentration (%)

Fig. 5.7. Effect of Li^6 absorber concentration on relative intensity of triton and α-groups from Li^6-Nd^{143} target.

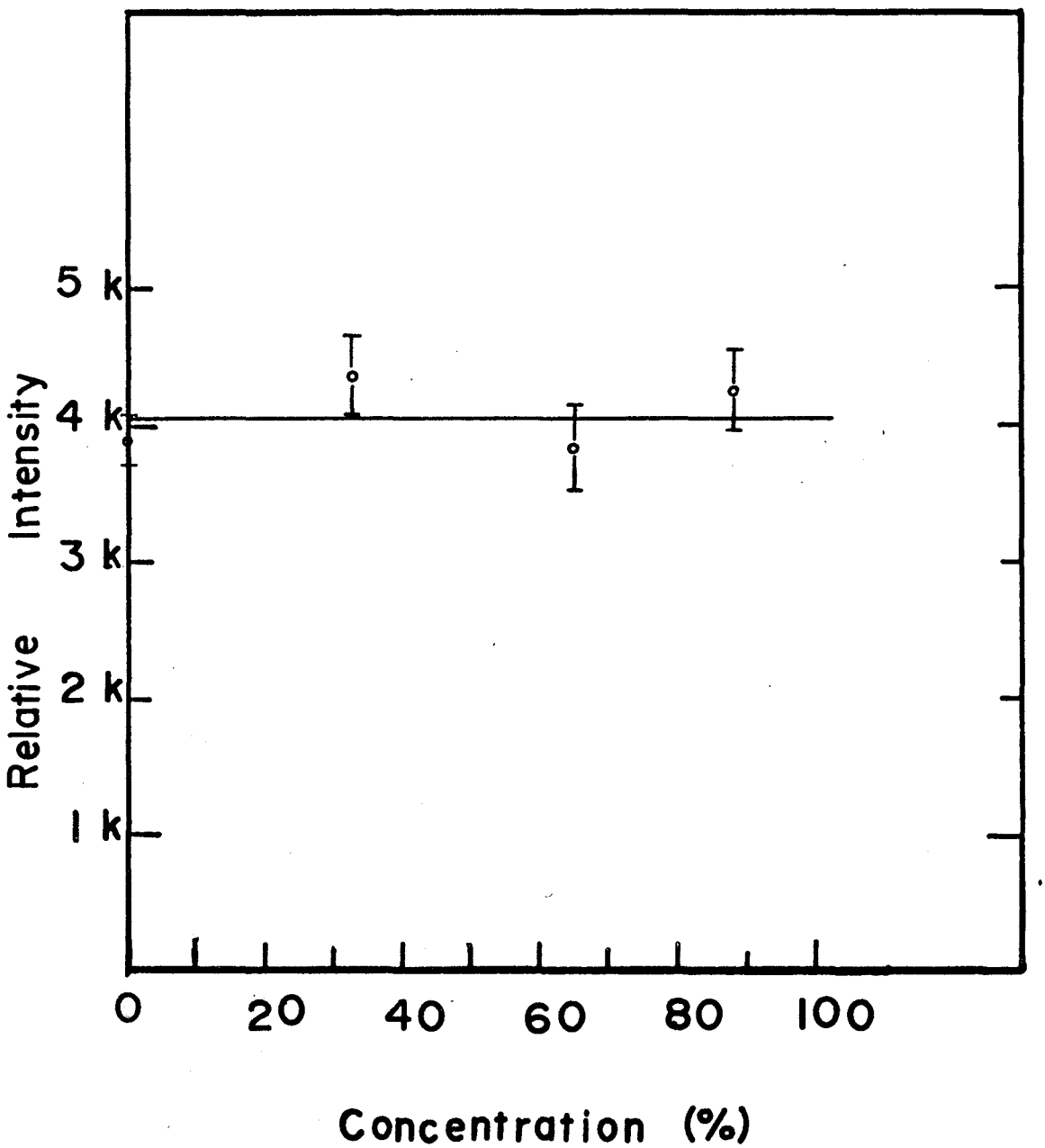
5 k
4 k
3 k
2 k
1 k
Relative Intensity
0
20
40
60
80
100
Concentration (%)

As shown in Fig.(5.6), most of the experimental points lie below the curve for I_{2^+}/I_{o^+} but there is reasonable agreement. There are reasons for expecting some departure from theoretical predictions:

(i) The flux distribution may not be a true Maxwellian.

(ii) The excitation function for the n,α reaction used for the 2^+ alpha transition may differ from the Breit-Wigner shape due to interference effects.

Because of the relatively large experimental uncertainties of the measurements this effect has not been pursued but it may be important.

Because of the low (n,α) cross sections, neutron transmission experiments could not be done on Sm^{147} and Gd^{155}. Experiments involving the study of the α-particle spectra using monoenergetic neutrons with high fluxes, when coupled with high resolution instruments such as the electrostatic particle guide should give interesting results on interference effects in the (n,α) reaction as well as more detail on the factors determining relative reduced alpha widths to excited states of the final nucleus.

To summarize the conclusions reached from these measurements:

(1) Most of the 2^+ α-transition in $Sm^{149}(n,\alpha)Nd^{146}$ reaction results from the 0.0967 eV resonance.

(ii) The 0.0967 eV resonance is a 4^- state.

(iii) The alpha transitions to the ground states in Sm^{149} and the $Nd^{143}(n,\alpha)$ reactions have their origins in the 1/v tails of bound 3^- resonances.

(iv) A significant contribution to the 2^+ alpha transition in the $Sm^{149}(n,\alpha)Nd^{146}$ reaction results from the bound 3^- state.

Ceulmans et al[7] in their recent studies of $Sm^{149}(n,\alpha)Nd^{146}$ reaction have also arrived at the same conclusions. They used monoenergetic neutrons with energies 0.004 eV, 0.025 eV and 0.0976 eV and obtained values 1.9, 6.5 and > 15 respectively for the ratios I_{2^+}/I_{o^+} for this reaction.

CHAPTER VI

SEARCH FOR A CHEMICAL EFFECT ON THE REACTION RATE IN $Sm^{149}(n,\alpha)Nd^{146}$ REACTION

Introduction

According to the theory of the compound nucleus[32,34], the neutron capture cross section near a resonance level of a nucleus at rest in free space is given by the Breit-Wigner formula. However, in its generally used form it is only valid for atoms at rest. Atoms in a crystal, however, are neither free nor at rest. Atoms in a gas may be considered as freely moving but at any given temperature, T, they have a Maxwellian distribution of velocities. Atoms in a solid, on the other hand, are held in a crystal lattice and vibrate with a frequency which is related to the characteristic Debye temperature, Θ_D.

Bethe and Placzek (1937)[81,82] treated theoretically the problem for a gaseous target. They changed the resonance energy denominator of the Breit-Wigner formula according to the relative velocities of the neutrons and the atoms and then averaged over the Maxwellian distribution

of velocities of the gas atoms. They showed that the capture cross section is then given to a very good approximation by

$$\sigma = \sigma^{o}\psi(\xi,x) \qquad (6.1)$$

where $x = 2(E-E_o)/\Gamma/2$; E is the energy of the neutron

$\xi = \Gamma/\Delta$. The quantity Δ is called the Doppler width and

$\Delta = 2(kTE_o m/M)^{\frac{1}{2}}$ where $\Delta << E_o$ (resonance energy);

k = Boltzmann constant,

T = Absolute temperature of the target,

m,M = Masses of neutron and target nucleus respectively,

Γ = Full width at half maximum of resonance,

σ^{o} = Cross section at the resonance energy E_o,

$$\psi(\xi,x) = \frac{\xi}{2\sqrt{\pi}} \int_{-\infty}^{\infty} \frac{e^{-\frac{1}{4}\xi^2(x-y)^2}}{1+y^2}\, dy \ .$$

Although the gas model gives a very good approximation for most of the resonances, Lamb (1939)[83] pointed out that in solid targets, where atoms are bound in a crystal, lattice effects due to lattice vibrations will be quite different from predictions of the gas model. Lamb derived a theoretical expression for the shape of the effective neutron absorption line for atoms bound in crystal lattices of varying degrees of strength. The mathematical detail of this treatment can be found in the original paper by Lamb[83]. Here we wish to give the relevant features of his

treatment. According to Lamb the absorption line is normal and should be centered about $E = E_o$ if the lattice binding is sufficiently strong ($\theta_D \to \infty$) and the resonance factor is then given by

$$W(E) = \frac{1}{(E-E_o)^2+(\Gamma/2)^2} \qquad (6.2)$$

In the weak binding limit, the absorption line is again normal but centered about an energy $E = E_o + R$. R is the recoil energy, $(m/M)E_o$, which is sometimes of the order of the natural line width of the resonance. This change in the position of the absorption curve can be experimentally important even though the recoil energy is quite small. This effect should be detectable by use of different crystals containing in common an element which shows resonant neutron capture in the thermal region, and it should be temperature dependent. Lamb treated the atoms of a weak binding lattice as if they were in a gas, not however with a temperature T but at a larger temperature corresponding to the average energy per vibrational degree of freedom (including the zero point energy) of the crystal. Using the condition for weak binding $[\frac{1}{2}\Gamma + (R\bar{\epsilon})^{\frac{1}{2}} >> \theta_D]$ Lamb showed that the shape of resonance can be given by

$$W(E) = \frac{4}{\Gamma^2}\,\psi(\xi,x) \qquad (6.3)$$

where $\psi(\xi,x)$, x, ξ are the same as defined before except that now an effective Doppler width

$$\Delta = 2\ (k\bar{\epsilon}E_o\ m/M)^{\frac{1}{2}} \qquad (6.4)$$

which involves $\bar{\epsilon}$ instead of T is used. This means, then, that the atoms in a weak crystal at a temperature T give the same absorption line as they would in a gas at a temperature $\bar{\epsilon}$ equal to the average energy per vibrational degree of freedom of the crystal.

For the intermediate cases the shape of the absorption line is in general much more complicated. For this case Lamb calculated the line shape for a substance at a temperature much lower than the Debye temperature of $\Theta_D = 210^oK$ (case of silver) with different Γ values and showed that for such a case the absorption line exhibited a fine structure. The area under the absorption curve, however, did not differ from that calculated on the basis of gas model. This behaviour is illustrated by Fig. 6.1 which has been reproduced from Lamb's paper.

Lamb[83,84] further remarked that the chemical binding can not cause any difference in the 1/v variation of the capture cross section as this arises from the normalization of the incident neutron wave function to unit flux required by the definition of a cross section.

It has been our intention for some time to study the effect of chemical binding and to test experimentally

Fig. 6.1 Plot of the neutron resonance absorption curve in silver for assumed $\Gamma = \Theta_D$ (case of intermediate binding). The curve one would obtain with free atoms is shown for comparison. The abscissa measures the distance from resonance in units of $\frac{1}{2}\Gamma$.

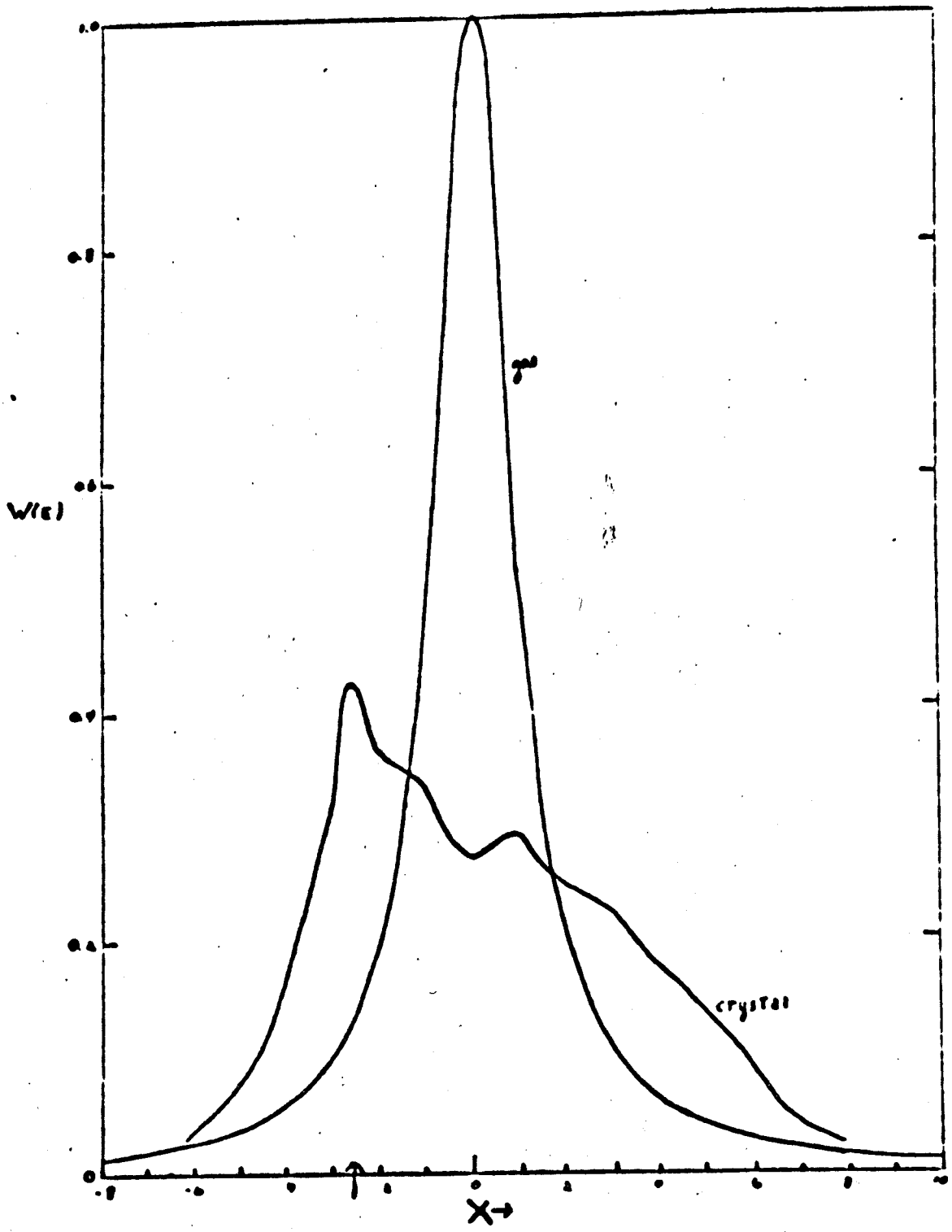
W(E)
X→
crystal

Lamb's theory. We feel that the $Sm^{149}(n,\alpha)Nd^{146}$ reaction should provide a unique case for such a study. In our work, it has been shown that the two main alpha transitions observed during the study of this reaction arise from two independent sources. While the ground state transition originates entirely from the negative resonance and shows a 1/v dependence, the 2^+ α-transition has its origin primarily in a positive resonance at 0.0967 eV. Therefore if a Sm^{149} nucleus is studied in crystalline states of differing lattice strengths the rate of the (n,α) reaction leading to the ground state should remain unaffected whereas that for the 2^+ state should be affected because of the crystal lattice effects.

Measurements and Results

The experimental procedure involved the study of the relative intensities of the main α-groups resulting from natural samarium metal and its oxide as targets. The method of studying the (n,α) reactions was the same as adopted earlier for the study of (n,α) reactions in Gd^{155} and Eu^{151}. A natural samarium metal-target corresponding to ~ 80 μg/cm^2 of Sm^{149} was deposited on an Al-backing (~ 44 cm^2 area) using a vacuum evaporation technique similar to the one described by Westgaard et al[85]. An alpha particle spectrum was accumulated for about 2 weeks. The same sample was then heated at 450°C for ~ 2 hours to convert the metal into oxide

and the operation was repeated with the same counting geometry and carried out for about the same length of time. During the process of oxidation it was observed that most of the metal had alloyed with aluminum and only a small fraction had, in fact, undergone oxidation. This was indicated by a large increase in tailing observed in the α particle spectrum and also by the general appearance of the target sample which showed metallic lustre. A new oxide sample was therefore made with approximately the same Sm^{149} content as above using the technique of electrodeposition[47]. The material used to obtain this target was the same as that used for the metal deposition. To prepare the target the metal was first converted into the nitrate which was then used for electrodeposition as described in ref. 48. Finally the target was heated for 2 hours at 450°C to ensure complete conversion of the deposit into the oxide form. This was then irradiated for about a week. In all the three measurements the accumulated α-spectra were printed out every two days and the data analyzed to determine the relative intensities of the two main α-groups resulting mainly from the $Sm^{149}(n,\alpha)$ reaction. The samarium metal target was also counted for 48 hours in a region outside the thermal column to check for the presence of any contamination from the natural radioactivity. The alpha particle spectrum did not show any contamination in the alpha energy region of interest (6 - 10 MeV).

Table 6.1 Chemical Effect on Intensities of α-Transitions in $Sm^{149}(n,\alpha)Nd^{146}$ reaction

Chemical State of Target	Counts*		$\frac{\alpha_{2^+}}{\alpha_{o^+}}$
	α_{2^+}	α_{o^+}	
Metal (sm)	170297	25548	6.67 ± 0.04
Alloy (Sm-Al)	125388	18501	6.78 ± 0.05
Oxide (Sm_2O_3)	41542	5909	7.03 ± 0.10

*These counts were not corrected for collection efficiency.

Results and Discussion

The results obtained in all the three measurements were finally combined to give overall results. These results are tabulated in Table 6.1. They clearly show that there is a significant difference in the ratios of the intensities of the 2^+ and 0^+ α-transitions for the metal and oxide. The ratio in the case of the alloyed target is, however, not as high as that observed in the case of the completely oxidized samarium target. The increase observed in both the cases is larger than can be accounted for from self-absorption or neutron resonance absorption. There is another possible source of error and this arises from the correction for tailing from the adjacent peaks. The upper limit of this error has been estimated to be of the order of 2%.

The only plausible explanation for this effect appears to be the chemical effect that we were looking for. In the light of Lamb's theory this would mean that the decrease in the ratio for the metal has resulted from the change in the effective position or shape of the 0.0967 eV resonance in the Sm^{149} capture cross section due to simultaneous lattice excitation and neutron capture. This change will cause the reaction rates to differ. Since the 1/v components remain unaffected, the 2^+ α-transition

should be the only one to show a change in the count rate. A decrease in the α-intensity ratio for the metal is expected if the effective neutron spectrum has shifted from E_o to E_o+R, $R = E_o(\frac{m}{M})$.

Natural samarium contains 15.0% Sm^{147}. This isotope also has a thermal neutron (n,α) reaction and shows two prominent α-groups. The more intense group lies at about the same energy as the ground state α-transition from the $Sm^{149}(n,\alpha)Nd^{146}$ reaction. Its contribution, though small, is significant and is about 12% of the total accumulated under the 0^+ α group from the $Sm^{149}(n,\alpha)Nd^{146}$ reaction. Fortunately the excitation function in the thermal region , as remarked earlier, has nearly a 1/v behaviour and should, therefore, be expected to behave as the 0^+ α group from Sm^{149}.

The Debye temperature, Θ_D, for the metal samarium is known. Its value is 147 ± 3°K.[86] The Debye temperature for its oxide is not known. However, its high melting point suggests that Θ_D for the oxide should be significantly higher than that of the metal. Using a computer programme of a type similar to the one shown in Appendix B, the ratio for the reaction rates for the resonance energy at 0.0967 and at 0.0967 + R were evaluated. The results of these calculations, according to Lamb's theory should correspond to the condition for strong binding (oxide) and weak binding (metal)

respectively. These calculations gave a value for

$$\left|\frac{(\alpha_{2^+}/\alpha_{o^+})_{oxide}}{(\alpha_{2^+}/\alpha_{o^+})_{metal}}\right|_{calculated} = 1.01$$

The quantities α_{2^+} and α_{o^+}, refer to the intensities for the 2^+ and 0^+ α-transitions respectively. This is lower than the experimental values for the same ratios. This ratio for the oxide and the metal was 1.05±0.02 and for the alloy and the metal was 1.02±0.02

The results described above are of preliminary nature and it is too early to make any quantitative comparison between theory and experiment. The general trend, nevertheless is quite clear and suggests that there is a significant chemical effect. This effect is presumably due to a perturbation of the effective line shape caused by excitation of the crystal lattice. More experimental work such as studying the effect of temperature and using the (n,γ) reaction rather than the weaker (n,α) reaction will determine whether the present interpretation has any validity.

BIBLIOGRAPHY

1. R. D. Griffioen and J. O. Rasmussen, UCRL-9566, 1961,P.147.
2. R. D. Macfarlane and I. Almodovar, Phys. Rev. 127, 1665 (1962).
3. E. Cheifetz, J. Gilat, A. I. Yavin and S. G. Cohen, Phys. Letters 1, 289 (1962).
4. M. W. Cresswell and R. R. Roy, Proc. Phys. Soc. 78, 1297 (1962).
5. V. N. Andreev and S. M. Sirotkin, Jadernaya Fizika 1, 252 (1965)
6. Par. H. Ceulemans, F. Poortmans and M. Neve De Mevergnies, Le Journal De Physique 24, 1003 (1963).
7. F. Poortmans, H. Ceulemans, A. J. Deruytter and M. Neve De Mevergnies, Nucl. Phys. 82, 331 (1966).
8. J. Kvitek and Yu. P. Popov; Phys. Letters 22, 186 (1966).
9. M. Dakowski, T. Krogulski, E. Piasecki, H. Piekarz and M. Sowinski; Nucl. Phys. A97, 187 (1967).
10. J. Kvitek and Yu. P. Popov, JINR Report E3-3029 (1966).
11. J. Kvitek and Yu. P. Popov, JINR Report P3-3104 (1967).
12. N. S. Oakey and R. D. Macfarlane, Phys. Letters 24B, 142 (1967).
13. E. Cheifetz, Y. Goss and I. A. Yavin; Nucl. Phys. 91A, 238 (1967).

14. G. Gamow, Z. Phys. 51, 204 (1928).

15. E. U. Condon and R. W. Gurney, Nature 122, 439 (1928).

16. F. Rasetti, 'Elements of Nuclear Physics', Prentice Hall Publication, 1936, p.100.

17. I. Perlman and J. O. Rasmussen, 'Alpha Radioactivity' Handbuch der Physik, 42, Springer-Verlag, Berlin (1957).

18. H. A. Bethe, Rev. Mod. Phys. 9, 161 (1938).

19. G. H.Winslow, Phys. Rev. 96, 1032 (1954).

20. P. J. Brussaard and H. A. Tolhoek, Physica 24, 263 (1958).

21. H. J. Mang, Z. Phys. 148, 582 (1957).

22. H. J. Mang, Phys. Rev. 119, 1069 (1960).

23. H. J. Mang, UCRL-8931 (1959).

24. H. J. Mang and J. O. Rasmussen, Mat. Fys. Skr. Dan. Vid Selsk. 2, No. 3 (1962).

25. H. D. Zeh and H. J. Mang, Nucl. Phys. 29, 529 (1962).

26. H. J. Mang, 'Alpha Radioactivity', Ann. Rev. Nucl. Sci. 14 (1964).

27. (i) G. Igo, Phys. Rev. Letters 1, 72 (1958).
(ii) G. Igo, Phys. Rev. 115, 1665 (1959).

28. (i) J. O. Rasmussen; Phys. Rev. 113, 1593 (1959).
(ii) J. O. Rasmussen, Phys. Rev. 115, 1675 (1959).

29. D. H. Wilkinson, Proc. Rutherford Jubilee Inter. Conf. (1961).

30. J. K. Poggenburg, Jr., UCRL-16187 (1965).

31. R. D.Woods and D. S. Saxon, Phys. Rev. 95, 577 (1954)

32. N. Bohr, Nature 137, 344 (1936).

33. R. D. Evans, 'The Atomic Nucleus', McGraw Hill Publication, 1955, P. 90.

34. G. Breit and E. Wigner, Phys. Rev. 49, 519 (1936).

35. V. L. Sailor, Phys. Rev. 104, 736 (1956).

36. J. M. Blatt and V. F. Weisskopf, 'Theoretical Nuclear Physics' John Wiley Publication, 1952, Chapter 8.

37. E. Segre, 'Experimental Nuclear Physics', John Wiley Publication, 1953. Vol. II, P.257.

38. A. Stolovy and J. A. Harvey, Phys. Rev. 108, 353 (1957).

39. J. S.Story, AERE report T/M-77.

40. C. H.Westcott, AECL-407 (1957).

41. C. H. Westcott, W. H. Walker and T. K. Alexander, 'Peaceful Uses of Atomic Energy', Paper P/202, 16, 70 (1958).

42. T. A. Eastwood, A. P. Baerg, C. B. Bigham, F. Brown, M. J. Cabell, W. E. Grummitt, J. C. Roy, L. P. Roy and R. P. Schuman, 'Peaceful Uses of Atomic Energy', Paper P/203, 16, 54 (1958).

43. C. G. Campbell and R. G.Freemantle , AERE report RP/R2031 (1956).

44. D. J. Hughes, 'Pile Neutron Research', Addison Wesley Publication,1953, P.175.

45. J. B. Radcliffe, Jr. and E. E. Hill, UCRL-4919-Rev (1960).

46. N. S. Oakey and R. D. Macfarlane, N.I.M., 49, 220 (1967).

47. W. Parker and A. Falk, N.I.M., 16, 355 (1962).

48. N. S. Oakey, Ph.D. Thesis, McMaster University (1967)

49. D. J. Hughes and R. B. Schwartz, BNL-325 2nd ed. (1958).

50. A. H. Wapstra, Nucl. Phys. 57, 48 (1964).

51. G. G. O'Kelley, 'Application of Computers to Nuclear and Radio Chemistry',NAS-NSB-107, U.S.A. 1962, P.67.

52. J. H. E. Mattauch, W. Thiele and A. W. Wapstra; Nucl. Phys. 67, 1 (1965).

53. H. W. Baer, J. J. Reidy and M. L. Wiedenbeck; Nucl. Phys. 86, 332-344 (1966).

54. Nuclear Data Sheets (appendix 1) (1965).

55. H. J. Hays, J. Nucl. Energy 7, 199 (1958).

56. D. J. Hughes and R. B.Schwartz, B.N.L.-325 (1957).

57. J. Kvitek and Y. P. Popov, JINR-P3104 (1967).

58. D. J. Buss, E. G. Funk and J. W. Mihelich, Phys. Rev. 144, 1193-1199 (1966).

59. A. V. Ramayya and Y. Yoshizawa, Phys. Rev. 137, 1B, 13-16 (1965).

60. H. Marshak and V. L. Sailor, Phys. Rev. 109, 1219 (1958).

61. N. J. Pattenden, Proceedings of the Second United Nations Conf. on the Peaceful Uses of Atomic Energy, 16, pp.44, paper P/11 U.K. (1958).

62. B. N. Brockhouse, Can. J. Phys. 31, 432 (1953).

63. L. D. Roberts, S. Bernstein, J. W. T. Dabbs and C. P. Stanford, Phys. Rev. 95, 105 (1954).

64. H. Marshak, H. K. Postma, V. L. Sailor, F. J. Shore, and C. A. Reynold, Phys. Rev. 128, 1287 (1962).

65. V. P. Hohne, Ann. Der. Physik, 7, 50 (1961).

66. K. Beg and R. D. Macfarlane, Bull. Am. Phys. Soc. 10, 724 (1965).

67. F. Poortman and H. Ceulemans, Nucl. Phys. A97, 657 (1967).

68. J. D. Macdougall, W. McLatchie, S. Whineray and H. E. Duckworth, (private communication) 1966.

69. B. S. Dzhelepov, L. K. Peker and V. O. Sergeev , 'Decay Scheme of Radioactive Nuclei, A>100' (Academy of Sciences of the USSR Press, Moscow-Leningrad, 1963).

70. N. A. Eissa, D. Berenyi, Gy. Mathe, D. Varga, I. Rezanka and L. Maly, Nucl. Phys. A100, 438 (1967).

71. R. T.Carpenter, Report ANL-6589 (1962).

72. L. Forman, F. A. White, Nucl. Sci. and Eng. 28, 139 (1967).

73. Nuclear Data Sheets.

74. E. T. Florance see H. B. Miller , F. J. Shore and V. L. Sailor, Nucl. Sci. and Eng. 8, 183 (1960).

75. A. Stolovy, Phys. Rev. 134, 1B, 68 (1964).

76. D. Ali, Nucl. Phys. 71, 441 (1965).

77. S. Tassan, A. Hellsten and V. L. Sailor, Nucl. Sci. and Eng. 10, 169 (1961).

78. F. Dominac and E. T. Patronis, Phys. Rev. 114, 1577 (1959).

79. N. Holt, Phys. Rev. 98, 1162A (1955).

80. D. J. Hughes and R. B. Schwartz, BNL-325 (Suppl.) 60-143-1 (1966).

81. H. Bethe and G. Placzek, Phys. Rev. 51, 462 (1937).

82. H. Bethe, Rev. Mod. Phys. 9, 140 (1937).

83. W. E. Lamb, Jr.,Phys. Rev. 55, 190 (1939).

84. W. E. Lamb, Jr.,Phys. Rev. 51, 187 (1937).

85. L. Westgaard and S. Bjornholm , N.I.M. 42, 77 (1966).

86. K. A. Gschneidner, Jr., 'Rare Earth Alloys', D. Van Nostrand Company Inc., 1961, p.38.

APPENDIX A

TREATMENT OF ERRORS

The uncertainties associated with the Q-value and cross section results arise from the propagation of errors. In those cross section measurements where less than four experiments were made, the final results were evaluated by a simple averaging method. In cases where more than four independent results were obtained the method of weighting was adopted.[1] The uncertainty associated with individual effective cross section values were evaluated by taking into account two main sources of error: statistical and systematic. These, however, do not include errors which may have resulted from corrections required for resolving gross alpha spectra into their components or from extrapolation of curves such as the one shown in Fig. 3.1. These effects were important for the Sm^{149} data given in Table 4.3 where the results show large scattering. The statistical errors varied from one nuclide to another depending on the magnitude of the capture cross section. In the case of Sm^{149} and Nd^{143}, for example, precisions of better than 1% could be achieved within a period of 1000 minutes. This was not possible for Sm^{147} or Gd^{155} where even long irradiations (> 4000 minutes) could not improve the counting precision to better than 2%. The errors associated with the

isotope abundance ratios were in general not greater than 0.1% and from target preparation, of the order of 1%. The uncertainty associated with the $Li^6(n,\alpha)T^3$ reaction cross section is not available. The cross section values were calculated by taking the cross section of the standard as an absolute value. Correction for errors due to "beam broadening" were not made. This error could be important only for Sm^{149} and Gd^{155}, since their total capture cross sections are large and both have contributing resonances in the thermal region. The results on the (n,α) reaction cross sections determined for various target thicknesses used in these investigations (Tables 4.3 and 4.4) did not show any definite trend of the effect of thickness on cross section. Furthermore the thickest sample used should not attenuate the neutron beam by more than 3%.

The uncertainties in energies were based on errors associated with the energy standards used. No correction for target thickness was made. The samples used were thin and uniform enough so that there was no serious perturbation of the relative energies of the alphas from the standard and those resulting from the isotope investigated.

The large errors quoted in the neutron transmission measurements are due to poor counting statistics. The

measurement of the ratios of the count rates eliminated corrections for flux hardening for individual peaks in the alpha particle spectra. The blank that was run was not a true blank because it did not contain any chloride. The effect of chloride and other impurities, however, appear to be very small. Like Li^6, Cl^{35} is also a '1/v' absorber and as such behaves in the same way as Li^6. Its total effect, however, cannot be greater than 2%. For measurements involving natural samarium as the absorber the effect of Sm^{147} was considered to be negligible.

Ref. 1. A. G. Worthing and J. Geffner "Treatment of Experimental Data" Wiley, New York, 1943, pp. 189-215

APPENDIX B

A COMPUTER PROGRAMME FOR CALCULATIONS IN NEUTRON TRANSMISSION MEASUREMENTS

```
$JOB            000501 BEG              100    0100
$IBJOB          NODECK
$IBFTC
C       CALCULATIONS FOR NEUTRON TRANSMISSION MEASUREMENTS
C       EFFECT OF CONC. OF ABSORBER ON RELATIVE INTENSITIES OF ALPHA PARTICLE
C       EFFECTIVE CROSS SECTION FOR GROUND STATE ALPHA=5.275MB
C       EFFECTIVE CROSS SECTION FOR  FIRST EXCITED STATE=38.70MB
C       38.70=34.50MB(FROM +IVE RESONANCE) + 4.20MB(FROM -IVE RESONANCE)
C       EO=RESONANCE ENERGY,TOTTAO=TOTAL RADIATION WIDTH,BOLC=BOLTZMAN CONST/
        READ 1,EO,TOTTAO,BOLC
        PRINT 1,EO,TOTTAO,BOLC
C       T=TEMPERATURE IN DEGREES KELVIN
        READ 2,T
        PRINT 2,T
C       SN ANS SM ARE NUMBER OF ATOMS OF LITHIUM-6 AND SAMARIUM-149 IN TARGE
        READ 3,SN,SM
        PRINT 3,SN,SM
        A=(3.14159*200.)/((3.14159*BOLC*T)**1.5)
        B=1.0/(BOLC*T)
        D=2.87/(2.*3.14159*10.**9)
        G=TOTTAO*TOTTAO/4.0
C       X=THICKNESS OF THE ABSORBER COLUMN USED
        READ 4,X
        PRINT 4,X
C       ESTART=ENERGY AT START,EINC=ENERGY INCREMENT,EEND=ENERGY AT THE END
        READ 5,ESTART,EINC,EEND
        PRINT 5,ESTART,EINC,EEND
C       NUMN=NUMBER OF ABSORBERS FOR WHICH CALCULATIONS ARE SOUGHT
        READ 6,NUMN
        PRINT 6,NUMN
```

```
      CON0=3.14159*D*D
      CON1=1.3823*1.0E+06*A*EINC
      CON2=149.41*1.0E-24
      CON3=CON0*0.293725*1.0E-10
      CON4=0.83403*1.0E-27
      CON5=5.832678*1.0E-28
      CON6=760.*1.0E-24
      CON7=CON0*TOTTAO*0.874*1.0E-03
      DO 17 I=1,NUMN
      E=ESTART
C     C=NUMBER OF ABSORBER ATOMS PER CC
      READ 7,C
      PRINT 7,C
      H=C*X
C     SRLI,SRSM2,SRSM0 ARE TOTAL RATES FOR LI AND SM(2+) AND SM(0+)
      SRLI=0.
      SRSM2=0.
      SRSM0=0.
C     TSRLI,TSRSM2,TSRSM0 CORRESPOND TO TOTAL RATES WITH TRANSMITTED FLUXE
      TSRLI=0.
      TSRSM2=0.
      TSRSM0=0.
      DO 15 J=1,1000
      ESQ=1.0/SQRT(E)
C     DEN= NUTRON FLUX DISTRIBUTION BASED ON 100 NEUTRONS PER CC.
      DEN=CON1*EXP(-E*B)*E
C     SIGLI REPRESENTS THE EXCITATION FUNCTION FOR LITHIUM-6
C     SIGSM2=EXCITATION FUNCTION FOR ALPHA TRANSITION TO FIRST EXCITED STA
C     SIGSM0=EXCITATION FUNCTION FOR ALPHA TRANSITION TO GROUND STATE
```

```
C       SIGTOT=EXCITATION FUNCTION FOR NUTRON CAPTURE BY ABSORBER
        SIGLI=CON2*ESQ
        SIGSM2=((CON3*ESQ/(G+(E-EO)*(E-EO)))+(CON5*ESQ))
        SIGSM0=CON4*ESQ
        SIGTOT=(CON7*ESQ/(G+((E-EO)*(E-EO)))+(CON6*ESQ))
C       DENT=TRANSMITTED DEN
        DENT=DEN*EXP(-SIGTOT*H)
C       RLI,RSM2,RSM0 ARE RATES(E) OF LI,SM(2+),SM(0+) (WITHOUT ABSORBER)
        RLI=DEN*SN*SIGLI
        RSM2=DEN*SM*SIGSM2
        RSM0=DEN*SM*SIGSM0
        SRLI=SRLI+RLI
        SRSM2=SRSM2+RSM2
        SRSM0=SRSM0+RSM0
C       RLIT,RSM2T,RSM0TCORRESPONDS TO RATES(E) WITH TRANSMITTED FLUXES.
        RLIT=DENT*SN*SIGLI
        RSM2T=DENT*SM*SIGSM2
        RSM0T=DENT*SM*SIGSM0
        TSRLI=TSRLI+RLIT
        TSRSM2=TSRSM2+RSM2T
        TSRSM0=TSRSM0+RSM0T
        E=E+EINC
        IF(E.GT.EEND) GO TO 16
   15 CONTINUE
   16 PRINT 9,EEND,SRLI,SRSM2,SRSM0,TSRLI,TSRSM2,TSRSM0
      RLS2=SRLI/SRSM2
      RLS0=SRLI/SRSM0
      RS2S0=SRSM2/SRSM0
      TRLS2=TSRLI/TSRSM2
```

```
      TRLSO=TSRLI/TSRSMO
      TRS2SO=TSRSM2/TSRSMO
   17 PRINT 10,RLS2,RLSO,RS2SO,TRLS2,TRLSO,TRS2SO
    1 FORMAT( 3E12.5)
    2 FORMAT( F20.5)
    3 FORMAT( 2E20.5)
    4 FORMAT( F20.5)
    5 FORMAT( 3F20.5)
    6 FORMAT( I10)
    7 FORMAT( E20.5)
    9 FORMAT( 7E10.5)
   10 FORMAT( 1HO,6E10.5)
      STOP
      END
C     SAMPLE DATA INPUT
$ENTRY
  .09670E-00  .05800E-00  .86166E-04
          300.
       1.00000E+17          6.00000E+17
            .35
         0.001                0.001              0.5
       10
        0.11807E+21
        0.10626E+21
        0.94456E+20
        0.82650E+20
        0.70842E+20
        0.59035E+20
        0.47228E+20
```

0.35421E+20

0.23614E+20

0.11807E+20

$IBSYS

CD TOT 0121